SCALE INVARIANCE IN BIOLOGICAL SYSTEMS

by

MAJA ŠKATARIĆ

A dissertation submitted to the

Graduate School-New Brunswick

Rutgers, The State University of New Jersey

In partial fulfillment of the requirements

For the degree of

Doctor of Philosophy

Graduate Program in Electrical and Computer Engineering

Written under the direction of

Professor Eduardo D. Sontag

And approved by

_____

_____

_____

_____

_____

New Brunswick, New Jersey

October, 2014

ABSTRACT OF THE DISSERTATION

Scale Invariance in Biological Systems

by MAJA ŠKATARIĆ

Dissertation Director:
Professor Eduardo D. Sontag

In this dissertation we will discuss various techniques related to modeling and identification problems arising in complex biological networks, and demonstrate how control theory approaches can be used to validate mathematical models coming from exhaustive computational experiments or noisy experimental data. The methodology based on systematic exploration of the basic dynamic processes, feedback control loops, and signal processing mechanisms in complex networks or their parts provides powerful tools for guiding the reverse-engineering of networks, and allows one to design artificial systems that are capable of achieving various objectives.

Adaptation is an essential property of many cellular systems and it means that the measured variables return to their basal levels after a transient response to a step increase in stimulus. By definition, neither the concepts of perfect nor approximate adaptation address the characteristics of the transient signaling which occurs prior to a return to steady state, which are physiologically relevant. It has been recently observed that some adapting systems, ranging from bacterial chemotaxis pathways to signal transduction mechanisms in eukaryotes exhibit an additional feature: scale invariance, meaning that transient behavior remains approximately the same when the background signal level is scaled. Recent interest in scale-invariance was triggered by a pair of papers published in 2009, in which scale-invariant behavior was experimentally

observed in several highly conserved eukaryotic signaling pathways that play roles in embryonic patterning, stem cell homeostasis, cell division, and other central processes, and their misregulation results in diseases including several types of cancer.

In this thesis we will review the biological phenomena of adaptation and scale invariance, and present the relevant mathematical results for several classes of systems that exhibit these properties. We will use a model from the literature which describes the class of enzyme networks, to prove the impossibility of perfect scale invariance, and develop the mechanism which gives rise to an approximate scale invariance. We will demonstrate results on a biological example of soil-living amoeba *Dictyostelium discoideum*. Additionally, it has been often remarked in the literature that certain systems whose output variables respond at a faster time scale than internal components, give rise to an approximate scale-invariant behavior. We will state a fundamental limitation of such a mechanism, showing that there is a minimal error that cannot be overcome, no matter how large the separation of time scales is. We will highlight the extensions and challenges in analyzing adaptation and scale-invariance in a stochastic setting.

Finally, we will discuss the development of tools for the identification of time-varying parameters in nonhomogeneous Poisson processes, in applications where discrete measurements such as "spikes" or "tumbles" are observed from the behavior of free swimming bacteria in response to the nutrient (input) signals. The objective is to estimate the underlying rate of a nonhomogeneous Poisson process that describes these events, which can then be used to analyze transient behaviors of various species and postulate a plausible model. This work has been motivated by the novel experimental methods for assaying various chemotactic bacteria based on microfluidics devices, with the goal to analyze scale invariance property and model the behavior of different species using various inputs (nutrients).

Acknowledgements

I would like to thank Dr. Sophocles Orfanidis, Dr. David Daut, Dr. Zoran Gajić and Dr. Melike Baykal-Gürsoy, for serving on my committee and spending their valuable time. In addition to serving in my panel, I am indebted to Dr. Zoran Gajić for his advice and help, through his roles as a graduate director and an instructor. Thanks to Dr. Sophocles Orfanidis for inspiring me to excel as a teaching assistant and as a course instructor. His courses in signal processing have helped me tremendously throughout the course of my doctoral studies.

I would like to thank the Department of Electrical and Computer Engineering for their support and funding during my Masters, and a part of my Ph.D. I am grateful to John Scafidi, Barbara Klimkiewitz, Noraida Martinez, John McCarthy and Justin Schlossberg, who were always there to help me throughout my program.

I was lucky to work with Dr. Jerry Nedelman, who hired me as an intern at Novartis Pharmaceuticals in 2013. In addition to being an extraordinary, dedicated scientist, and the best manager and mentor one could ever ask for, he inspired me strive for excellence and passion in everything I do, both professionally and personally. I would also like to thank him for his efforts to advertise me and recommend me while I was on the job market. I am indebted to Dr. Smaine Zeroug, Dr. Sandip Bose and Dr. Bikash Sinha of Schlumberger-Doll Research, for their support. Thanks to our group members, Zahra Aminzare, Michael de Freitas, and Evgeni Nikolaev. I would like to extent my gratitude to my friends and colleagues, Ashwin Ashok, Prashanth Kumar Gopala, Jim Housell, Dragoslav Stojadinovic, Pavel Reyes, John McGarvey and Tuan Le, for their friendship, support and inspiration.

I cannot find the words to express my deepest and sincerest gratitude to my dissertation advisor, Dr. Eduardo Sontag, who has supported me throughout my Masters

and Ph.D. with his guidance and patience. His energy to work, teach, publish and communicate has been inspirational. He has taught me how to do research, look for relevant scientific questions, explain concepts in clear and simple terms, and has given me plenty of opportunities to present my work in front of experts in the field. He has also taught me many important lessons in life which will always guide me throughout my career.

Finally, I would like to thank my parents, for their unconditional and selfless love and support.

Dedication

Mojim roditeljima,

Dobrili i Veselinu Škatarić

To my parents

Table of Contents

List of Figures

Chapter 1

Introduction

The survival of organisms depends upon their ability to formulate appropriate responses to sensed chemical and physical environmental stimuli [93]. Signal transduction and gene regulatory networks in individual cells mediate the processing of measured external signals, such as ligand concentrations or stresses, eventually leading to regulatory changes in metabolism and gene expression.

Research in the field of molecular systems biology seeks to unravel the basic dynamic processes, feedback control loops, and signal processing mechanisms in single cells and entire organisms, both for understanding and for guiding drug design [82, 4]. One of the key questions is: how can one relate phenotype (function) to interaction maps (gene networks, protein graphs, and so forth) derived from experimentation? Answers to this question provide powerful tools for guiding the reverse-engineering of networks, by focusing on mechanisms that are consistent with experimentally observed behaviors, and, conversely, from a synthesis viewpoint, allow one to design artificial biological systems that are capable of adaptation [11] and other objectives. In biology, an adapting system is one that has a property of disturbance rejection with respect to a specific class of inputs, typically zero inputs [94]. For linear systems and certain classes of nonlinear systems, the internal model principle says that such systems must have a model of the disturbance-generating system [57, 96, 37]. For example, if there is adaptation with respect to constant inputs, one expects to find an integrator, after a suitable coordinate change (integral feedback). Such systems are also found in biology, see [4, 65]. In this manner, adaptation is defined as an asymptotic property, and hence does not refer to transient behavior. In the recent years, the research interest has shifted in part towards the understanding of physiologically relevant transient behaviors, and more

specifically on the phenomenon of scale invariance, also referred to as Fold Change Detection (FCD), which is the invariance of the complete output trajectory with respect to a rescaling of the input magnitudes.

This thesis discusses these two robust properties that arise in the modeling of biological systems, namely adaptation and scale invariance, and presents relevant mathematical results for several classes of systems that exhibit these properties.

Experimental verification of scale invariant behaviors and other relevant physiological responses for arbitrary inputs and classes of systems is often not an easy task. One would like to understand and quantify adaptation and scale-invariance property for an arbitrary class of experimentally controlled stimuli, understand the molecular mechanisms underlying the robust signal detection which these properties entail, [65], and the novel experimental methods provide powerful tools to design a controlled experiment where a behavior of individual cells and a population of cells can be assayed. Hence, motivated by experimental challenges, this dissertation tackles estimation problems arising from modeling biological phenomena in which discrete measurements such as "spikes" or "tumbles" are measured from free swimming bacteria, with the objective to estimate the underlying rate of a nonhomogeneous Poisson process (NHPP) that describes these events, which can then be used to analyze input- output relationship and postulate a plausible biological model. We here propose an approach based on observers and Kalman filters.

1.1 Adaptation and scale invariance

Adaptation is an essential property of many cellular systems and it means that the measured variables return to their basal (steady-state) levels after a transient response to a step increase in stimulus [4]. This stimulus might be physical or biochemical, such as a light input to a photoreceptor, or a ligand to an olfactory receptor. Often, a return to such steady-state values of outputs occurs even in the face of a sustained step or periodic excitation: the study of such exact (or at least approximate) adaptation to a persistent input has been the subject of extensive investigations in both the experimental and the

modeling literature [9, 117, 4].

Physiological adaptation is a trait of many sensory systems, allowing them to accurately detect changes in input signals, and maintain essential variables within acceptable bounds, distinguish meaningful information from background through a shifting of dynamic range. Thus, the human eye distinguishes features across nine orders of magnitude, even though its sensors can only detect a three order of magnitude contrast; this is achieved through both the pupillary light reflex and the adjustment of sensitivity of rods and cones [23]. Similarly, humans adapt to constant touches, smells, or background noises, detecting new information only when a substantial change occurs. Physiological examples of adaptation include also the regulation of key metabolites in the presence of environmental variations [43]. At the single-cell level, one of the best understood examples of adaptation is exhibited by the *E. coli* chemotaxis sensory system, which responds to gradients of nutrient and ignores constant concentration [12, 86].

By definition, neither the concept of perfect nor the concept of approximate adaptation address the characteristics of the transient signaling which occurs prior to a return to steady-state. The amplitude and other characteristics of transient behaviors, however, are physiologically relevant. In this more general context, we are interested here in a finer property than mere adaptation, namely logarithmic sensing or scale-invariance of responses, a phenomenon exhibited by several human and animal sensory systems [43, 51, 104]. This means that responses are functions of ratios (in contrast to actual magnitudes), of a stimulus relative to the background. This phenomenon appears in bacterial chemotaxis [41, 68], in the sensitivity of *S. cerevisiae* to fractional rather than absolute pheromone gradients [73], and in two mammalian signaling systems: transcriptional as well as embryonic phenotype responses to β-catenin levels in Wnt signaling pathways [29], and nuclear ERK localization in response to EGF signaling [22]. Scale invariance allows systems to react to inputs ranging over several orders of magnitude, and is speculated to help make behaviors robust to external noise as well as to stochastic variations in total expressed concentrations of signaling proteins [88]. Scale invariance implies adaptation, but not every adaptive system is scale invariant

[88]. To explain this property intuitively, consider two step inputs u_1 and u_2 which are scaled versions of each other: $u_2(t) = pu_1(t)$, for some positive number or "scale factor" p, see Fig. 1.1(a). Adaptation means that, whether excited by u_1 or u_2, the output signal will return to the same value, as shown in Fig. 1.1(b). On the other hand, scale-invariance means that the entire actual transient response will be the same under either excitation, as shown in Fig. 1.1(d). An intermediate property between mere adaptation and scale-invariance is the "Weber-like" property in which the temporal, transient response may be different, but the peak intensities are the same, as shown in Figure 1.1(c). The term "Weber-like" is used to draw a connection to the

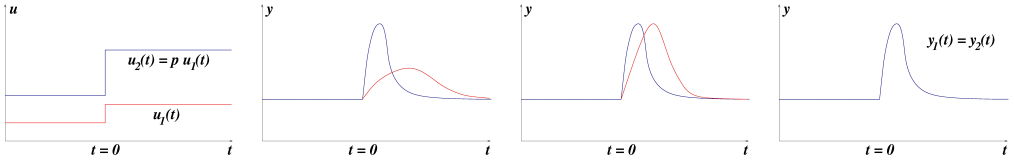

(a) (b) (c) (d)

Figure 1.1: (a) Scaled step inputs and corresponding responses: (b) perfect adaptation; (c) Weber-like (same peak amplitude responses); (d) scale-invariance (same transient responses)

Weber-Fechner law in psychophysics, which relates physical magnitudes of stimuli and perceived intensities in human sensing. Ernst Weber in the 1840s founded the field of experimental psychology, performing experiments in which a subject was asked to hold a weight, and then the weight was gradually increased until a change was first noticed. It was discovered that the smallest noticeable difference was proportional to the starting value and not to the absolute weight; in other words, two scaled versions of the input result in the same reaction. A similar phenomenon has been observed in other sensory systems, including perception of pitch in sound, light intensity, smell, pain, and taste. Gustav Fechner went on to establish a logarithmic relation between physical and perceived quantities [113, 44, 51, 80].

Recent interest in scale-invariance was triggered by a pair of papers [29] and [22] published in late 2009, in which scale-invariant behavior was experimentally observed in a Wnt signaling pathway and an EGF pathway, respectively. These are highly conserved eukaryotic signaling pathways that play roles in embryonic patterning, stem cell

homeostasis, cell division, and other central processes, and their misregulation results in diseases including several types of cancer, see Figure 1.2. The paper [29] focused

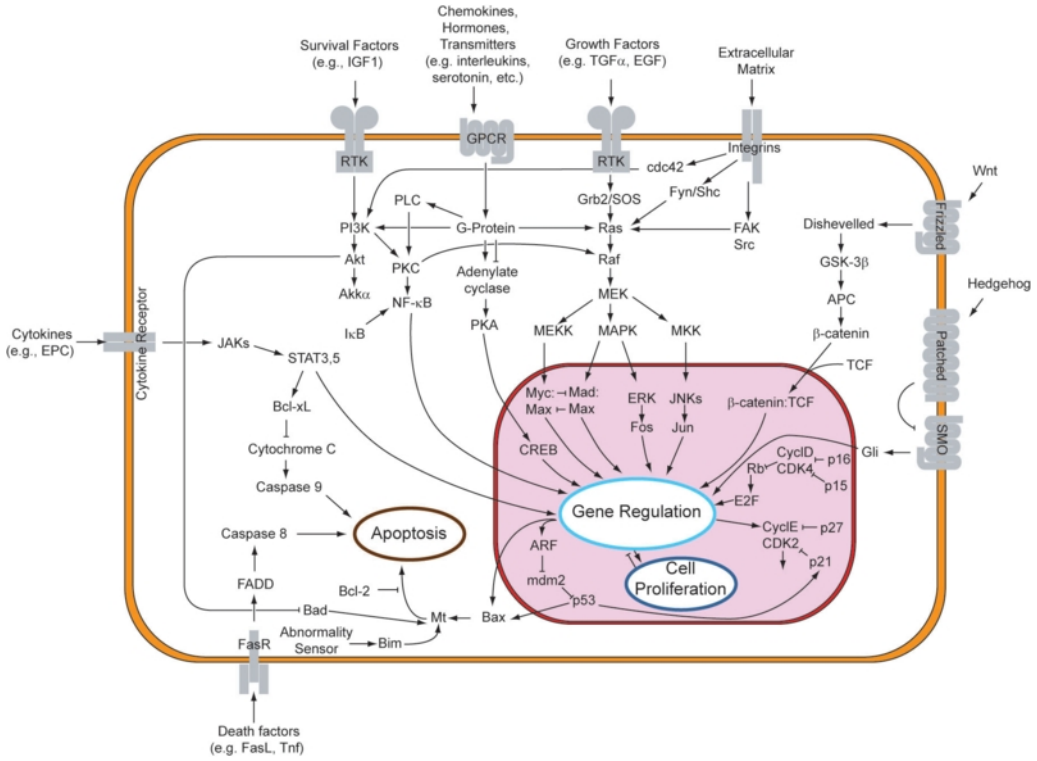

Figure 1.2: Various eukaryotic signaling pathways. Open-sourced figure reproduced from Wikipedia: The Free Encyclopedia. Wikimedia Foundation Inc.

on the effect of binding of Wnt ligand on the levels of a key protein in the Wnt signal transduction pathway, β-catenin, which in turn activates transcription of specific target genes. It was observed that, in a given population, cells might differ substantially in the β-catenin level after stimulation by Wnt, but that the effects downstream, measured either through gene expression or phenotype (in *Xenopus* embryos), appear to be a function only of the relative changes in Wnt, and not its absolute amount, Fig. 1.3. Analogous results, for an EGFR pathway, were reported in the paper [22]. Scale-invariance is also found in certain bacterial signaling systems. A prediction, for the *E. coli* chemotaxis sensory circuit in response to the ligand α-methylaspartate, was made in [87], based on a model proposed by Tu, Shimizu and Berg [86]. This predicition was later verified in a microfluics population experiment carried out in Stocker's lab as

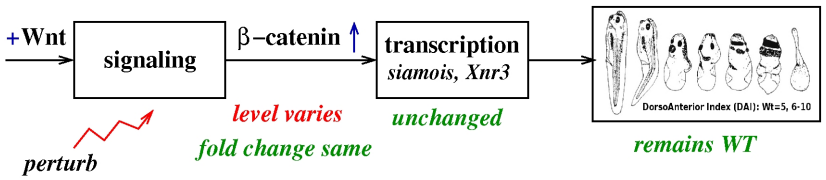

Figure 1.3: Diagram explaining some of the conclusions from [29].

well as an in FRET measurements on genetically altered bacteria in Shimizu's lab [52]. A mathematical analysis of scale-invariance was initiated in [88], [87]. For consistency we restate here the main result from [88]. To check for scale invariance we consider a system with:

$$\begin{aligned} \dot{x} &= f(x, y, u) \\ \dot{y} &= g(x, y, u) \end{aligned} \tag{1.1}$$

where x represents internal variables, u input signal and y output signal. Scale invariance holds if system (1.1) is stable, shows exact adaptation to a steady state output $y = y_0$, and if g and f satisfy the following homogeneity conditions for any $p > 0$:

$$\begin{aligned} f(px, y, pu) &= pf(x, u, y) \\ g(px, y, pu) &= g(x, u, y) \end{aligned} \tag{1.2}$$

If f is linear then this condition is also necessary for FCD [88]. More generally, the mathematical definition of perfect scale invariance [87] imposes the ideal requirement that the same response invariance property is exhibited if $u = u(t), t \geq 0$ is any time-varying input. While adaptation can be often understood in terms of control-theoretic tools based on linearizations [95, 117, 96, 37, 57], scale invariance is a genuinely nonlinear property; as a matter of fact, a linear system can never display scale-invariance, which will be described in detail the next chapter.

1.1.1 Robustness to total protein levels is guaranteed by scale invariance of downstream components

Scaled inputs in molecular sensing may arise as follows. Suppose P is a signaling protein, whose total concentration P_T is assumed to be constant at the signaling timescale. This protein can be found in inactive or active forms P_i and P_a, respectively. The active form P_a is a transcription factor that controls the level of expression of a target gene and can be thus viewed as an input to a downstream system. The rates of transition between these two forms depend, in turn, on a signal $w(t)$ (for example, an extracellular ligand concentration) through functions $k_{\text{on}}(w(t))$ and $k_{\text{off}}(w(t))$:

$$P_i \underset{k_{\text{off}}(w(t))}{\overset{k_{\text{on}}(w(t))}{\rightleftharpoons}} P_a \,, \tag{1.3}$$

as shown in Fig. 1.4.

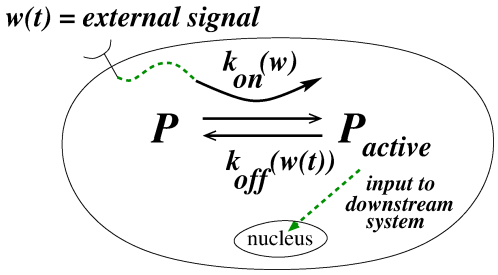

Figure 1.4: Activation and inactivation of a protein by an external signal. Active form is input to downstream gene expression.

The simplest differential equation model describing the temporal dynamics of this process would be given by:

$$\dot{u}(t) = k_{\text{on}}(w(t))(P_T - u(t)) - k_{\text{off}}(w(t))u(t)$$

(dot indicates time derivative), where we denote by $u(t)$ the amount of active protein P_a at time t; we use this notation to emphasize that this function $u(t)$ is what will be sensed by the downstream system as an input. The key observation is that, for any

number $p > 0$, the function $v(t) := pu(t)$ satisfies

$$\dot{v}(t) = k_{\text{on}}(w(t))(pP_T - v(t)) - k_{\text{off}}(w(t))v(t)\,,$$

which means that $v(t)$ solves the new differential equation in which the total protein level P_T has been scaled by p. Another way to say this is that if P_T changes to some other value P_T' , then the temporal signal $u(t)$, the input to a downstream system, will be scaled by the constant factor $p = P_T'/P_T$. This implies that the cell's response to $w(t)$ will be robust to uncertainty in P_T provided that the response to u be scale-invariant. (A similar discussion, but based on a much more restrictive Michaelis-Menten quasi-steady state approximation, can be found in [88].) As total protein concentrations are highly variable from cell to cell, and even in the same cell over time [77, 89, 25, 40, 103], this robustness might explain the experimental results in [29, 22].

Scale-invariance means that the downstream system cannot distinguish between an input $u(t)$ and a scaled version $pu(t)$. For step inputs that jump at $t = 0$, we can reformulate this property by saying that the response can *only* depend on the "*fold change*" of the input at time 0:

$$\frac{v(t)}{v(0)} = \frac{pu(t)}{pu(0)} = \frac{u(t)}{u(0)}\,,$$

hence motivating the terminology "fold change detection" (FCD), which we will use interchangeably from now on.

1.1.2 Bacterial chemotaxis as a motivating example of a scale-invariant system

Chemotaxis is the ability of organisms to sense gradients in their chemical environment and adjust their motile behavior accordingly [2]. Bacteria are often able to measure chemical gradients and move towards higher concentrations of a favorable chemical ("attractants") or lower concentrations of an unfavorable chemical ("repellents"). *E. coli* bacteria possess up to six flagella for movement, propelling themselves using one or

more of them, in a direction that is determined by chance. Flagella are rotary motors powered by ion gradients across the plasma membrane. This motor drives a helical propeller. In the presence of a spatial gradient of chemoeffectors (attractor or repellent inputs), a movement in a favorable direction happens, i.e. either towards higher concentrations of attractants, or lower concentrations of repellents. *E. coli* swimming consists of periods of smooth translation, or "runs" (corresponding to counterclockwise (CCW) direction of flagellar motor rotation), interrupted by periods of reorientation, or "tumbles" (corresponding to clockwise (CW) direction) [39, 86]. Swimming direction is chosen randomly, but swimming in a favorable direction results in longer runs, while swimming in an unfavorable direction causes a cell to revert to its baseline behavior. The sensory system responds to chemical cues (inputs) by modulating the fraction of time spent in each of these two states. *E. coli* represents the best-studied system of bacterial chemotaxis, but a wide range of other chemotactic strategies exists among bacteria. *Bacillus subtilis* and *Salmonella typhimurium* swim in a run and tumble manner, similar to *E. coli* [2]. On the other hand, some marine bacteria, i.e. *Vibrio alginolyticus* swim using a run and reverse strategy. It is of great interest to develop models of transient behavior for these systems.

1.1.3 *E. coli* model

On the molecular level, *E. coli* chemotactic description is very well characterized [39]. In the *E. coli* system, external stimuli are sensed by membrane-bound chemoreceptors called methyl-accepting chemotaxis proteins (MCP), which form a functional complex with two types of cytoplasmic proteins: the adaptor protein $CheW$ and the histidine kinase $CheA$. Upon binding to an attractant (repellent) ligand molecule, the receptor suppresses (enhances) the autophosphorylation activity of the attached $CheA$, and transduces the external chemical signal to inside the cell. $CheA$ phosphorylates itself and then transfers phosphoryl group to the two regulator proteins $CheY$ and $CheB$. The small protein $CheY-$phosphate ($CheY-P$), before it gets dephosphorylated by the phosphatase enzyme $CheZ$, can diffuse from the receptor complex to the flagellar

motor. $CheY-P$ can bind to the proteins of the flagellar motor, increasing the probability of changing its rotation from counterclockwise (CCW) to clockwise (CW), which in turn causes the motion of the *E. coli* cell to change from run to tumble. After a brief tumble, the cell runs again in a new random direction. *E. coli* chemotaxis signaling pathway has the ability to adapt to a wide range of environments. The response of the E. coli flagellar motor to $CheY-P$ level was measured quantitatively at the single cell level [21]. Knowledge of the key pathway components can be integrated in a model of the signaling network to quantitatively study various chemotaxis behaviors in spatiotemporally varying environments. One such model is Signaling Pathway-based *E. coli* Chemotaxis Simulator (SPECS) model developed in [39]. The aim of this model is to help understand how the chemotaxis motion is controlled by the cell's internal molecular signaling processes, in particular to further to explore adaptation and scale invariance.

The input for the signaling pathway is the instantaneous ligand concentration $[L](x(t),t)$, at the physical location $x(t)$ of the cell. The internal dynamics is described by the interactions between the average receptor methylation level $m(t)$ and the kinase activity, $a(t)$ which determines the switching probability $p(t)$ of the flagellar motor. The switching probability is then used to determine the cell motion (run or tumble), see Fig. 1.5.

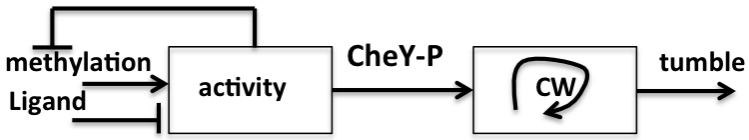

Figure 1.5: The schematic representation of the SPECS model

The general SPECS model can be written as:

$$\begin{aligned} \frac{dm(t)}{dt} &= F(a,m,[L]), \\ a &= G(m,[L]). \end{aligned} \tag{1.4}$$

The kinase activity can be determined by the quasi-equilibrium approximation:

$$a = \frac{1}{1 + exp(N\varepsilon(m, [L]))}, \tag{1.5}$$

$$\begin{aligned} \varepsilon(m, [L]) &= f_m(m) - \ln\left(\frac{1 + [L]/K_A}{1 + [L]/K_I}\right), \\ f_m(m) &= \alpha(m_0 - m). \end{aligned} \tag{1.6}$$

The usual ligand input (chemo-attractant) in an experimental setup, MeAsp, yields typical values $K_I = 18.2\mu M$, $K_A = 3mM$, $N = 6$ determined by fitting the pathway model to the data. The parameters α and m_0 for MeAsp are roughly $\alpha \approx 1.7$, $m_0 \approx 1$. The kinetics of the methylation level can be described by

$$\frac{dm}{dt} = F(a) = k_R(1 - a) - k_B a \tag{1.7}$$

where, k_R and k_B are linear rates for methylation and demethylation processes. For simplicity, $k_R \approx k_B$, to fix the steady-state activity $a_0 = 0.5$. The methylation rates can be estimated by the adaptation time from experiments with step inputs, for MeAsp $k_R \approx 0.0051$/sec.

In order to model the *E. coli* cell motion, let $s = 0, 1$, represent the tumble and run states of the cell. For the time period $t \to t + \Delta t$, a cell switches from state s to state $(1 - s)$ with probability $p_s([Y])\Delta t$. From experiments in [21] the ratio between the two probability rates for one flagellar motor can be found, and tumble time is estimated to be roughly constant (independent of $[Y]$) $\tau_0 \approx 0.2$ sec. It is assumed that $[Y]$ is proportional to the kinease activity: $[Y] = Y_a a(t)$ without considering the nonlinear dependence. In steady-state, $a \approx a_0 = k_R/(k_R + k_B)$ and the average run time is $\tau_1 \approx 0.8$sec.

1.2 Assays used for measuring the chemotaxis properties

The classical experimental method to assay the effect of controlled stimuli in controlled microenvironments on the bacterial behavior is tethering: *E. coli* is pre-treated chemically, genetically or mechanically to be attached by a single flagellum to a glass slide and the counterrotation of the bacterial body is visualized at the microscope [12]. The experimentally measured quantity is the fraction of time spent by the flagellum rotating CCW or CW (averaged over the population). Limitations of this method are long and stressful procedure of preparing the bacteria, the fact that dynamics of the flagellar bundle does not simply reflect the behavior of individual flagella, and the strong noise which requires averages over tens of bacteria for a good-quality estimate.

Another method used to measure bacterial chemotaxis in immobilized populations is to measure the activity of $CheY - P$ by using FRET microscopy [99]. FRET assays rely on nonradiative distance-dependent energy transfer from one fluorescent molecule (donor) to another (acceptor) and permit study of interactions of fluorescently labeled proteins in living cells. The major advantages of FRET are that the measurements are noninvasive, and performed in real time. FRET measurement determines stimulation-dependent interactions between the response regulator $CheY$ and its phosphatase $CheZ$ in a population bacteria and can be used to measure intracellular kinase activity or response times.

1.2.1 Methods for free swimming bacteria

Microfluidics is a method for studying the motile behavior of single cells or the population, by enabling observations at high spatial and temporal resolution in carefully controlled microenvironments [2]. Spatial coordinates of individual bacteria can be extracted from acquired images by automated image analysis. These coordinates are used to construct spatial distribution profiles of bacteria, which can be used to compute various chemotactic response properties, and hence, chemotaxis can be assessed at the population level. Additionally, cells can be tracked through a sequence of frames using

particle-tracking software, and the trajectories thus obtained yield information on swimming speeds, turning angles/frequencies, run lengths, adaptation responses allowing a quantification of chemotaxis at the single-cell level and help in formulating theoretical models of bacterial chemotaxis. The main limitation of cell tracking is imposed by the finite depth of field of the microscope, which only permits acquisition of relatively short segments of a bacterial trajectory before the cell swims out of focus. The advanced microdevices are able to generate flow-free, steady gradients of arbitrary shape. Under steady flow rates, the gradient is steady at each location along the channel.

1.2.2 Generation of high-fidelity temporal signals for free-swimming bacteria

In order to study the behavior of an unknown system, having full control of the input allows one to craft stimuli that are maximally informative for distinguishing between several proposed models of an unknown species. Ultimately, this methodology can be used for detailed comparisons between experimental data and mathematical models of transient behaviors. To achieve that goal, our collaborators designed the microfluidic signal generator (MSG), a microfluidic device, to enable these type of experiments for freely swimming microorganisms, by generating signals of nutrients that vary quickly in time, with minimal spatial and flow perturbations.

The goals established by the collaborators in Professor Stocker's lab located at MIT, were to achieve reliable, high frequency signal generation and then to proceed to the measurement portion of the experiment, where the goal is to develop procedures for reliable tracking of bacteria as they respond to the temporally varying stimuli. In particular, the focus is on reliable identification of tumble events in chemotactic bacteria. In turn, from the tumbles we can retrieve the underlying activity, $a(t)$, which is the ultimate goal, as shown on Fig. 1.5.

With the successful completion of the MSG, the focus has now shifted towards the measurement of the behavior characteristics of the bacteria in the test chamber. Two primary behavioral characteristics are the speed and tumbling rate. The collaborators

have also developed protocols to make decisions on the state of individual bacteria based on their tracked motion, and are in the last phase of the process, where the experimental data are collected, and which will allow us to probe the chemotactic response of a population of bacteria with unprecedented temporal control, and acquiring unprecedented data for comparison with mathematical models of transient behaviors. Therefore, there is a need for a good estimation algorithm, which will reconstruct the underlying activity function, based on the discrete data. The proposed method will be explained in Chapter 4.

1.3 Thesis Overview

In this dissertation, we analyze and mathematically describe a robust property, termed the scale invariance property, for several classes of systems found in biology, and demonstrate how this property can help in model discrimination. Motivated by the experimental limitations and challenges in modeling of bacterial chemotaxis, the contribution of this thesis also lies in developing an observer-based approach to the problem of estimation of an unknown rate function of a nonhomogeneous Poisson process.

The thesis is organized in six chapters, as follows.

In **Chapter 2**, we study the scale invariance property for a class of three-dimensional nonlinear systems which have been widely studied as a generic model of enzymatic networks [57], common in eukaryotic as well as prokaryotic systems, and are found in intracellular signal processing. We start by proving the impossibility of perfect scale invariance for these enzymatic networks, so that a purely numerical study of approximate scale invariance is called for. Computational results are then outlined, and they lead us to postulate a novel property, "uniform linearizations with fast output" (ULFO): after a singular perturbation reduction on the output variable, the linearizations of the obtained two-dimensional system at all steady-states (corresponding to constant inputs) must all be identical. Numerically, we find that all networks in our study which are (approximately) scale invariant must necessarily (approximately) satisfy ULFO. In

converse direction, we prove that the ULFO property implies approximate scale invariance. Additionally, for approximately scale invariant systems, the two states in the reduced system are computationally found to satisfy an homogeneity property with respect to the input scalings. Conversely, we present a proof that equal linearizations are necessary for reduced systems to satisfy the homogeneity property. Results are then demonstrated on a biological example of soil-living amoeba *Dictyostelium discoideum*. This example contains an incoherent feedforward (IFFL) motif, in which an external stimulus u activates a molecular species x, which in turn, activates or represses a downstream species y (our output of interest). This effect entailed in the IFFL possesses powerful signal processing properties [4], and has been proposed as one of the two biomolecular mechanisms that can help produce approximate scale invariance, [30, 88, 87]. Additionally, it was observed that multiple time scales, corresponding to slow and fast subsystems, are typically inherent in such motifs. The property of time scale separation for the IFFL's was in particular analyzed in the generic example of three-node enzymatic networks in Section 1.4.1, where we concluded through numerical and theoretical analysis, that every three node enzyme network which has an approximate scale invariance property must rely on this mechanism of time scale separation.

In **Chapter 3**, we analyze incoherent feedforward circuits in detail, and show that no matter how small the time separation parameter ε is, there is always an irreducible minimal possible difference in the instantaneous values of the outputs when comparing the response to an input $u(t)$, and to a scaled version of this input $pu(t)$.

In **Chapter 4** we discuss challenges in experimental verification and modeling of scale invariant behaviors and other relevant physiological responses for arbitrary inputs and classes of systems. Novel experimental techniques based on microfluidics devices provide powerful tools to design a controlled experiment where a behavior of individual cells and a population of cells can be assayed, and they require new estimation methods.

Bacterial chemotaxis plays a fundamental role in a broad range of processes, including disease pathogenesis, biofilm formation, bioremediation, etc [2]. Because of its simplicity, bacterial chemotaxis of *E. coli* is among the best characterized signaling systems in

biology, and its molecular level description of how the signal is received, transduced, and regulated has been well studied [66]. Not much is known nor modelled for chemotaxis process of other bacterial species such as *Bacillus subtilis*, *Salmonella typhimurium*, *Vibrio alginolyticus*, etc. It is of great interest to develop models of transient behavior for these species, as well.

Using the data from the experiments, multiple models can be created, each representing one of the possible interconnections between the key players in the system. Engineering tools can then be applied to determine whether there is an optimal input to the system that can differentiate between the behaviors of the different models, so that if this input was applied in the laboratory it would result in discrimination [112, 79]. Motivated by experimental challenges arising from modeling biological phenomena, and novel assays using microfluidics devices, in Chapter 4 we develop an estimation method for the rate of a nonhomogeneous Poisson process. Experimentally, discrete events such as "spikes" or "tumbles" are observed and expracted from the images of free swimming bacteria, and the objective is to estimate the underlying rate of a nonhomogeneous Poisson process (NHPP) that describes these events, which can then be used to analyze input-output relationships and postulate a plausible biological model. The schematic shown in Fig. 1.5 depicts the basic idea behind the estimation problem: the same inputs are fed to a population of chemotactic bacteria, and microscope based observations of tumbling events will be used for the estimation of the tumbling rate (a function of chemotactic protein concentrations). We propose an approach based on observers and Kalman filters and compare these to other methods (not model-based) in the literature.

This alternate method of collecting measurements allows to collect the measurements for a large class of inputs, where both single cells and populations of bacteria can be assayed under the same conditions, the experiments can be repeated and applied to different classes of bacteria. Additionally with the advancement in the experimental setup various types of environments where bacteria live could be mimicked and the effect on the dynamics modeled appropriately.

In **Chapter 5** we provide some remarks regarding the adaptation and scale invariance

properties in stochastic setting.

The final conclusions are drawn in **Chapter 6**, which also contains a brief section on passible avenues for the extension of the presented work.

1.4 Thesis Contribution

The major contributions of this thesis are summarized as follows.

1.4.1 Scale invariance in enzymatic networks

We developed a novel mathematical property termed "uniform linearization with fast output" (ULFO) on a study of three-node enzyme networks, that explains approximate scale invariance for the class of enzyme networks. Then we mathematically prove that ULFO yields approximate scale invariance, and extend the results of this study to examples relevant in systems biology. Finally, we show how we can use scale invariance and our developed mechanism for model invalidation, on an example of a published model of soil-living amoeba *Dictyostelium discoideum*. This work was published in a journal and a conference paper, [93, 94].

1.4.2 Feedforward circuits and a fundamental limitation of time-scale based scale-invariance

Another key contribution to this topic of scale invariance is in the analysis of feedforward circuits, a motif commonly used in the biological research community as a "signal processing" mechanism that gives rise to an approximate scale invariance, due to the presence of different time scales in its dynamics. We provide a fundamental limitation to this mechanism, and give a lower bound result for the scale invariance error. This work was published in a journal article [90].

1.4.3 Estimation of a rate function of a nonhomogeneous Poisson process (NHPP)

Motivated by the work with our experimental collaborators who are designing novel experimental methods, our contribution lies also in developing tools for the identification of time-varying parameters in nonhomogeneous Poisson processes based on observers and Kalman filters. Experimentally, discrete events such as "tumbles" or "spikes" are observed, based on images of swimming bacteria in response to the nutrient signal, and the goal is to identify a hidden continuous time variable that drives the tumbling behavior. The method we developed is novel in its application to biology, but it is also superior to other methods commonly used in the literature, for instance in communication networks, or neural science, where estimation of a NHPP arises as well, in the sense that our method takes into account the fact that we are using information about the inputs to our estimator. We support this claim on several examples. The results are published in a conference article [92].

1.4.4 Adaptation property in stochastic setting

We remark that commonly used structures in deterministic setting, such as incoherent feedforward loop, and a feedback loop fail to exhibit adaptation (and hence, the scale invariance property) assuming that "copy numbers" of species (ions, atoms, molecules, individuals) are very small, which is a realistic assumption in molecular biology at the single-cell level. In such cases the occurrence of chemical reactions in this setting, involves discrete and random events, and in order to predict the progress of chemical reactions in terms of observables such as copy number, we generate sample paths of the stochastic process for the copy number, which is referred to as a stochastic simulation. For our two typical motifs, we analytically and numerically demonstrate that the adaptation of the moments in the stochastic setting is lost. This work is accepted for publication, see [91].

Chapter 2

Approximate scale invariance for a class of enzymatic networks

In this chapter, we focus on enzymatic signal transduction systems, which involve the activation/deactivation cycles that typically mediate transmission of external signals (inputs) to transcription factors and other effectors. Networks involving such enzymatic cycles are involved in signal transduction networks from bacterial two-component systems and phosphorelays [10, 31] to actin treadmilling [19], guanosine triphosphatase cycles [24], glucose mobilization [42], metabolic control [100], cell division and apoptosis [101], cell-cycle checkpoint control [56], and the eukaryotic Mitogen-Activated Protein Kinase (MAPK) cascades which mediate growth factor inputs and determine proliferation, differentiation, and apoptosis [8, 18, 36, 114, 6].

2.1 Dynamic model for three-node enzymatic networks

We are interested in exploring which enzymatic networks do not merely adapt, but also display scale invariance. To analyze this problem we first consider networks consisting of three types of enzymes, denoted respectively as A, B, and C. Each of these enzymes can be in one of two states, active or inactive. The fractional concentration of active enzyme A is represented by a variable $x_A = x_A(t)$, so $\widetilde{x}_A = 1 - x_A$ is the fraction of inactive enzyme A. Similar notations are used for B and C. Only enzyme A is directly activated by an external input signal, and the response of the network is reported by the fraction of active C. Enzyme B acts as an auxiliary element.

Each enzyme may potentially act upon each other through activation (positive regulation), deactivation (negative regulation), or not at all. If a given enzyme is not

deactivated by any of the remaining two, we assume that it is constitutively deactivated by a specific enzyme; similarly, if a given enzyme is not activated by any other, there is a constitutively activating enzyme for it.

One represents networks by 3-node directed graphs, with nodes labeled A, B, C, and with edges between two nodes labeled + and − (or "$\rightarrow$" and "$\dashv$") to denote positive or negative regulation respectively; no edge is drawn if there is no action. There are $3^2 = 9$ potential directed edges among the three nodes (A to A, A to B, etc.), each of whose labels may be +, −, or "none" if there is no edge. This gives a total of $3^9 = 19,683$ possible graphs. One calls each of these possible graphs a *topology*. Discarding the 3,645 topologies that have no direct or indirect links from the input to the output, there remain 16,038 topologies.

We quantify the effects of each existing regulatory interaction by a Michaelis-Menten term and write a three-variable ordinary differential equation (ODE) that describes the time evolution of $x_A(t)$, $x_B(t)$, and $x_C(t)$:

$$\dot{x}_A = \sum_i \frac{k_{V_iA} v_i \cdot \widetilde{x}_A}{\widetilde{x}_A + K_{V_iA}} - \sum_i \frac{k_{W_iA} w_i \cdot x_A}{x_A + K_{W_iA}} \tag{2.1a}$$

$$\dot{x}_B = \sum_i \frac{k_{V_iB} v_i \cdot \widetilde{x}_B}{\widetilde{x}_B + K_{V_iB}} - \sum_i \frac{k_{W_iB} w_i \cdot x_B}{x_B + K_{W_iB}} \tag{2.1b}$$

$$\dot{x}_C = \sum_i \frac{k_{V_iC} v_i \cdot \widetilde{x}_C}{\widetilde{x}_C + K_{V_iC}} - \sum_i \frac{k_{W_iC} w_i \cdot x_C}{x_C + K_{W_iC}} \tag{2.1c}$$

The K's denote Michaelis-Menten, and the k's catalytic rate constants associated to each regulatory interaction. All the summations range over $i = 1, \ldots, 6$. Each "V_i" represents one of A, B, C, E_A, E_B, E_C, the activating enzymes in the respective equations, and each "W_i" one of A, B, C, F_A, F_B, F_C, the deactivating enzymes; E and F are the constitutively activating and deactivation enzymes, buffered at constant concentrations. (Lower-case variables $v_i, w_i = x_A, \ldots, x_{F_C}$ denote active fractions) As an exception, the equation for node A does not include an E_A term, but instead includes a term $k_{UA} u \frac{\widetilde{x}_A}{\widetilde{x}_A + K_{UA}}$ that models activation of A by an external input whose strength at time t is given by $u = u(t)$ and whose values $u(t)$ stay within a range $[\underline{u}, \overline{u}]$. No enzyme appears both an activator and as a deactivator of any given component, that

is, $k_{X_iA}k_{Y_iA} = 0$, $k_{X_iB}k_{Y_iB} = 0$, and $k_{X_iC}k_{Y_iC} = 0$, and constitutive enzymes are included only if the reaction would be otherwise irreversible.

For example, the topology shown in Figure 2.1 is described by the following set of ODE's:

$$\dot{x}_A = \frac{k_{UA}u \cdot \widetilde{x}_A}{\widetilde{x}_A + K_{UA}} - \frac{k_{BA}x_B \cdot x_A}{x_A + K_{BA}} - \frac{k_{CA}x_C \cdot x_A}{x_A + K_{CA}} \tag{2.2a}$$

$$\dot{x}_B = \frac{k_{AB}x_A \cdot \widetilde{x}_B}{\widetilde{x}_B + K_{AB}} - \frac{k_{F_BB}x_{F_B} \cdot x_B}{x_B + K_{F_BB}} \tag{2.2b}$$

$$\dot{x}_C = \frac{k_{AC}x_A \cdot \widetilde{x}_C}{\widetilde{x}_C + K_{AC}} - \frac{k_{BC} \cdot x_B x_C}{x_C + K_{BC}} - \frac{k_{CC}x_C \cdot x_C}{x_C + K_{CC}} \tag{2.2c}$$

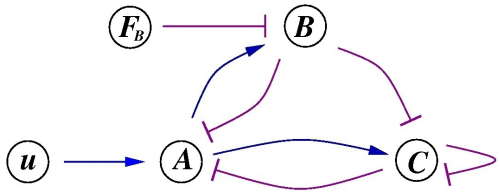

Figure 2.1: An example of a topology

The term *circuit* is used to refer to a given topology together with a particular choice of the K and k parameters. The three-node model in (2.1) was employed by Ma et al. [57], in order to classify the minimal enzymatic circuits that (approximately) adapt. (With the model in [57] that we adopted, there is no direct connection from the input to the output node, and two-node networks are not sufficient for adaptation, while larger adapting networks contain these three-node networks [57]. If one allows direct connections from input to outputs, then two-node networks are able to display adaptation.)

The same paradigm has since been used to investigate other network characteristics as well [84], [116].

The restriction to three-node networks is made for both practical and biological reasons. As argued in several papers that use a similar approach [57, 84, 116], even though adaptation (as well as scale invariant) behaviors can, and do, arise in larger networks, the coarse-graining involved in restricting the computational search to minimal networks

leads to a tractable search problem, and allows also one to intuitively understand the basic principles. The same motifs are observed in larger networks, in which several nodes may represent a single node in the three-node networks that we study.

Before we proceed to the description and results of a numerical study we performed on all three-node enzyme networks, in the next section, we will revisit and demonstrate the concepts of (approximate) adaptation and (approximate) scale invariance, and motivate our analysis using an example that demonstrates that adaptation is not sufficient for scale invariance.

2.2 Adaptation and scale invariance metrics

We will see in the consequent sections that examples of three-node networks should be analyzed only in terms of approximate adaptation and scale invariance metrics.

Following the methodology introduced in [28], we define approximate adaptation in terms of two metrics: *adaptation precision* and *signal detection* or *sensitivity*.

The first metric quantifies the following effect: if we start at steady-state, and then step the input at time $t = 0$ from a value u_0 to a different constant value u_1, then the system's output, as reported by a response variable $y(t)$ (where $y(t) = x_C(t)$ in (2.1)), should return asymptotically to a value that is close to the original value $y(0)$. The relative difference in initial and final response $\Delta_y^\infty = |y(+\infty) - y(0)|$ provides a measure of adaptation precision. We say that a system is *(approximately) adaptive* provided that, for all inputs in the valid range, $\Delta_y^\infty/\Delta_u < 0.1$, where $\Delta_u = |u_1 - u_0| \,/\, |u_0|$ is the relative change in input.

In particular, **exact or perfect adaptation** means that $\Delta_y^\infty = 0$. The 10% error tolerance is natural in applications, and the qualitative conclusions are not changed by choosing a smaller cutoff [57].

A second metric relies upon the maximal transient difference in output, normalized by the steady-state output, $\Delta_y^{\max} = \max |y(t) - y(0)| \,/\, |y(0)|$. A *signal-detection* property for adaptation [96], [5], should be imposed in order to rule out the trivial situation $\Delta_y^{\max} \approx 0$ in which a system's output is independent of the input. To avoid having to

pick an arbitrary threshold, in this study we follow the convention in [57] of requiring the *sensitivity* $\Delta_y^{\max}/\Delta_u$ to be greater than one.

Scale invariance is the property that if a system starts from a steady-state condition that was pre-adapted ($t < 0$) to a certain background level u_0, and the input is subsequently set to a new level u at $t = 0$, then the entire time response of the system $y_{u_0,u}(t)$ is the same as the response $y_{pu_0,pu}(t)$ that would result if the stimulus had changed, instead, from pu_0 to pu. This property should hold for scale changes $p > 0$ that respect the bounds $\underline{u} \leq u \leq \overline{u}$ on inputs. More generally, the mathematical definition of (perfect) scale invariance [87], imposes the ideal requirement that the same response invariance property is exhibited if $u = u(t)$, $t \geq 0$ is any time-varying input. The experiments in [52] included excitation by certain oscillatory inputs, for example. In practice, however, this property will always break down for high-frequency inputs, since there are limits to the speed of response of biological systems. In this study, for an approximate scale invariance, we will ask that the relative difference between the responses $y_{pu_0,pu}(t)$, and $y_{u_0,u}(t)$ be at most 10%: $\max_t \{|y_{pu_0,pu}(t) - y_{u_0,u}(t)| \,/\, \max(y_{pu_0,pu}(t) - y_{u_0,u}(t))\} < 0.1$, with bounds $\underline{u} \leq u \leq \overline{u}$ on the input, and for $p > 0$.

Adaptive systems need not be scale invariant

As an illustration of a (perfectly) adaptive yet not scale invariant system, consider the following equations:

$$\dot{x}_A = k_1 u - k_2 x_B \tag{2.3a}$$

$$\dot{x}_B = k_3 x_A - k_4 x_B \tag{2.3b}$$

$$\dot{x}_C = k_5 x_A - k_6 x_B x_C \tag{2.3c}$$

which is a limiting case of the system described by (2.2) when $k_{CA}, k_{CC}, K_{UA}, K_{BA}, K_{AB}$, $K_{AC} \approx 0$, $k_{BC} = k_6 K_{BC}$, $K_{BC} \gg 1$ (so $-k_{BC} x_B x_C/(x_C + K_{BC}) \approx -k_6 x_B x_C$), and $k_{F_B B} x_{F_B} = k_2 K_{F_B B}$ and $K_{F_B B} \gg 1$.

This network perfectly adapts, since at steady state the output is $x_C = \overline{x}_C = k_4 k_5/(k_3 k_6)$,

no matter what is the magnitude of the constant input u, and in fact the system returns to steady state after a step change in input u, with $x_C(t) \to \overline{x}_C$ as $t \to \infty$ (general stability properties of feedforward circuits shown in [98]).

On the other hand, the example in Eq.2.3 does not display scale invariance. Indeed, consider the solution from an initial state pre-adapted to an input level u_0, that is $x_A(0) = k_1k_4u_0/(k_2k_3)$, $x_B(0) = k_1u_0/k_2$, and $x_C(0) = k_4k_5/(k_3k_6)$, and the input $u(t) \equiv u_1$ for $t \geq 0$. Then, $x_C(t) = k_4k_5/(k_3k_6) + k_1k_5(u_1 - u_0)t^2/2 + O(t^3)$ for small $t \geq 0$. Since the t^2 coefficient in this Taylor expansion gets multiplied by p when u_0 is replaced by pu_0 and u_1 is replaced by pu_1, it follows that the transient behavior of the output $x_C(t)$ depends on p.

Interestingly, if the equation for the third node is replaced by $\dot{x}_C = k_5x_A/x_B - k_6x_C$, that is to say the activation of C is repressed by B, instead of its de-activation being enhanced by A, then scale invariance does hold true, because $x_A(t)$ and $x_B(t)$ both scale by p when $u_0 \mapsto pu_0$, $u_1 \mapsto u_0$, and $x_C(t)$ depends on the ratio of these two functions (in particular, the $t^2/2$ term is $k_2k_5(u_1 - u_0)/u_0$). Such a repression is typical of genetic interaction networks, but is not natural in enzymatic reactions.

It fact, the example described by Eq.2.3 is typical: no enzymatic network described by Eq.2.1 can display perfect scale invariant behavior, and this fact is a consequence of the equivariance theorem proved in [87].

Thus, a meaningful study of enzymatic networks, even for perfectly adaptive ones, must rely upon a test of approximate scale invariance, as explained in Section 2.2. Instead of asking that $y_{u_0,u}(t) = y_{pu_0,pu}(t)$, as was the case in the theory developed in [88, 87], and given by (1.2), one should require only that the difference be small, as given in the Section 2.2. We next prove the impossibility of a perfect scale invariance for this class of systems.

2.3 Impossibility of perfect scale invariance

Consider any system with state $x = (x_A, x_B, x_C)$, output x_C, and equations of the general form:

$$\begin{aligned} \dot{x}_A &= f(x) + G(x_A)u \\ \dot{x}_B &= g(x) \\ \dot{x}_C &= h(x) \;=\; x_A a(x_C) + x_B b(x_C) + c(x_C)\,. \end{aligned}$$

It is assumed that $a(x_C) \neq 0$ for all x_C, $G(x_A) \neq 0$ for all x_A, $\overline{G} := \sup_x G(x) < \infty$, and the system is irreducible [87]. We now prove that such a system cannot be scale invariant. Suppose by way of contradiction that it would be, and pick any fixed $p \neq 1$. The main theorem in [87] insures that there are two differentiable functions $\alpha(x)$ and $\beta(x)$ such that the algebraic identities:

$$\begin{aligned} \alpha_x(x)[f(x) + G(x_A)u] + \alpha_y(x)g(x) + \alpha_z(x)h(x) &= f(\alpha(x), \beta(x), x_C) + G(\alpha(x))pu, \\ \beta_x(x)[f(x) + u] + \beta_y(x)g(x) + \beta_z(x)h(x) &= g(\alpha(x), \beta(x), x_C) \\ \alpha(x)a(x_C) + \beta(x)b(x_C) + c(x_C) &= x_A a(x_C) + x_B b(x_C) + c(x_C) \end{aligned}$$

hold for all constant $x = (x_A, x_B, x_C)$ and u, and the vector function $x \mapsto (\alpha(x), \beta(x), z)$ is one-to-one and onto, which implies in particular that

$$\sup_x G(\alpha(x)) = \overline{G}\,.$$

Dividing by u and taking the limit as $u \to \infty$ in the first identity, we conclude that $\alpha_x(x)G(x_A) \equiv pG(\alpha(x))$. Doing the same in the second identity, we conclude that $\beta_x(x) \equiv 0$. Finally, taking partial derivatives with respect to x_A in the third identity:

$$a(x_C)pG(\alpha(x))/G(x_A) = \alpha_x(x)a(x_C) + \beta_x(x)b(x_C) = a(x_C)$$

is true for all x. Since $a(x_C) \not\equiv 0$, it follows that

$$pG(\alpha(x)) = G(x_A)$$

for all x. We consider two cases: (a) $p < 1$ and (b) $p > 1$. Suppose $p < 1$. Pick any sequence of points $x^{(i)}$ with $G(x^{(i)}) \to \overline{G}$ as $i \to \infty$. Then $G(\alpha(x^{(i)})) \to \overline{G}/p > \overline{G}$, contradicting $G(x) \leq \overline{G}$. If $p > 1$, picking a sequence such that $G(\alpha(x^{(i)})) \to \overline{G}$ as $i \to \infty$ gives the contradiction $G(x^{(i)}) \to p\overline{G} > \overline{G}$. This shows that the scale invariance property cannot hold.

2.4 Numerical study

Given that we proved that no enzymatic network described by (2.1) can display perfect scale invariant behavior, we perform an exhaustive computational study of all 3-node networks, finely sampled in parameter space, to see if there are those that exhibit an approximate scale invariance as we described in Section 2.2.

We generalized and extended the computational protocol developed for adaptation in [57] to an investigation of approximate scale invariance. MATLAB® scripts were used, in conjunction with the software developed in [57].

To investigate this issue, we computationally screened all 160,380,000 circuits, obtained from the 16,038 nontrivial 3-node topologies, each one with 10,000 parameters sampled in logarithmic scale using the Latin hypercube method [38], testing for small differences in responses to scaled steps. (We picked the ranges k_{cat}=0.1-10 and K_m=0.001-100. A finer sampling does not affect the conclusions in any significant way [57].) In order to test inputs in ranges of the form $a \leq u(t) \leq 2a$, redefining the constant k_{UA} if needed, we take simply $\underline{u} = 0.3$ and $\overline{u} = 0.6$.

We found that approximately 0.01% (16,304) of the circuits showed adaptation, meaning that, as in [57], when making a 20% step from $u_0 = 0.5$ to $u_1 = 0.6$ the precision is 10% or better, and the sensitivity is at least unity. Of the adapting circuits, about 0.15% (25 circuits, classified into 21 different topologies) were determined to be approximately scale invariant. Approximate scale invariance (ASI) was then tested by also performing a 20% step experiment from $u_0 = 0.3$ to $u_1 = 0.36$ and requiring that the relative difference between the responses be at most 10%: $\max_t \{|y_{0.6}(t) - y_{3.6}(t)| \,/\, \max(y_{0.6}(t) - y_{3.6}(t))\} < 0.1$

We provide the graphs for 21 topologies, together with their parameter sets that correspond to the identified 25 circuits. As an example of the behavior of one of these, Fig. 2.2 shows a response resulting from a 20% step, from 3 to 3.6, compared to the response obtained when stepping from 5 to 6; the graphs are almost indistinguishable. In the following discussion, we will refer to these surviving circuits, an their topologies, as being "approximately scale invariant".

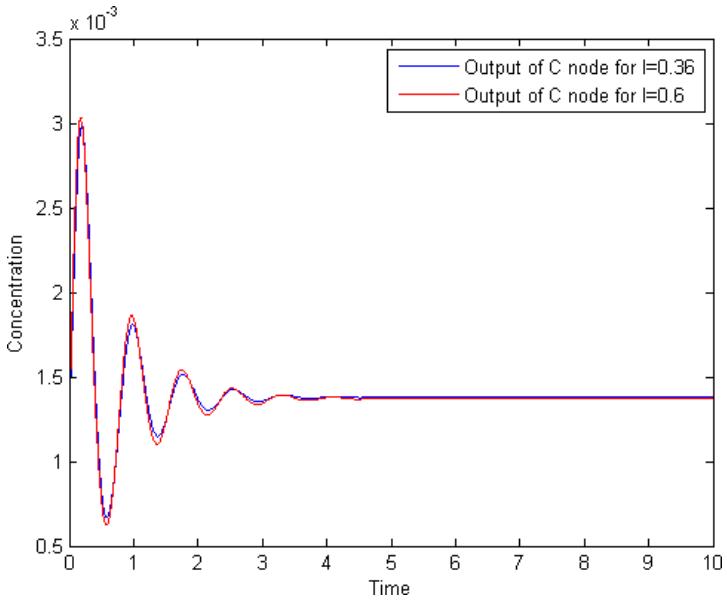

Figure 2.2: Scale invariance: plots overlap, for responses to steps 3→1.2∗3 and 5→1.2∗5. Network is the one described by 2.2. Random parameter set: K_{UA}=0.093918 k_{UA}=11.447219, K_{BA}=0.001688 k_{BA}=44.802268, K_{CA}=90.209027 k_{CA}=96.671843, K_{AB}=0.001191 k_{AB}=1.466561, K_{F_B}= 9.424319 k_{F_B}=22.745736, K_{AC}=0.113697 k_{AC}=1.211993, K_{BC}=0.009891 k_{BC}=7.239357, K_{CC}=0.189125 k_{CC}=17.910182

Once that this small subclass was identified, we turned to the problem of determining

what network characteristics would explain the results of these numerical experiments.

2.5 Approximate scale invariance (ASI)

Continuing with the example in (2.3), let us suppose that $k_1, k_2, k_3, k_4 \ll k_5, k_6$, so that the output variable $y = x_C$ reaches its steady-state much faster than x_A and x_B do. Then, we may approximate the original system by the planar linear system represented by the differential equations for x_A and x_B together with the new output variable $\widetilde{y}(t) = h(x_A(t), x_B(t)) = kx_A(t)/x_B(t)$, where $k = k_5/k_6$. This reduced planar system, obtained by a quasi-steady state approximation (or time-scale separation, which is the term we will be using in the next chapter), has a perfect scale invariance property: replacing the input u by pu results in the solution $(px_A(t), px_B(t))$, and thus the output is the same: $h(x_A(t), x_B(t)) = h(px_A(t), px_B(t))$. The exact invariance of the reduced system translates into an approximate scale invariance property for the original three-dimensional system because, except for a short boundary-layer behavior (the relatively short time for x_C to reach equilibrium), the outputs of both systems are essentially the same, $y(t) \approx \widetilde{y}(t)$. The assumption $k_1, k_2, k_3, k_4 \ll k_5, k_6$ is often written symbolically as $\dot{x}_A = k_1 u - k_2 x_B$, $\dot{x}_B = k_3 x_A - k_4 x_B$, $\varepsilon \dot{x}_C = k_5 x_A - k_6 x_B x_C$, where $0 < \varepsilon \ll 1$ and where k_5, k_6 are now the original k_5, k_6 multiplied by ε. The quality of approximate scale invariance will depend on how small "ε" is. In the next chapter, we will look at this example, which is entails a motif called an incoherent feedforward loop more closely, and elaborate on the "smallness" of the parameter ε, as well as the error one makes by assuming the quasi-steady state approximation for the output variable.

Generality of the planar reduction

We found that, just as in the example of (2.3) when $k_1, k_2, k_3, k_4 \ll k_5, k_6$, in every ASI circuit the time scale of node C is much shorter than that of A and B. Therefore, the same two-dimensional reduction is always valid. It follows that one can drop the last equation, approximating these circuits by planar systems that are described by only the two state variables x_A and x_B, where every occurrence of x_C in the first two

equations of the right-hand side of (2.1) is replaced by $h(x_A, x_B)$, the function obtained by setting the right-hand side of the third equation in (2.1) to zero and solving for the unique root in the interval $[0, 1]$ of the quadratic equation. This reduced system, with $\widetilde{y}(t) = h(x_A(t), x_B(t))$ as an output, provides an excellent approximation of the original dynamics. Fig. 2.3 compares the true response with the response obtained by the quasi-steady state approximation, for one ASI circuit. The parameter sets for all ASI circuits are given in 2.8 and their graphical representations are given on Fig. 2.7.

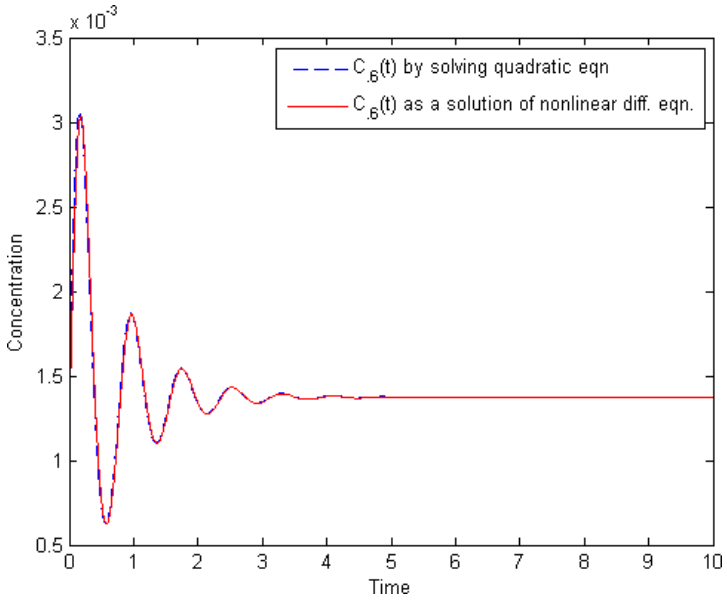

Figure 2.3: QSS quadratic approximation. Network is the one described by (2.2). Random parameter set is as in Fig. 2.2

.

2.5.1 Generality of dependence on x_A/x_B

In the example given by (2.3), there were two additional key mathematical properties that made the planar reduction scale invariant (and hence the original system approximately so). The first property was that, at equilibrium, the variable x_C must be a function of the ratio x_A/x_B, and the second one was that each of x_A and x_B must scale by the same factor when the input scales by p. Neither of these two properties need to hold, even approximately, for general networks. Surprisingly, however, we discovered that both are valid with very high accuracy for every ASI circuit. The

equilibrium value of x_C is obtained from setting the last right-hand side of (2.1) to zero and solving for x_C. A solution $x_C = h(x_A, x_B)$ in the interval $[0, 1]$ always exists, because at $x_C = 0$ one has $\widetilde{x}_C = 1$ and thus the term is positive, and at $x_C = 1$ one has $\widetilde{x}_C = 0$ and so the term is negative. This right-hand side has the general form $x_A\phi(x_C) + x_B\gamma(x_C) + \kappa(x_C, x_{E_C}, x_{F_C})$, where ϕ and γ are increasing functions, each a constant multiple of a function of the form $\widetilde{x}_C/(\widetilde{x}_C+K)$ or $-x_C/(x_C+K)$. If the term κ is negligible, then $x_A\phi(x_C)+x_B\gamma(x_C) = 0$ means that also $(x_A/x_B)\phi(x_C)+\gamma(x_C) = 0$, and therefore x_C at equilibrium is a (generally nonlinear) function of the ratio x_A/x_B. There is no a priori reason for the term κ to be negligible. However, we discovered that in every ASI circuit, $\kappa \approx 0$. More precisely, there is no dependence on the constitutive enzymes, and this "self-loop" link, when it exists, contributes to the derivative $\dot{x}_C$ much less than the x_A and x_B terms, see Fig. 2.4.

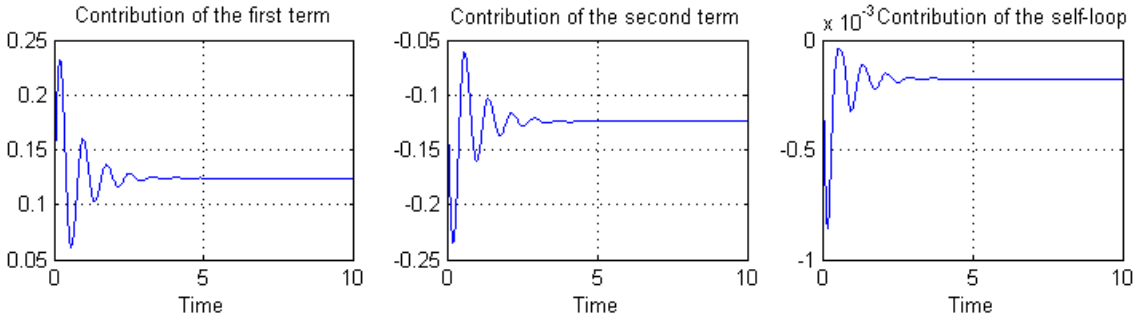

Figure 2.4: Relative contribution of terms in the equation for node C. The first two terms range in $[-0.25, 0.25]$ but self-loop magnitude is always less than 10^{-3}. i.e. contribution or self-loop to $\dot{x}_C$ is less than 1%. Similar results hold for all ASI circuits. Network is the one described by (2.2). Random parameter set is as in Fig. 2.2.

2.5.2 Generality of homogeneity of x_A, x_B

The last conclusion from (2.3) that plays a role in approximate scale invariance is that each of x_A and x_B must scale proportionately when the input is scaled. In that example, the property holds simply because the equations for these two variables are linear. In general, however, the dynamics of (x_A, x_B) are described by nonlinear equations. We tested the property by plotting $x_A(t)/x_B(t)$ in a set of experiments in which a system was pre-adapted to an input value u_0 and the input was subsequently set to a new level

u at $t = 0$. When going from pu_0 to pu, we found that the new value $x_A(t)/x_B(t)$ was almost the same, meaning that x_A and x_B scaled in the same fashion. A representative plot is shown in Fig. 2.5.

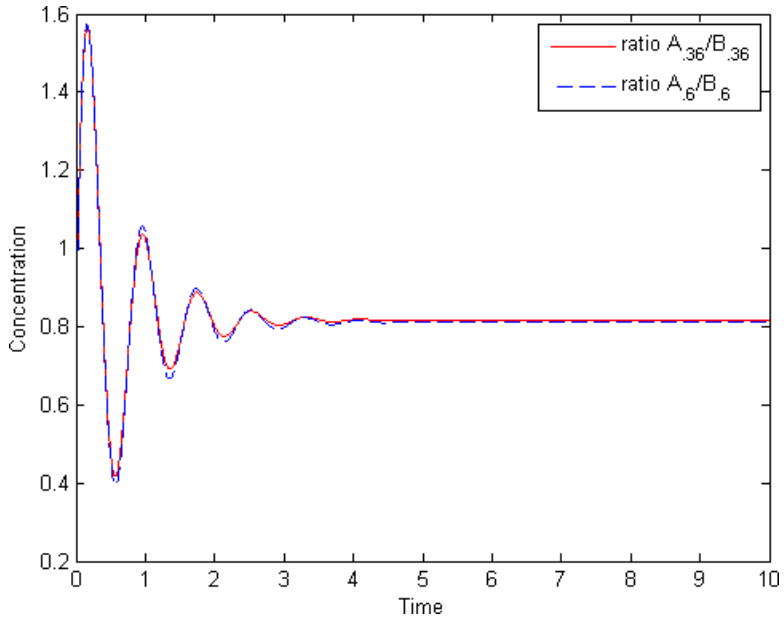

Figure 2.5: Constant A/B ratio in responses to $3 \rightarrow 1.2 * 3$ and $5 \rightarrow 1.2 * 5$. Network is the one described by (2.2). Random parameter set is as in Fig. 2.2. Similar results are available for all ASI circuits.

2.5.3 Emerging motifs

We found that all ASI networks possess a feedforward motif, meaning that there are connections (positively or negatively signed) $A \rightarrow B \rightarrow C$ and as well as $A \rightarrow C$. Such feedforward motifs have been the subject of extensive analysis in the systems biology literature [4] and are often involved in detecting changes in signals [60]. They appear in pathways as varied as *E. coli* carbohydrate uptake via the carbohydrate phosphotransferase system [47], control mechanisms in mammalian cells [58], nitric oxide to NF-κB activation [59, 62], EGF to ERK activation [81, 70], glucose to insulin release [67, 71], ATP to intracellular calcium release [78], and microRNA regulation [107]. The feedforward motifs in all ASI networks are incoherent, meaning such that the direct effect $A \rightarrow C$ has an opposite sign to the net indirect effect through B. An example of an incoherent feedforward connection is provided by the simple system

described by (2.3), where the direct effect of A on C is positive, but the indirect effect is negative: A activates B which in turn deactivates C. Not every incoherent feedforward network provides scale invariance; a classification of those that provide exact scale invariance is known [87]. The study of a scale invariance property of an incoherent feedforward motif, given by its various molecular representations will be done in detail in the next chapter.

It is noteworthy that all ASI circuits have a positive regulation from A to B and a negative regulation from B to A. Thus, they all include a negative feedback loop which is nested inside the incoherent feedforward loop. In addition, as discussed below, all ASI circuits have only a weak (or no) self-loop on the response node C.

2.6 A new property: uniform linearizations with fast output

The (approximate) independence of $x_A(t)/x_B(t)$ on input scalings is not due to linearity of the differential equations for x_A and $x_B(t)$. Instead, the analysis of this question led us to postulate a new property, which we call *uniform linearizations with fast output (ULFO)*. To define this property, we again drop the last equation, and approximate circuits by the planar system that has only the state variables x_A and x_B, where every occurrence of x_C in their differential equations shown in (2.1) is replaced by $h(x_A, x_B)$. We denote by $f(x_A, x_B, u) = (f_1(x_A, x_B, u), f_2(x_A, x_B, u))$ the result of these substitutions, so that the reduced system is described in vector form by $\dot{x} = f(x, u)$, $x = (x_A, x_B)$. We denote by $\sigma(u)$ the unique steady-state corresponding to a constant input u, that is, the solution of the algebraic equation $f(\sigma(u), u) = 0$. We denote by $\mathcal{A}(u) = (\partial f/\partial x)(\sigma(u), u)$ the Jacobian matrix of f with respect to x, and by $\mathcal{B}(u) = (\partial f/\partial u)(\sigma(u), u)$ the Jacobian vector of f with respect to u.

The property ULFO is then defined by requiring the following properties:

1. time-scale separation for x_C;

2. $h(x_A, x_B)$ depends only on the ratio x_A/x_B;

3. for every u , v, and p such that u, v, and pu are in the range $[\underline{u}, \overline{u}]$:

$$\sigma(pu) = p\sigma(u), \;\; \mathcal{A}(u) = \mathcal{A}(v), \;\; \mathcal{B}(u) = \mathcal{B}(v) \tag{2.4}$$

Notice that we are not imposing the far stronger property that the Jacobian matrices should be constant. We are only requiring the same matrix at every steady state.

The first condition in (2.4) means that the vector $\sigma(u)/u$ should be constant. We verified that this requirement holds with very high accuracy in every one of the ASI circuits. With $\underline{u} = 0.3$ and $\overline{u} = 0.6$, we have the following $\sigma(u)/u$ values, rounded to 3 decimal digits: $(0.195, 0.239)$, $(0.193, 0.237)$, $(0.192, 0.236)$, $(0.191, 0.235)$ when $u = 0.3$, 0.4, 0.5, and 0.6 respectively, for the network described by (2.2) and the random parameter set in Fig. 2.2. Similar results are realized for all ASI circuits.

The Jacobian requirements in (2.4) are also verified with high accuracy for all the ASI circuits. We illustrate this with the same network and parameter set. Let us we compute the linearizations $\mathcal{A}_{0.3} = \mathcal{A}(0.3)$, $\mathcal{A}_{0.4} = \mathcal{A}(0.4)$, $\ldots$, $\mathcal{B}_{0.6} = \mathcal{B}(0.6)$ and the average relative differences

$$\mathcal{A}^{\text{err}}_{ij} = \sum_{u=0.3,0.4,0.5,0.6} \left| \frac{(\mathcal{A}_u)_{ij} - (\mathcal{A}_{0.45})_{ij}}{(\mathcal{A}_{0.45})_{ij}} \right|$$

and we define similarly $\mathcal{B}^{\text{err}}$. These relative differences are very small (shown to 3 decimal digits):

$$\mathcal{A}^{\text{err}} = \begin{pmatrix} 0.069 & 0.004 \\ 0 & 0.005 \end{pmatrix}, \quad \mathcal{B}^{\text{err}} = \begin{pmatrix} 0.002 \\ 0 \end{pmatrix},$$

thus justifying the claim that the Jacobians are practically constant. Similar results are available for all ASI circuits.

Tables

The following three tables for the 25 identified ASI circuits are shown:

- Table 1. Relative differences in linearization matrices corresponding to different linearizations, $\mathcal{A}_{0.3} = \mathcal{A}(0.3)$, $\mathcal{A}_{0.4} = \mathcal{A}(0.4)$, $\ldots$, $\mathcal{B}_{0.6} = \mathcal{B}(0.6)$, rounded to 3 decimal places. The corresponding expressions are given by:

$$\mathcal{A}_{ij}^{\text{err}} = \sum_{u=0.3,0.4,0.5,0.6} \left| \frac{(\mathcal{A}_u)_{ij} - (\mathcal{A}_{0.45})_{ij}}{(\mathcal{A}_{0.45})_{ij}} \right|$$

  and similarly for $\mathcal{B}^{\text{err}}$. These relative differences are very small. The entries in the table are of the following form: $\mathcal{A}^{\text{err}}$ displayed as $[a_{11}\ a_{12}; a_{21}\ a_{22}]$ and $\mathcal{B}^{\text{err}}$ displayed as $[b_1\ b_2]^T$.

- Table 2. Relative error between original (nonlinear) system with an initial state $\xi = (x_A, x_B)$ corresponding to $u = 0.3$, and applied input $u = 0.36$, and the approximation is $\xi + z(t)$, where z solves the linear system with an initial condition of zero and a constant input of 0.06. Additionally, we provide relative errors between the original (nonlinear) system with an initial state corresponding to $u = 0.5$, and applied input of $u = 0.6$, and the approximation given by $\xi + z(t)$, where z solves the linear system with an initial condition of zero and a constant input of 0.1. The corresponding expressions are given by:

  $x_{A_{max,u=0.36}^{err}} = \max_{t\geq 0} \left| \frac{x_{A_{0.36}^{\text{L}}}(t) - x_{A_{0.36}^{\text{N}}}(t)}{x_{A_{0.36}^{\text{N}}}(t)} \right|,$
  $x_{A_{max,u=0.6}^{err}} = \max_{t\geq 0} \left| \frac{x_{A_{0.6}^{\text{L}}}(t) - x_{A_{0.6}^{\text{N}}}(t)}{x_{A_{0.6}^{\text{N}}}(t)} \right|,$
  where N denotes a nonlinear system, and L denotes a linear system.
  We define similarly for $x_{B_{max,u=0.36}^{err}}$ and $x_{B_{max,u=0.6}^{err}}$.

- Table 3. Homogeneity property of the states x_A and x_B. For a constant input u, it holds that $\sigma(pu) \approx p\sigma(u)$, where $\sigma(u)$ is a unique steady state (x_A, x_B).

Circuit	$\mathcal{A}^{\mathbf{err}}$	$\mathcal{B}^{\mathbf{err}}$
1	$[0.069\ 0.004; 0\ 0.005]$	$[0.002\ 0]^T$
2	$[0.084\ 0.006; 0.019\ 0.015]$	$[0.004\ 0]^T$
3	$[0.069\ 0.004; 0\ 0.005]$	$[0.002\ 0]^T$
4	$[0.114\ 0.007; 0.011\ 0.003]$	$[0.002\ 0]^T$
5	$[0.045\ 0.003; 0.01\ 0.033]$	$[0\ 0]^T$
6	$[0.075\ 0.012; 0.021\ 0.012]$	$[0.015\ 0]^T$
7	$[0.057\ 0.012; 0.021\ 0.012]$	$[0.012\ 0]^T$
8	$[0.055\ 0.012; 0.019\ 0.009]$	$[0.016\ 0]^T$
9	$[0.069\ 0.004; 0\ 0.005]$	$[0.002\ 0]^T$
10	$[0.037\ 0.022; 0.009\ 0.0707]$	$[0.002\ 0]^T$
11	$[0.037\ 0.022; 0.007\ 0.009]$	$[0.002\ 0]^T$
12	$[0.025\ 0.029; 0.007\ 0.006]$	$[0.012\ 0]^T$
13	$[0.037\ 0.022; 0.009\ 0.007]$	$[0.002\ 0]^T$
14	$[0.036\ 0.022; 0.007\ 0.009]$	$[0.002\ 0]^T$
15	$[0.07\ 0.004; 0\ 0.005]$	$[0.002\ 0]^T$
16	$[0.07\ 0.004; 0\ 0.005]$	$[0.002\ 0]^T$
17	$[0.073\ 0.012; 0.017\ 0.009]$	$[0.015\ 0]^T$
18	$[0.051\ 0.004; 0\ 0.005]$	$[0.002\ 0]^T$
19	$[0.066\ 0.013; 0.018\ 0.009]$	$[0.015\ 0]^T$
20	$[0.048\ 0.013; 0.018\ 0.009]$	$[0.016\ 0]^T$
21	$[0.051\ 0.004; 0\ 0.005]$	$[0.002\ 0]^T$
22	$[0.233\ 0; 0.011\ 0.003]$	$[0.002\ 0]^T$
23	$[0.069\ 0.004; 0\ 0.005]$	$[0.002\ 0]^T$
24	$[0.051\ 0.004; 0\ 0.005]$	$[0.002\ 0]^T$
25	$[0.233\ 0; 0.011\ 0.003]$	$[0.002\ 0]^T$

Table 2.1: Relative error in linearization matrices

Circuit	$x_{A_{max,u=0.36}}^{err}$	$x_{B_{max,u=0.36}}^{err}$	$x_{A_{max,u=0.6}}^{err}$	$x_{B_{max,u=0.6}}^{err}$
1	0.055	0.011	0.028	0.005
2	0.008	0.007	0	0.002
3	0.055	0.010	0.028	0.005
4	0.03	0.007	0.012	0.004
5	0.031	0.006	0.003	0
6	0.015	0.016	0.011	0.005
7	0.023	0.021	0.005	0.004
8	0.023	0.021	0.004	0.004
9	0.055	0.01	0.028	0.005
10	0.097	0.020	0.081	0.016
11	0.010	0.020	0.084	0.016
12	0.033	0.021	0.024	0.010
13	0.097	0.020	0.081	0.016
14	0.010	0.02	0.084	0.016
15	0.056	0.010	0.028	0.005
16	0.056	0.010	0.028	0.005
17	0.027	0.022	0.004	0.004
18	0.047	0.010	0.028	0.006
19	0.027	0.023	0.005	0.004
20	0.023	0.021	0.005	0.004
21	0.04	0.009	0.034	0.004
22	0.116	0.027	0.05	0.013
23	0.055	0.010	0.028	0.005
24	0.045	0.01	0.027	0.005
25	0.117	0.03	0.05	0.013

Table 2.2: Relative error between nonlinear and linearized system

Circuit	$\sigma(u_{0.3})/0.3$	$\sigma(u_{0.4})/0.4$	$\sigma(u_{0.5})/0.5$	$\sigma(u_{0.6})/0.6$
1	$(0.195, 0.239)$	$(0.193, 0.237)$	$(0.192, 0.236)$	$(0.19, 0.234)$
2	$(0.199, 0.364)$	$(0.197, 0.359)$	$(0.194, 0.356)$	$(0.192, 0.353)$
3	$(0.195, 0.239)$	$(0.193, 0.237)$	$(0.192, 0.236)$	$(0.191, 0.234)$
4	$(0.132, 0.172)$	$(0.131, 0.170)$	$(0.131, 0.169)$	$(0.13, 0.168)$
5	$(0.591, 0.11)$	$(0.58, 0.109)$	$(0.57, 0.109)$	$(0.561, 0.108)$
6	$(0.206, 0.526)$	$(0.198, 0.507)$	$(0.192, 0.493)$	$(0.188, 0.481)$
7	$(0.208, 0.529)$	$(0.2, 0.512)$	$(0.194, 0.498)$	$(0.19, 0.486)$
8	$(0.206, 0.530)$	$(0.199, 0.512)$	$(0.193, 0.499)$	$(0.189, 0.486)$
9	$(0.195, 0.239)$	$(0.194, 0.237)$	$(0.192, 0.236)$	$(0.190, 0.234)$
10	$(0.078, 0.083)$	$(0.075, 0.08)$	$(0.073, 0.078)$	$(0.071, 0.076)$
11	$(0.077, 0.083)$	$(0.074, 0.08)$	$(0.072, 0.078)$	$(0.071, 0.076)$
12	$(0.153, 0.09)$	$(0.145, 0.086)$	$(0.139, 0.082)$	$(0.135, 0.08)$
13	$(0.078, 0.083)$	$(0.075, 0.08)$	$(0.073, 0.078)$	$(0.071, 0.076)$
14	$(0.077, 0.083)$	$(0.074, 0.08)$	$(0.072, 0.078)$	$(0.071, 0.076)$
15	$(0.195, 0.239)$	$(0.193, 0.237)$	$(0.191, 0.235)$	$(0.190, 0.234)$
16	$(0.195, 0.239)$	$(0.193, 0.237)$	$(0.191, 0.236)$	$(0.19, 0.234)$
17	$(0.204, 0.526)$	$(0.197, 0.508)$	$(0.191, 0.494)$	$(0.186, 0.48)$
18	$(0.196, 0.24)$	$(0.193, 0.238)$	$(0.192, 0.236)$	$(0.19, 0.235)$
19	$(0.205, 0.528)$	$(0.197, 0.509)$	$(0.192, 0.494)$	$(0.187, 0.481)$
20	$(0.206, 0.532)$	$(0.199, 0.513)$	$(0.193, 0.5)$	$(0.189, 0.487)$
21	$(0.196, 0.24)$	$(0.194, 0.237)$	$(0.192, 0.236)$	$(0.191, 0.235)$
22	$(0.136, 0.177)$	$(0.134, 0.173)$	$(0.133, 0.171)$	$(0.132, 0.17)$
23	$(0.195, 0.239)$	$(0.193, 0.237)$	$(0.192, 0.236)$	$(0.191, 0.234)$
24	$(0.196, 0.240)$	$(0.194, 0.237)$	$(0.192, 0.236)$	$(0.190, 0.235)$
25	$(0.136, 0.178)$	$(0.134, 0.173)$	$(0.133, 0.171)$	$(0.132, 0.17)$

Table 2.3: $\sigma(u)/u$ for constant inputs $u = 0.3, 0.4, 0.5, 0.6$

The key theoretical fact is that the property ULFO implies approximate scale invariance, which will be proved in Section 2.6.1. The term "uniform" refers to the fact that the linearizations at every steady state are the same, and proved in Section 2.6.2. If the linearizations are not all the same, it is easy to see that scale invariance does not hold. The uniformity of linearizations provides a "global" way to tie together behaviors at different scales. The conditions give us the approximate homogeneity property $f(px, pu) \approx pf(x, u)$ when near steady states, because, for $u \approx u^*$ and $x \approx \sigma(u^*)$:

$$\begin{aligned} f(px, pu) &\approx \mathcal{A}(pu^*)(px - \sigma(pu^*)) + \mathcal{B}(pu^*)(pu - pu^*) \\ &= \mathcal{A}(u^*)(px - p\sigma(u^*)) + \mathcal{B}(u^*)(pu - pu^*) \quad \approx pf(x, u)\,. \end{aligned}$$

These conditions are satisfied in various combinations of parameter regimes. As a purely theoretical example, consider the following system (denoting $x = x_A$, $y = x_B$, $z = x_C$):

$$\begin{aligned} \dot{x} &= -\frac{x}{1+x/K}z + u \\ \dot{y} &= x - y \\ \varepsilon\dot{z} &= x - zy, \end{aligned}$$

which can be viewed as a limiting case of the system described by (2.2) when

$$k_{UA} = 1, k_{AB} = 1, k_{CC}, K_{UA}, k_{BA}, K_{AB}, K_{AC} \approx 0, k_{BC} = K_{BC}, K_{BC} \gg 1,$$

$$k_{AC} = 1, k_{F_BB}x_{F_B} = K_{F_BB}, K_{F_BB} \gg 1, K_{BA} \approx 0, k_{CA}/K_{CA} = 1.$$

Substituting $z = x/y$ in the first equation, we have:

$$\dot{x} = f_1(x, y, u) = -\frac{x^2}{y + xy/K} + u$$

The linearization of the system evaluated at a steady state corresponding to a constant input u has

$$\mathcal{A}(u) = \begin{pmatrix} -2 + 3u/K - u^2/K^2 & 0 \\ 1 & -1 \end{pmatrix}$$

(and $\mathcal{B}(u)$ constant), and is therefore approximately constant provided that K is large or that the input u is small in relative magnitude. Similarly, if we use $\sigma(pu)$ as initial state and pu as inputs, we get a similar expression (with $o(pu)$ instead of $o(u)$ and the p's in the fraction canceling out).

2.6.1 ULFO implies approximate scale invariance, for any number of nodes

Consider a system of n differential equations with input signal u,

$$\dot{x} = f(x, u)$$

with the variables x evolving on some closed bounded set and f differentiable, and suppose that for each constant input $\bar{u^*}$ there is a unique steady state $\bar{x^*} = \sigma(\bar{u^*})$ with the conditions in (2.4) and an output

$$y(t) = h(x(t))$$

such that h is differentiable and homogeneous of degree zero ($h(px) = h(x)$ for nonzero p). We view 3-node enzymatic networks as obtained from a set of $n+1$ equations

$$\begin{aligned} \dot{x} &= F(x,z,u) \\ \varepsilon \dot{z} &= G(x,z) \end{aligned}$$

with $n = 2$, $x = (x_A, x_B)$, and $z = x_C$ ($0 < \varepsilon \ll 1$ represents the faster time scale for x_C), and we are studying the reduced system $\dot{x} = f(x,u) = F(x, \alpha(x), u)$ obtained by solving $G(x,z) = 0$ for $z = \alpha(x)$ and substituting in F. Consider a time interval $[0,T]$, a constant input $\bar{u^*}$, and a possibly time-varying input $u(t)$, $t \geq 0$, as well as a scaling $p > 0$, such that all values $\bar{u^*}$, $p\bar{u^*}$, $u(t)$, $pu(t)$ are in the input range $[\underline{u}, \overline{u}]$. The solutions of $\dot{x} = f(x,u)$ with initial condition $x(0) = \sigma(\bar{u^*})$ and of $\dot{z} = f(z,pu)$ with initial condition $z(0) = \sigma(p\bar{u^*})$ are denoted respectively by $x(t)$ and $z(t)$, and the respective outputs are $y(t) = h(x(t))$ and $y_p(t) = h(z(t))$. We wish to show that these two responses are approximately equal on $0 \leq t \leq T$.

More precisely, we will prove that the relative error

$$\frac{\sup_t |y_p(t) - y(t)|}{\sup_t |u(t) - \bar{u^*}|} \to 0$$

as a function of the input perturbation $u(t) - \bar{u^*}$.

Proof. Write $\delta(t) = u(t) - \bar{u^*}$. From Theorem 1 in [95] we know that

$$x(t) = x(0) + \xi(t) + o(\|\delta\|)$$

where $\|\delta\| = \sup_{0\leq t\leq T} |\delta(t)|$ and ξ is the solution of the variational system

$$\dot{\xi}(t) = \mathcal{A}\xi(t) + \mathcal{B}\delta(t)$$

with $\xi(0) = 0$, and that

$$z(t) = z(0) + \zeta(t) + o(\|pu - p\bar{u^*}\|) = z(0) + \zeta(t) + o(\|\delta\|),$$

where

$$\dot{\zeta} = \mathcal{A}\zeta(t) + \mathcal{B}p\delta(t)$$

with $\zeta(0) = 0$. Recall that $\mathcal{A}(u) = (\partial f/\partial x)(\sigma(u), u)$ is the Jacobian matrix of f with respect to x, and $\mathcal{B}(u) = (\partial f/\partial u)(\sigma(u), u)$ is the Jacobian vector of f with respect to u, and the assumptions are that these matrices are in fact independent of u. By linearity, $\zeta = p\xi$. Using $z(0) \equiv \sigma(p\bar{u^*}) = p\sigma(\bar{u^*}) = px(0)$, we have that $px(t) - z(t) = o(\|\delta\|)$. Thus,

$$y(t) = h(x(t)) = h(px(t)) = h(z(t) + o(\|\delta\|)).$$

If K is an upper bound on the gradient of h, then

$$|y_p(t) - y(t)| = |h(z(t)) - h(z(t) + o(\|\delta\|))| \leq Ko(\|\delta\|).$$

Thus, the relative error $\sup_t |y_p(t) - y(t)| \,/\, \sup_t |u(t) - \bar{u^*}|$ converges to zero as a function of the input perturbation $u(t) - \bar{u^*}$, as claimed. □

As a numerical illustration, we consider again the the network described by (2.2) and the random parameter set in Fig. 2.2. We compare the relative error between the original nonlinear system, with initial state $\xi = (x_A, x_B)$ corresponding to $u = 0.3$, and applied input $u = 0.36$, and the approximation is $\xi + z(t)$, where the z solves the linear system with initial condition zero and constant input 0.06. The maximum approximation error is about 5% (to 3 decimal places, 0.055 for x_A and 0.01 for x_B). When stepping from $u = 0.5$ to $u = 0.6$, the error is less than 3% (0.028 and 0.005

respectively). Similar results are available for all ASI circuits.

2.6.2 Equilinearization in scale invariant systems

We consider systems of the form:

$$\dot{x} = f(x, u)\,, \quad y = h(x)$$

(more generally, one may consider $y = h(x, u)$). The input values $u(t)$, states $x(t)$, and output values $y(t)$ have dimensions m, n, p respectively.

We suppose that for each $\bar{u}$ constant, there is a unique steady state $\bar{x} = \sigma(\bar{u})$:

$$f(\sigma(\bar{u}), \bar{u}) = 0\,.$$

Let $F_t^{\bar{x}}(u)$ be the output at time $t \geq 0$ if the initial state is $\bar{x}$ and the input is u.

We say that the system is *homogeneous* if

$$F_t^{\sigma(p\bar{u})}(pu) \;=\; p\, F_t^{\sigma(\bar{u})}(u)$$

for each $p > 0$ and $t > 0$, each constant $\bar{u}$, and each input function u.

This is the property satisfied by our enzymatic systems when a singular perturbation analysis has already been performed and we are reduced to a two-dimensional system describing the dynamics of A and B, with C substituted by its quasi-steady state values. Observe that in that example, x has dimension 2 and the output is $y = x$, i.e. C is an identity matrix.

We prove next that, for such systems, the linearizations at all steady-state conditions are the same. This is consistent with the results of our numerical exploration.

Consider the linearizations at each steady-state $\bar{x} = \sigma(\bar{u})$ and respective input $\bar{u}$:

$$A_{\bar{u}} = \frac{\partial f}{\partial x}(\bar{x}, \bar{u})\,, \quad B_{\bar{u}} = \frac{\partial f}{\partial u}(\bar{x}, \bar{u})\,, \quad C_{\bar{u}} = \frac{\partial h}{\partial x}(\bar{x})$$

and the respective Hankel parameters

$$H_{\bar{u}}(k) = C_{\bar{u}} A_{\bar{u}}^{k-1} B_{\bar{u}}\,, \quad k = 1, 2, \ldots\,.$$

Lemma 1. *For homogeneous systems, $H_u^{(k)}$ is independent of u and for each k (same input/output behavior of all linearizations).*

Proof. Consider any $\bar{u}$ and let $\bar{x} = \sigma(\bar{u})$. Let v be any input function. Fix any $t \geq 0$. Expanding around $\bar{u}$, and for h small:

$$F_t^{\bar{x}}(\bar{u} + hv) = F_t^{\bar{x}}(\bar{u}) + hJ_t^{\bar{x}}(\bar{u})v + o(h) \tag{2.5}$$

where $J_t^{\bar{x}}(\bar{u})$ is the Jacobian of $F_t^{\bar{x}}$, seen as mapping inputs on the interval $[0, t]$ to the last output $y(t)$, and evaluated at $\bar{u}$. This Jacobian maps inputs $v(\cdot)$ into states.
Pick any $p > 0$ and let $\bar{z} = \sigma(p\bar{u})$. Then, by the same argument,

$$F_t^{\bar{z}}(p\bar{u} + phv) = F_t^{\bar{z}}(p\bar{u}) + hJ_t^{\bar{z}}(p\bar{u})pv + o(h)\,. \tag{2.6}$$

We also know, by the homogeneity property, that

$$F_t^{\bar{z}}(p(\bar{u} + hv)) = pF_t^{\bar{x}}(\bar{u} + hv) \quad \text{and} \quad F_t^{\bar{z}}(p\bar{u}) = pF_t^{\bar{x}}(\bar{u})\,. \tag{2.7}$$

Combining (2.5)-(2.7), dividing by h, and taking the limit as $h \to 0$, we conclude that:

$$J_t^{\bar{x}}(\bar{u})v = J_t^{\bar{z}}(p\bar{u})v\,. \tag{2.8}$$

Now, Theorem 1 in [95] says that $J_t^{\bar{x}}(\bar{u})v$ is the solution $y(t)$ at time t of

$$\begin{aligned} \dot{x} &= A_{\bar{u}}x + B_{\bar{u}}v\,, \quad x(0) = 0 \\ y &= C_{\bar{u}}x \end{aligned}$$

and $J_t^{\bar{z}}(p\bar{u})v$ is the solution $y(t)$ at time t of

$$\begin{aligned} \dot{x} &= A_{p\bar{u}}x + B_{p\bar{u}}v\,, \quad x(0) = 0 \\ y &= C_{p\bar{u}}x\,. \end{aligned}$$

Since (2.8) holds for any v, we conclude, by elementary linear systems theory [95], that

$$C_{\bar{u}}A_{\bar{u}}^{k-1}B_{\bar{u}} = C_{p\bar{u}}A_{p\bar{u}}^{k-1}B_{p\bar{u}}\,, \tag{2.9}$$

as we wanted to prove. □

Corollary 1. *Suppose that, for all $\bar{u}$. The triplet $(A_{\bar{u}}, B_{\bar{u}}, C_{\bar{u}})$ is reachable and observable, $m = 1$, $n = p$, and $C_{\bar{u}} = I$. Then $(A_{\bar{u}}, B_{\bar{u}}, C_{\bar{u}}) = (A_{\bar{v}}, B_{\bar{v}}, C_{\bar{v}})$ for all $\bar{u} > 0$ and $\bar{v} > 0$.*

Proof. Pick any two positive $\bar{u}$ and $\bar{v}$. Since we can use $p = \bar{v}/\bar{u}$ in (2.9), we know that $C_{\bar{u}}A_{\bar{u}}^{k-1}B_{\bar{u}} = C_{\bar{v}}A_{\bar{v}}^{k-1}B_{\bar{v}}$ for all k, and hence by elementary linear systems theory [95] we know that there is an invertible matrix T such that

$$T^{-1}A_{\bar{u}}T = A_{\bar{v}}\,, T^{-1}B_{\bar{u}} = B_{\bar{v}}\,, C_{\bar{u}}T = C_{\bar{v}}\,.$$

Using that $C_{\bar{u}} = C_{\bar{v}} = I$, we have that $T = I$. □

2.6.3 Extensions of three-node enzymatic networks

The conditions that we obtained for three-node networks are also sufficient for an arbitrary number of nodes [93], in the following sense. Suppose that we consider a set of $n + 1$ nodes, where n nodes are described by variables $x = (x_1, \ldots, x_n)$ and an additional node is described by a variable z. Suppose that the z variable evolves at a faster time scale than the x variables. Then, the ULFO property implies approximate scale invariance. A variation of this situation is that in which a three-node network already displays scale invariance through an output node x_C, and this output feeds into an additional node x_D which evolves in a linear mode; then the entire four-node

network will display scale invariance as well. Yet another variation is that in which an input is processed linearly before being fed into a three-node network. The example of a published chemotaxis pathway in *Dictyostelium discoideum* that we provide in the next Section combines these variations.

A full numerical study as performed for three-node networks is already infeasible for four-node networks, due to the combinatorial explosion in the number of possible networks and of parameters to be randomly tested. A theoretical proof is also very difficult to envision, because (a) exact scale invariance is impossible for enzymatic networks, as shown in this paper, and (b) approximate adaptation and scale invariance are mathematically very hard to formalize in such a manner that impossibility can be rigorously proved for systems that do not satisfy our characterizations. In any event, as has been argued in other recent papers dealing with biological adaptation by enzymatic networks [57, 84, 116], a restriction to three-node networks is biologically reasonable, both as a coarse-graining of the problem and because many eukaryotic biological pathways, such as MAPK pathways, have at their core a three-component architecture.

2.7 A concrete biological model

In a recent paper [102] Takeda and collaborators studied the adaptation kinetics of a eukaryotic chemotaxis signaling pathway, employing a microfluidic device to expose *Dictyostelium discoideum* to changes in chemoeffector cyclic adenosine monophosphate (cAMP). Specifically, they focused on the dynamics of activated Ras (Ras-GTP), which was in turn reported by RBD-GFP, and showed almost perfect adaptation of previously unstimulated cells to cAMP concentrations ranging from 10^{-2}nM to 1μM. Furthermore, inspired by [57], the authors proposed alternative models for adaptation, and concluded that the best fit was obtained by using an incoherent feedforward structure. The model

that they identified is given by:

$$\begin{aligned}
\frac{dR_1}{dt} &= k_{R_1}(v+r_1)(R_1^{\text{tot}} - R_1) - k_{-R_1}R_1 \\
\frac{dR_2}{dt} &= k_{R_2}(v+r_2)(R_2^{\text{tot}} - R_2) - k_{-R_2}R_2 \\
u &= R_1 + R_2 \\
\frac{dGEF}{dt} &= k_{GEF}\,u - k_{-GEF}GEF \\
\frac{dGAP}{dt} &= k_{GAP}\,u - k_{-GAP}GAP \\
\frac{dRas^{GTP}}{dt} &= k_{RAS}\,GEF\,(RAS^{\text{tot}} - Ras^{GTP}) - k_{-RAS}\,GAP\,Ras^{GTP} \\
\frac{dRBD^{\text{cyt}}}{dt} &= k_{RBD}^{\text{off}}\,(RBD^{\text{tot}} - RBD^{\text{cyt}}) - k_{RBD}^{\text{on}}\,Ras^{GTP}\,RBD^{\text{cyt}}\,.
\end{aligned}$$

The symbol v stands for the chemoeffector cAMP, and the authors assumed the existence of two different receptor populations (R_1 and R_2, with very different K_d's) which when bound pool their signals to downstream components (through u). The constants r_1 and r_2 represent levels of constitutive activation. The variables GEF and GAP represent activation and deactivation of RasGEF and RasGAP, Ras^{GTP} represents the activated Ras, and RBD^{cyt} describes the cytosolic reporter molecule RBD-GFP.

The best-fit parameters obtained in [102] are as follows: $R_1^{\text{tot}} = 0.1$, $R_2^{\text{tot}} = 0.9$, $r_1 = 0.012\text{nM}$, $r_2 = 0.115\text{nM}$, $k_{R_1} = 0.00267\text{nM}^{-1}\text{sec}^{-1}$, $k_{-R_1} = 0.16\text{sec}^{-1}$, $k_{R_2} = 0.00244\text{nM}^{-1}\text{sec}^{-1}$, $k_{-R_2} = 1.1\text{sec}^{-1}$, $k_{GEF} = 0.04\text{sec}^{-1}$, $k_{-GEF} = 0.4\text{sec}^{-1}$, $k_{GAP} = 0.01\text{sec}^{-1}$, $k_{-GAP} = 0.1\text{sec}^{-1}$, $RAS^{\text{tot}} = 1$, $k_{RAS} = 390\text{sec}^{-1}$, $k_{-RAS} = 3126\text{sec}^{-1}$, $RBD^{\text{tot}} = 1$, $k_{RBD}^{\text{off}} = 0.53\text{sec}^{-1}$, $k_{RBD}^{\text{on}} = 1.0\text{sec}^{-1}$. With these parameters, and cAMP concentrations which are small yet also satisfy $r_1 \ll v(t)$ and $r_2 \ll v(t)$, it follows that $\dot{R}_1 \approx k_{R_1}R_1^{\text{tot}}v - k_{-R_1}R_1$ and $\dot{R}_2 \approx k_{R_2}R_2^{\text{tot}}v - k_{-R_2}R_2$, so we may view $u(t)$ as an input (linearly dependent on the external $v(t)$) to the three-variable system described by $x_A = GEF$, $x_B = GAP$, $x_C = Ras^{GTP}$. Since RBD^{cyt} depends only on x_C, we may view x_C as the output. This three-variable system (interpreted as having limiting values of Michaelis-Menten constants) has the ULFO property provided that the dynamics of x_C are fast compared to x_A and x_B, which the identified parameters insure. So, we expect scale invariant behavior. Indeed, Fig. 2.6 shows a simulation

of the entire six-dimensional system (not merely of our 3-dimensional reduction) when using a step from 1 to 2 nM of cAMP, and shows that essentially the same response is obtained when stepping from 2 to 4 nM.

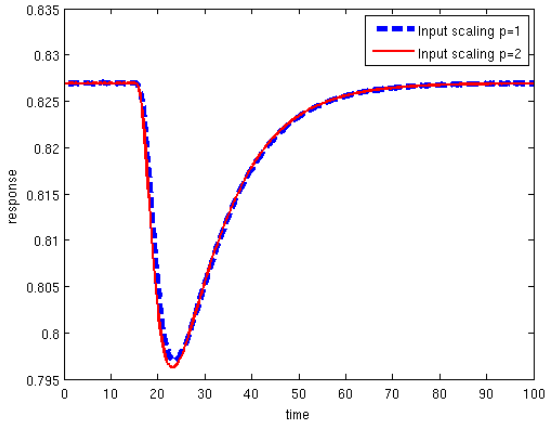

Figure 2.6: Scale invariance computed when using the model in [102]: Responses to steps 1→2 and 2→4 coincide.

This prediction of scale invariant behavior was tested experimentally, and the experimental resuts do not indicate scale invariant behavior. Hence, based on the mathematical model, one can suggest viable experiments to verify a mechanism that a certain organism may possess, and by doing so validate or (in this case) invalidate a mathematical model. Hence, our contribution lies in the model invalidation of [102].

2.8 Parameters for the identified ASI Circuits

Circuit 1.

$K_{AB} = 0.001191$; $k_{AB} = 1.466561$; $K_{AC} = 0.113697$; $k_{AC} = 1.211993$; $K_{BA} = 0.001688$; $k_{BA} = 44.802268$; $K_{BC} = 0.009891$; $k_{BC} = 7.239357$; $K_{uA} = 0.093918$; $k_{uA} = 11.447219$; $k_{AC} = 1.211993$; $K_{AC} = 0.1136927$; $K_{F_B} = 9.424319$; $k_{F_B} = 22.745736$

Circuit 2.

$K_{uA} = 0.093918$; $k_{uA} = 11.447219$; $K_{BA} = 0.001688$; $k_{BA} = 44.802268$; $K_{CA} = 90.209027$; $k_{CA} = 96.671843$; $K_{AB} = 0.001191$; $k_{AB} = 1.466561$; $K_{F_B} = 9.424319$; $k_{F_B} = 22.745736$; $K_{AC} = 0.113697$; $k_{AC} = 1.211993$; $K_{BC} = 0.009891$; $k_{BC} = 7.239357$

Circuit 3.

$K_{AA} = 7.633962$; $k_{AA} = 86.238263$; $K_{AB} = 20.265158$; $k_{AB} = 5.428752$; $K_{AC} = 0.258375; k_{AC} = 62.416585$; $K_{BA} = 0.003960$; $k_{BA} = 17.705166$; $K_{BB} = 31.604578$; $k_{BB} = 3.692326$; $K_{BC} = 44.386408$; $k_{BC} = 65.027941$; $K_{CB} = 0.701052$; $k_{CB} = 26.091557$; $K_{uA} = 0.464248$; $k_{uA} = 1.882348$

Circuit 4.

$K_{AA} = 7.633962$; $k_{AA} = 86.238263$; $K_{AB} = 20.265158$; $k_{AB} = 5.428752$; $K_{AC} = 0.258375$; $k_{AC} = 62.416585$; $K_{BA} = 0.003960$; $k_{BA} = 17.705166$; $K_{BC} = 44.386408$; $k_{BC} = 65.027941$; $K_{CB} = 0.701052$; $k_{CB} = 26.091557$; $K_{uA} = 0.464248$; $k_{uA} = 1.882348$

Circuit 5.

$K_{AB} = 63.277600$; $k_{AB} = 6.638959$; $K_{AC} = 0.133429$; $k_{AC} = 55.731406$; $K_{BA} = 0.011188$; $k_{BA} = 2.749793$; $K_{BC} = 0.013374$; $k_{BC} = 45.175191$; $K_{CB} = 1.457975$; $k_{CB} = 2.114949$; $K_{uA} = 24.589517$; $k_{uA} = 5.346875$

Circuit 6.

$K_{AA} = 7.633962$; $k_{AA} = 86.238263$; $K_{AB} = 20.265158$; $k_{AB} = 5.428752$; $K_{AC} = 0.258375$; $k_{AC} = 62.416585$; $K_{BA} = 0.003960$; $k_{BA} = 17.705166$; $K_{BB} = 31.604578$; $k_{BB} = 3.692326$; $K_{BC} = 44.386408$; $k_{BC} = 65.027941$; $K_{CA} = 26.714681$; $k_{CA} = 2.806080$; $K_{CB} = 0.701052$; $k_{CB} = 26.091557$; $K_{uA} = 0.464248$; $k_{uA} = 1.882348$

Circuit 7.

$K_{AA} = 7.633962$; $k_{AA} = 86.238263$; $K_{AB} = 20.265158$; $k_{AB} = 5.428752$; $K_{AC} = 0.258375$; $k_{AC} = 62.416585$; $K_{BA} = 0.003960$; $k_{BA} = 17.705166$; $K_{BC} = 44.386408$; $k_{BC} = 65.027941$; $K_{CA} = 26.714681$; $k_{CA} = 2.806080$; $K_{CB} = 0.701052$; $k_{CB} = 26.091557$; $K_{uA} = 0.464248$; $k_{uA} = 1.882348$

Circuit 8.

$K_{uA} = 0.093918$; $k_{uA} = 11.447219$; $K_{BA} = 0.001688$; $k_{BA} = 44.802268$; $K_{AB} = 0.001191$; $k_{AB} = 1.466561$; $K_{F_B} = 9.424319$; $k_{F_B} = 22.745736$; $K_{AC} = 0.113697$; $k_{AC} = 1.211993$; $K_{BC} = 0.009891$; $k_{BC} = 7.239357$; $K_{CB} = 30.602013$; $k_{CB} = 3.811536$; $K_{CC} = 0.189125$; $k_{CC} = 17.910182$

Circuit 9.

$K_{uA} = 0.093918$; $k_{uA} = 11.447219$; $K_{BA} = 0.001688$; $k_{BA} = 44.802268$; $K_{CA} = 90.209027$; $k_{CA} = 96.671843$; $K_{AB} = 0.001191$; $k_{AB} = 1.466561$; $K_{F_B} = 9.424319$; $k_{F_B} = 22.745736$; $K_{Ac} = 0.113697$; $k_{AC} = 1.211993$; $K_{BC} = 0.009891$; $k_{BC} = 7.239357$; $K_{CB} = 30.602013$; $k_{CB} = 3.811536$; $K_{CC} = 0.189125$; $k_{CC} = 17.910182$

Circuit 10.

$K_{AA} = 24.989065$; $k_{AA} = 53.174082$; $K_{AB} = 0.444375$; $k_{AB} = 12.053134$; $K_{F_B} = 1.716920$; $k_{F_B} = 11.601122$; $K_{AC} = 0.013988$; $k_{AC} = 8.521185$; $K_{BA} = 0.005461$; $k_{BA} = 7.103952$; $K_{BC} = 51.850148$; $k_{BC} = 80.408137$; $K_{CB} = 5.392001$; $k_{CB} = 3.086740$; $K_{CC} = 1.962230$; $k_{CC} = 17.382010$; $K_{uA} = 4.387832$; $k_{uA} = 19.638124$

Circuit 11.

$K_{AB} = 0.444375$; $k_{AB} = 12.053134$; $K_{F_B} = 1.716920$; $k_{F_B} = 11.601122$; $K_{AC} = 0.013988$; $k_{AC} = 8.521185$; $K_{BA} = 0.005461$; $k_{BA} = 7.103952$; $K_{BC} = 51.850148$; $k_{BC} = 80.408137$; $K_{CB} = 5.392001$; $k_{CB} = 3.086740$; $K_{CC} = 1.962230$; $k_{CC} = 17.382010$; $K_{uA} = 4.387832$; $k_{uA} = 19.638124$

Circuit 12.

$K_{uA} = 0.093918$; $k_{uA} = 11.447219$; $K_{BA} = 0.001688$; $k_{BA} = 44.802268$; $K_{CA} = 5.026318$; $k_{CA} = 45.803641$; $K_{AB} = 0.001191$; $k_{AB} = 1.466561$; $K_{F_B} = 9.424319$; $k_{F_B} = 22.745736$; $K_{AC} = 0.113697$; $k_{AC} = 1.211993$; $K_{BC} = 0.009891$; $k_{BC} = 7.239357$;

$K_{CB} = 30.602013$; $k_{CB} = 3.811536$; $K_{CC} = 0.189125$; $k_{CC} = 17.910182$

Circuit 13.

$K_{AA} = 24.989065$; $k_{AA} = 53.174082$; $K_{AB} = 0.444375$; $k_{AB} = 12.053134$; $K_{F_B} = 1.716920$; $k_{F_B} = 11.601122$; $K_{AC} = 0.013988$; $k_{AC} = 8.521185$; $K_{BA} = 0.005461$; $k_{BA} = 7.103952$; $K_{BC} = 51.850148$; $k_{BC} = 80.408137$; $K_{CB} = 5.392001$; $k_{CB} = 3.086740$; $K_{CC} = 1.962230$; $k_{CC} = 17.382010$; $K_{uA} = 4.387832$; $k_{uA} = 19.638124$; $K_{CA} = 15.479253$; $k_{CA} = 4.903430$

Circuit 14.

$K_{AB} = 0.444375$; $k_{AB} = 12.053134$; $K_{F_B}1.716920$; $k_{F_B} = 11.601122$; $K_{AC} = 0.013988$; $k_{AC} = 8.521185$; $K_{BA} = 0.005461$; $k_{BA} = 7.103952$; $K_{BC} = 51.850148$; $k_{BC} = 80.408137$; $K_{CB} = 5.392001$; $k_{CB} = 3.086740$; $K_{CC} = 1.962230$; $k_{CC} = 17.382010$; $K_{uA} = 4.387832$; $k_{uA} = 19.638124$; $K_{CA} = 15.479253$; $k_{CA} = 4.903430$

Circuit 15.

$K_{AB} = 0.709169$; $k_{AB} = 7.445605$; $K_{F_B} = 1.495375$; $k_{F_B} = 7.282827$; $K_{AC} = 0.002566$; $k_{AC} = 1.115065$; $K_{BA} = 0.002522$; $k_{BA} = 5.753075$; $K_{BC} = 0.017051$; $k_{BC} = 2.777794$; $K_{CC} = 0.195997$; $k_{CC} = 1.480130$; $K_{uA} = 0.225814$; $k_{uA} = 2.492872$

Circuit 16.

$K_{AB} = 0.001191$; $k_{AB} = 1.466561$; $K_{F_B} = 9.424319$; $k_{F_B} = 22.745736$; $K_{AC} = 0.113697$; $k_{AC} = 1.211993$; $K_{BA} = 0.001688$; $k_{BA} = 44.802268$; $K_{BC} = 0.009891$; $k_{BC} = 7.239357$; $K_{CC} = 0.189125$; $k_{CC} = 17.910182$; $K_{uA} = 0.093918$; $k_{uA} = 11.447219$

Circuit 17.

$K_{AB} = 1.620877$; $k_{AB} = 2.306216$; $K_{F_B} = 2.012565$; $k_{F_B} = 2.700847$; $K_{AC} = 0.010933$; $k_{AC} = 8.968091$; $K_{BA} = 0.001812$; $k_{BA} = 10.039221$; $K_{BC} = 0.014199$; $k_{BC} = 17.762333$; $K_{CC} = 2.686891$; $k_{CC} = 4.139044$; $K_{uA} = 0.161715$; $k_{uA} = 1.933303$

Circuit 18.

$K_{AA} = 17.569120$; $k_{AA} = 2.198366$; $K_{AB} = 9.435176$; $k_{AB} = 3.134007$; $K_{F_B} = 0.469083$; $k_{F_B} = 1.934194$; $K_{AC} = 0.062914$; $k_{AC} = 2.742206$; $K_{BA} = 0.003245$; $k_{BA} = 75.352905$; $K_{BB} = 27.463128$; $k_{BB} = 10.551155$; $K_{BC} = 0.041615$; $k_{BC} = 61.333818$; $K_{CC} = 0.039332$; $k_{CC} = 4.756637$; $K_{uA} = 0.005167$; $k_{uA} = 8.186533$

Circuit 19.

$K_{uA} = 4.387832$; $k_{uA} = 19.638124$; $K_{BA} = 0.005461$; $k_{BA} = 7.103952$; $K_{AA} = 24.989065$; $k_{AA} = 53.174082$; $K_{AB} = 0.444375$; $k_{AB} = 12.053134$; $K_{F_B} = 1.716920$; $k_{F_B} = 11.601122$; $K_{BC} = 51.850148$; $k_{BC} = 80.408137$; $K_{AC} = 0.013988$; $k_{AC} = 8.521185$; $K_{CC} = 1.962230$; $k_{CC} = 17.382010$

Circuit 20.

$K_{uA} = 4.387832$; $k_{uA} = 19.638124$; $K_{BA} = 0.005461$; $k_{BA} = 7.103952$; $K_{AB} = 0.444375$; $k_{AB} = 12.053134$; $K_{F_B} = 1.716920$; $k_{F_B} = 11.601122$; $K_{BC} = 51.850148$; $k_{BC} = 80.408137$; $K_{AC} = 0.013988$; $k_{AC} = 8.521185$; $K_{CC} = 1.962230$; $k_{CC} = 17.382010$

Circuit 21.

$K_{uA} = 0.093918$; $k_{uA} = 11.447219$; $K_{BA} = 0.001688$; $k_{BA} = 44.802268$; $K_{CA} = 5.026318$; $k_{CA} = 45.803641$; $K_{AB} = 0.001191$; $k_{AB} = 1.466561$; $K_{F_B} = 9.424319$; $k_{F_B} = 22.745736$; $K_{AC} = 0.113697$; $k_{AC} = 1.211993$; $K_{BC} = 0.009891$; $k_{BC} = 7.239357$; $K_{CC} = 0.189125$; $k_{CC} = 17.910182$

Circuit 22.

$K_{AB} = 1.620877$; $k_{AB} = 2.306216$; $K_{F_B} = 2.012565$; $k_{F_B} = 2.700847$; $K_{AC} = 0.010933$; $k_{AC} = 8.968091$; $K_{BA} = 0.001812$; $k_{BA} = 10.039221$; $K_{BC} = 0.014199$; $k_{BC} = 17.762333$; $K_{CA} = 0.002690$; $k_{CA} = 1.506954$; $K_{CC} = 2.686891$; $k_{CC} = 4.139044$; $K_{uA} = 0.161715$; $k_{uA} = 1.933303$

Circuit 23.

$K_{uA} = 0.093918$; $k_{uA} = 11.447219$; $K_{BA} = 0.001688$; $k_{BA} = 44.802268$; $K_{CA} = 90.209027$; $k_{CA} = 96.671843$; $K_{AB} = 0.001191$; $k_{AB} = 1.466561$; $K_{F_B} = 9.424319$; $k_{F_B} = 22.745736$; $K_{AC} = 0.113697$; $k_{AC} = 1.211993$; $K_{BC} = 0.009891$; $k_{BC} = 7.239357$; $K_{CC} = 0.189125$; $k_{CC} = 17.910182$

Circuit 24.

$K_{uA} = 0.093918$; $k_{uA} = 11.447219$; $K_{BA} = 0.001688$; $k_{BA} = 44.802268$; $K_{CA} = 5.026318$; $k_{CA} = 45.803641$; $K_{AB} = 0.001191$; $k_{AB} = 1.466561$; $K_{F_B} = 9.424319$; $k_{F_B} = 22.745736$; $K_{AC} = 0.113697$; $k_{AC} = 1.211993$; $K_{BC} = 0.009891$; $k_{BC} = 7.239357$

Circuit 25.

$K_{AB} = 1.620877$; $k_{AB} = 2.306216$; $K_{F_B} = 2.012565$; $k_{F_B} = 2.700847$; $K_{AC} = 0.010933$; $k_{AC} = 8.968091$; $K_{BA} = 0.001812$; $k_{BA} = 10.039221$; $K_{BC} = 0.014199$; $k_{BC} = 17.762333$; $K_{CA} = 0.002690$; $k_{CA} = 1.506954$; $K_{uA} = 0.161715$; $k_{uA} = 1.93330$

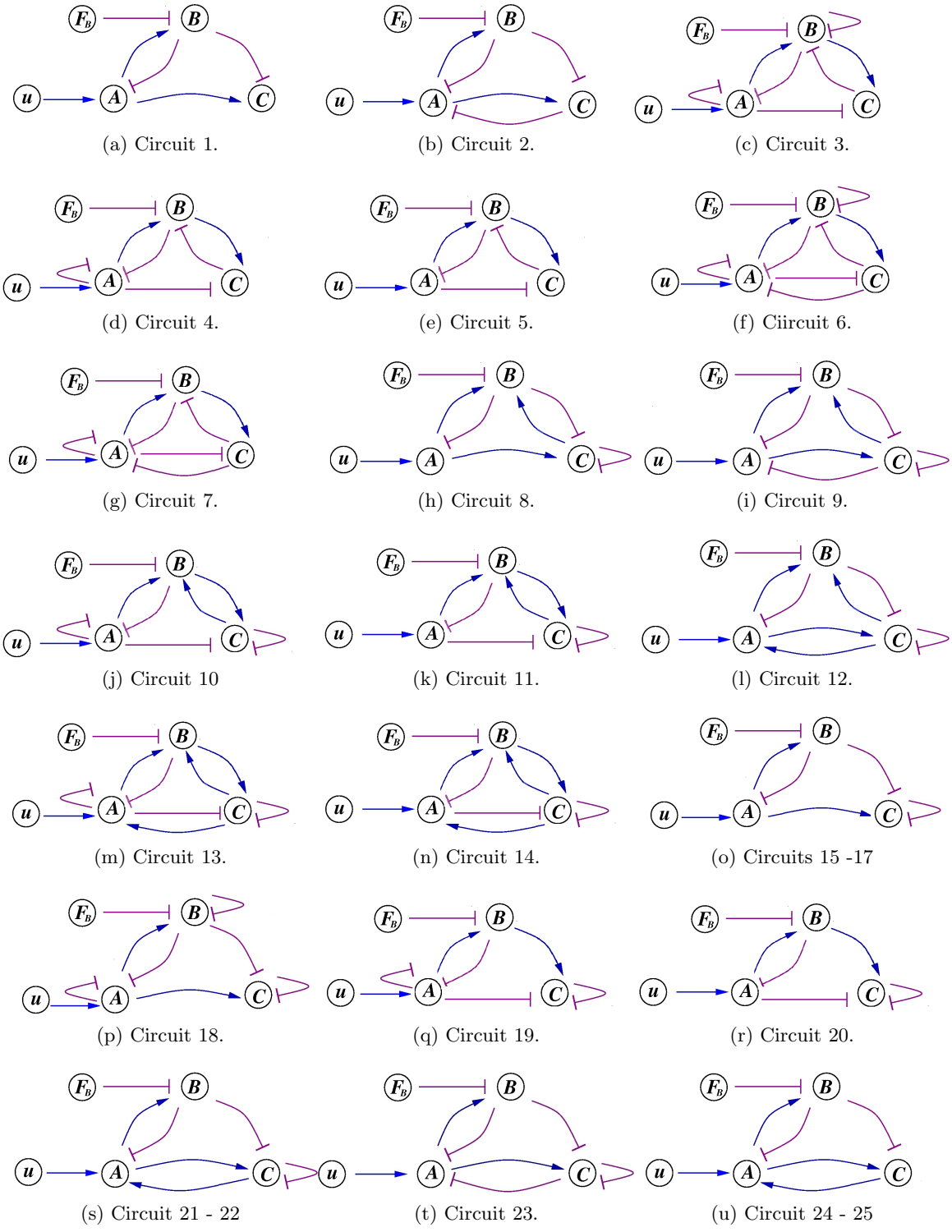

(a) Circuit 1. (b) Circuit 2. (c) Circuit 3.

(d) Circuit 4. (e) Circuit 5. (f) Ciircuit 6.

(g) Circuit 7. (h) Circuit 8. (i) Circuit 9.

(j) Circuit 10 (k) Circuit 11. (l) Circuit 12.

(m) Circuit 13. (n) Circuit 14. (o) Circuits 15 -17

(p) Circuit 18. (q) Circuit 19. (r) Circuit 20.

(s) Circuit 21 - 22 (t) Circuit 23. (u) Circuit 24 - 25

Figure 2.7: Identified ASI Circuits

Chapter 3

Scale Invariance in singularly-perturbed systems

The material in this chapter is based on joint work with Dr. Evgeni Nikolaev in the laboratory of Dr. E. Sontag.

It has been often remarked in the systems biology literature that certain systems whose output variables respond at a faster time scale than internal components, give rise to an approximate scale invariant behavior, allowing approximate scale invariance in stimuli. We have seen such examples on the study of three-node enzyme networks in Chapter 2, and also on a model of *Dictyostelium discoideum* in [102]. Both models contain an incoherent feedforward loop (IFFL), a pattern known to play a central role in processing external stimuli and signals by myriads of molecular circuits inherent in various cellular systems ranging from bacteria to mammalian cells. It was observed that multiple time scales, corresponding to slow and fast subsystems, are typically inherent in such motifs. Among many physiologically relevant properties that this motif can achieve, it has been experimentally shown that certain incoherent feedforward molecular circuits can (approximately) exhibit scale invarance property.

3.1 Feedforward circuits

In this section, we present the IFFL motif, as represented generically by the directed graphs in Fig. 3.1, which has been proposed as one of the two main biomolecular mechanisms (the other is integral feedback) that can help produce scale-invariance or FCD [30, 88, 87]. In IFFL's, an external cue or stimulus u activates a molecular species x which, in turn, activates or represses a downstream species y. Through a different path, the signal u represses or activates, respectively, the species y. This antagonistic ("incoherent") effect endows the IFFL motif with powerful signal processing properties

Figure 3.1: Two incoherent feedforward motifs: (a) Input activates and intermediate species represses output; (b) Input represses and intermediate species activates output.

[4].

The conceptual diagrams shown in Fig. 3.1 describe, in fact, various alternative molecular realizations. Different molecular realizations of the given motif can differ significantly in their dynamic response and, ultimately, biological function. Two realizations of the diagram in Fig. 3.1(b) are shown in Fig. 3.2, and similar alternatives exist for the diagram in Fig. 3.1(a).

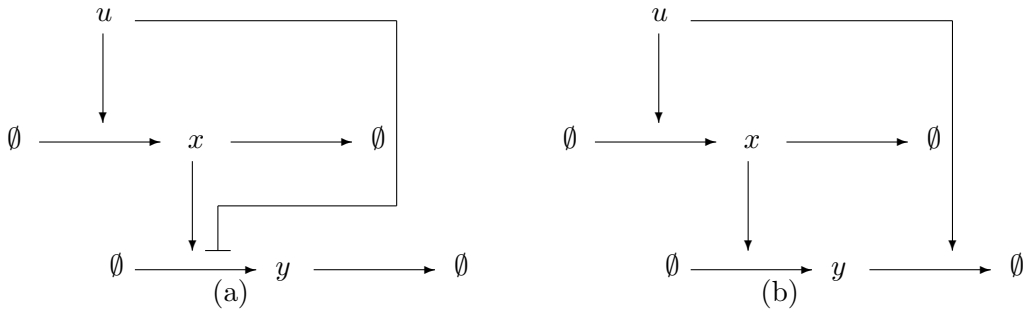

Figure 3.2: Two realizations of the "input repressing output" motif in Fig. 3.1(b): (a) Input inhibits the formation of output; (b) Input enhances the degradation of output.

These two realizations differ in a fundamental way in regards to their scale invariance properties. The biological mechanism in Fig. 3.2(a) exhibits scale invariance, but the one in Fig. 3.2(b) does not.

3.2 Time scale separation in IFFL models

We analyze the simplest ordinary differential equation (ODE) models for these IFFL processes, in which the concentrations of the input u and species x and y are described by scalar time-dependent quantities.

Suppose that $(x(t), y(t))$ is any solution corresponding to the input $u(t)$, for the system described by Fig. 3.2(a). Then, $(px(t), y(t))$ is a solution corresponding to the input

$pu(t)$:

$$\begin{array}{rclcrcl} \dot{x} & = & \alpha u - \delta x & \Rightarrow & (\dot{px}) & = & \alpha(pu) - \delta(px), \\ \dot{y} & = & \beta\frac{x}{u} - \gamma y & \Rightarrow & \dot{y} & = & \beta\frac{\not{p}x}{\not{p}u} - \gamma y\,. \end{array} \tag{3.1}$$

In particular, given a step input that jumps at time $t = 0$ and an initial state at time $t = 0$ that has been pre-adapted to the input $u(t)$ for $t < 0$ (that is, $x(0) = \alpha u_0/\delta$, where u_0 is the value of u for $t < 0$), the solution is the same as when instead applying $pu(t)$ for $t > 0$, but starting from the respective pre-adapted state $(p\alpha u_0/\delta)$. A simulation showing this effect is shown in Fig. 3.3.

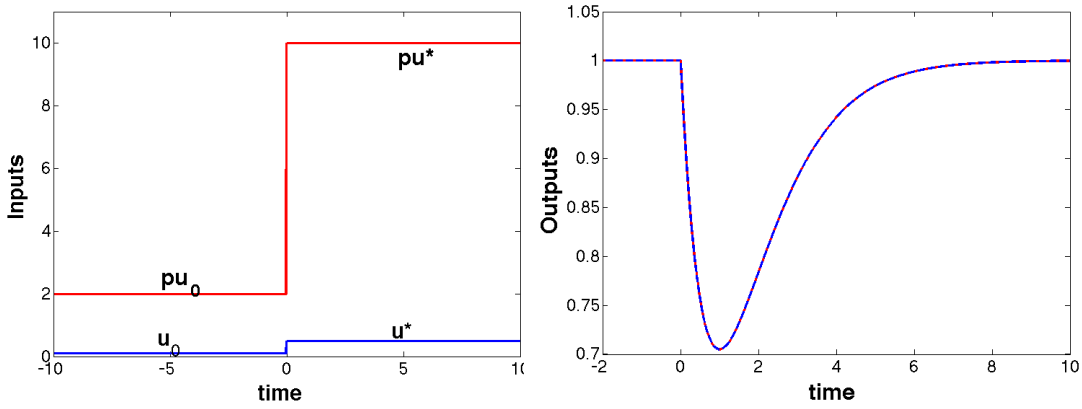

Figure 3.3: Dynamic response of the circuit in Fig. 3.2(a) and described by the model (3.1) and all parameters set to 1. Pre-adaptation value of input is $u_0 = 0.1$, stepping to $u^* = 0.5$ at $t = 0$. Original and p-scaled responses ($p = 20$) overlap perfectly. Here, $\alpha = \beta = \delta = \gamma = 1$.

On the other hand, the scale invariance property *fails for the system in which the input enhances the degradation of output*, shown in Fig. 3.2(b). The same "trick" of scaling states x by p does not work for this second system, when modeled in the obvious manner:

$$\begin{array}{rcl} \dot{x} & = & \alpha u - \delta x, \\ \dot{y} & = & \beta x - \gamma u y, \end{array}$$

because the scaling $x \mapsto px$ and $u \mapsto pu$ does not leave the y equation invariant. Moreover, one can prove that no possible equivariant group action on states is compatible

with output invariance, which means that no possible symmetries are satisfied by the input/output behavior of the system [88].

However, it has been observed that systems such as the one in Fig. 3.2(b) satisfy an *approximate* scale invariance property provided that the parameters β and γ are large enough so that a time-scale separation property holds. Multiple time scales, corresponding to slow and fast subsystems, are typically inherent in cellular systems [33]. Let us nondimensionalize all variables and parameters as follows:

$$\begin{aligned} &x = X_0\bar{x}, \quad y = Y_0\bar{y}, \quad u = U_0\bar{u}, \quad t = \tfrac{X_0}{\alpha_0 U_0}\bar{t}, \quad \alpha = \alpha_0\bar{\alpha}, \\ &\beta = \beta_0\bar{\beta}, \quad \bar{\delta} = \tfrac{\delta X_0}{\alpha_0 U_0}, \quad \bar{\gamma} = \tfrac{\gamma U_0 Y_0}{\beta_0 X_0}, \quad \varepsilon = \tfrac{\alpha_0}{\beta_0}\cdot\tfrac{Y_0 U_0}{X_0^2}. \end{aligned} \tag{3.2}$$

Here, X_0, Y_0, and U_0 are some mean or typical values of the variables x, y, and u, respectively, and $\bar{x}$, $\bar{y}$, and $\bar{u}$ are the corresponding dimensionless variables. The parameters α and β can be interpreted as the dimensionless rates of formation or activation, while $\bar{\delta}$ and $\bar{\gamma}$ can be interpreted as the dimensionless rates of degradation or inactivation of the species x and y, respectively. In what follows, the bar used in the notations will be omitted, and we think of $\bar{t}$ as the original time scale, so that we simply write the system in the following "singular perturbation" form:

$$\begin{aligned} \dot{x} &= \alpha u - \delta x, \\ \varepsilon\dot{y} &= \beta x - \gamma u y\,. \end{aligned} \tag{3.3}$$

Assuming that the corresponding pairs of parameters, $\alpha \sim \delta$ and $\beta \sim \gamma$ are of the same order of magnitude, while the ratio $\alpha/\beta \ll 1$ is small, we can think of $0 < \varepsilon \ll 1$ in (3.2) and (3.3) as a small parameter, where the remaining parameters are all $O(1)$. When viewed at a slow time-scale, we may assume that $y(t)$ quickly equilibrates (set $\varepsilon = 0$ in the second equation) so that, in effect, the resulting system is given by a one-dimensional differential equation together with a readout which is an instantaneous

ratio of states and inputs:

$$\begin{aligned} \dot{x} &= \alpha u - \delta x, \\ y(t) &\approx \frac{\beta x(t)}{\gamma u(t)} \end{aligned}$$

(we include the time argument in y to emphasize the instantaneous nature of the quasi-steady state dependence). Now a scaling $u \mapsto pu$ and $x \mapsto px$ results in (approximately) the same output, since

$$y = \frac{\beta \not{p} x}{\gamma \not{p} u}.$$

The property of time-scale separation for IFFL's can be traced back to work in [55, 115] and [30], and systems of this form were theoretically analyzed in [98].

3.3 Limitations of time-scale based (approximate) scale invariance

We were particularly motivated to look at the question of time scale separation by the analysis described in the Chapter 2, in which we concluded, that *every three node enzymatic network* (as studied in [57]) *which has an approximate scale invariance property must rely upon this mechanism of time scale separation.*

The study of this time-scale separation for scale invariance, and the dependence of the magnitude of the scale invariance error on the input scaling, not only for feedforward systems but in a general context, is to be shown next.

Our main result is that, *no matter how small ε is, there is always an irreducible minimal possible difference in instantaneous values of outputs when comparing the response to an input $u(t)$ and to a scaled version of this input, $pu(t)$.*

This claim is illustrated by the simulation shown in Fig. 3.4.

We call such an irreducible difference an scale invariance error. As a matter of fact, one can show that the scale invariance error (difference between the original output $y_1(t)$ and the output $y_p(t)$ arising from a p-scaled input) is not merely nonzero, but is in fact bounded below by a positive number that is independent of the value of the small parameter ε. Fig. 3.5 shows this effect.

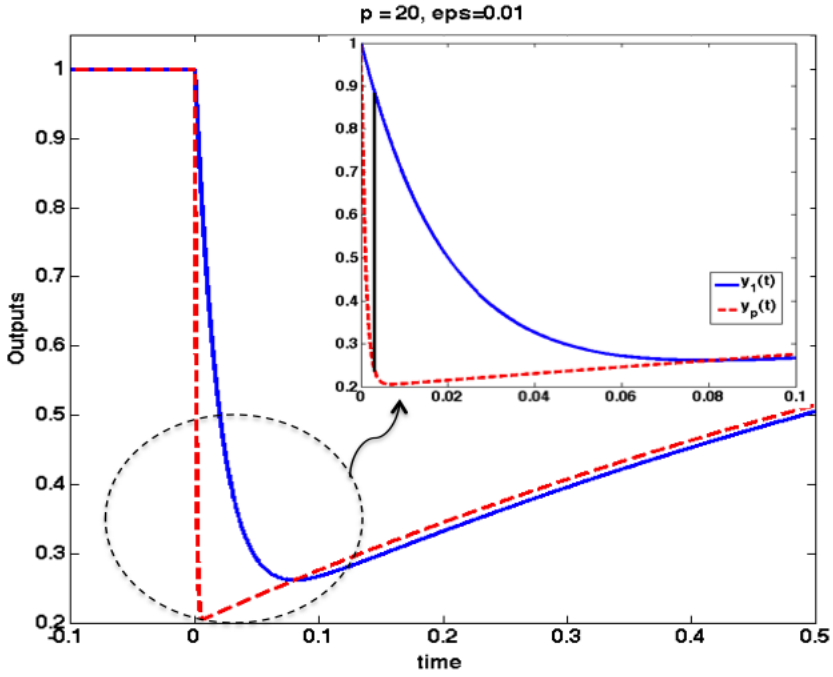

Figure 3.4: Dynamic response of the circuit in Fig. 3.2(b) and described by the model (3.3) with all parameters except ε set to 1. Original (blue) and p-scaled (red) responses. Pre-adaptation value of input is $u_0 = 0.1$, stepping to $u^* = 0.5$ at $t = 0$. The p-scaled output is denoted by $y_p(t)$. Here $\varepsilon = 0.01$ and $p = 20$. The maximal magnitude of the scale invariance error is depicted by a black segment (inset). Here, $\alpha = \beta = \delta = \gamma = 1$.

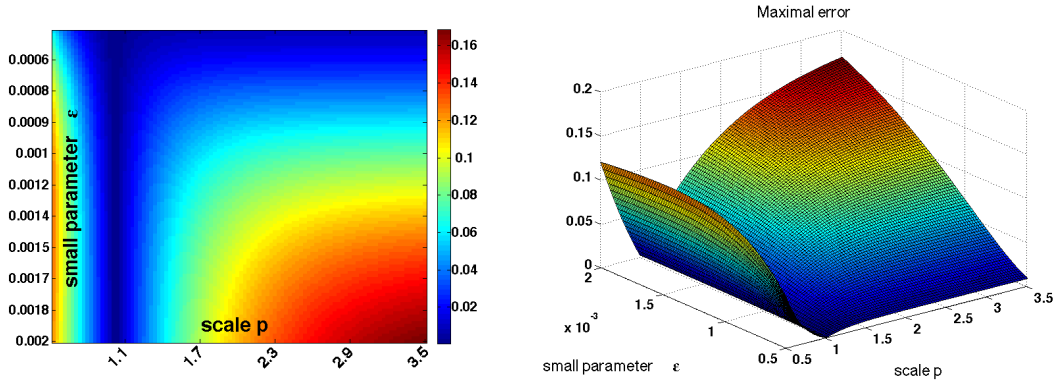

(a) (b)

Figure 3.5: System with input-dependent degradation. Heat-map and a 3D plot representing the largest absolute value of the difference between the two outputs $y_p(t)$ and $y_1(t)$. Observe that, for any fixed p, except for the trivial case $p = 1$, the values approach a positive number as $\varepsilon \to 0$. Pre-adaptation value of input is $u_0 = 1$, stepping to $u^* = 2$ at $t = 0$. The parameter ε was sampled in the range $[0.0005, 0.002]$. The parameter p was sampled in the range $[0.5, 3.5]$. 100 different samples for each were selected. Here, $\alpha = \beta = \delta = \gamma = 1$.

An entirely analogous situation holds for systems in which the state degrades the output, modeled by switching the roles of u and x in the y equation:

$$\begin{aligned} \dot{x} &= \alpha u - \delta x, \\ \varepsilon \dot{y} &= \beta u - \gamma x y, \end{aligned} \tag{3.4}$$

and error behavior is illustrated by Fig. 3.6.

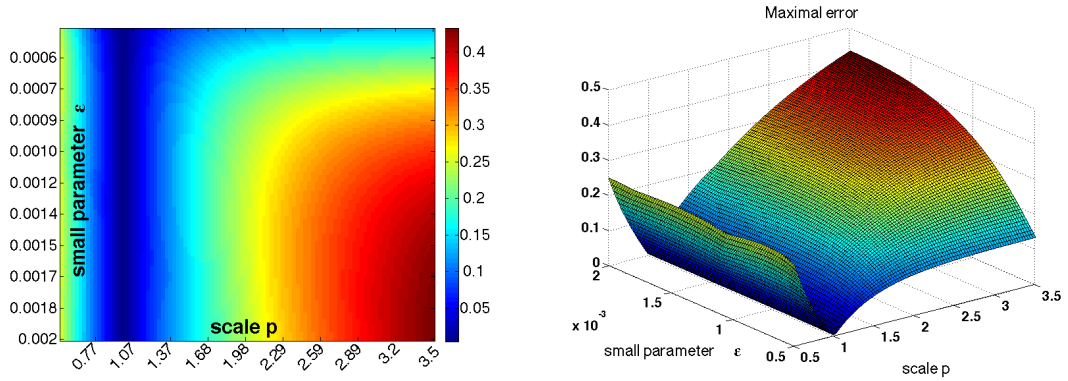

(a) (b)

Figure 3.6: System with state-dependent degradation. Heat-map and a 3D plot representing the largest absolute value of the difference between the two outputs $y_p(t)$ and $y_1(t)$. Pre-adaptation value of input is $u_0 = 1$, stepping to $u^* = 2$ at $t = 0$. Observe that, for any fixed p, except for the trivial case $p = 1$, the values approach a positive number as $\varepsilon \to 0$. The parameter ε was sampled in the range $[0.0005, 0.002]$. The parameter p was sampled in the range $[0.5, 3.5]$. 100 different samples for each were selected. Here, $\alpha = \beta = \delta = \gamma = 1$.

This irreducible error, no matter how small $\varepsilon > 0$ is, establishes a *fundamental limitation* to fold-sensing systems based on time-scale separation, such as those proposed in the context of state-degradation or input-degradation feedforward systems. The existence of such an irreducible error can also be understood through a geometric interpretation based on singular perturbation theory [72, 45, 111]: a step change in the input changes the ODE, with the net result that, even though the output remains the same, the internal state, whose activity is hidden from the output measurement, has in fact "jumped" away from the slow manifold. A derivation of estimates from that point of view, establishing asymptotic expansions to obtain precise bounds on the error for specific systems, will be conducted in Section 3.6.

3.3.1 A motivating example

We start by considering the input-induced degradation IFFL circuit under time-scale separation described in (3.3), the ODE model which we repeat here for convenience:

$$\begin{aligned} \dot{x} &= \alpha u - \delta x, \\ \varepsilon \dot{y} &= \beta x - \gamma u y\,, \end{aligned}$$

where α, β, δ and γ are positive constants and we think of ε as a small parameter. We wish to study the response of this system to a step input $u(t)$ which switches from the value $u(t) = u_0$ for $t < 0$ to a different value $u(t) = u^*$ for $t > 0$, under the assumption ("pre-adaptation") that the states x and y had converged to a steady state by time $t = 0$, and want to compare this response to the response to the input $pu(t)$.

In the first case, the steady state at time $t = 0$ can be found by setting $\alpha u^0 - \delta x = 0$ and $\beta x - \gamma u^0 y = 0$, and then solving for (x, y). The response for $t > 0$ will be, therefore, given by the solution of the ODE with initial condition $x(0) = \frac{\alpha}{\delta} u_0$ and $y(0) = \frac{\alpha\beta}{\delta\gamma}$, and input $u(t) \equiv u^*$ for $t > 0$.

In the second (p-scaled) case, the initial state will be $x(0) = \frac{\alpha}{\delta} p u_0$, and the same $y(0)$, now using the input $u(t) \equiv pu^*$ for $t > 0$.

We will take $\alpha = \beta = \delta = \gamma = 1$ in our subsequent analysis. This involves no loss of generality, because a change of scale in x, u, y and time via: $u = \delta u'/\gamma$, $x = \alpha x'/\gamma$, $y = \alpha\beta y'/(\delta\gamma)$, and $t = t'/\delta$ reduces to that case.

The main result for this example given in Proposition 1 below.

We use the notation $\|y - w\|_{[0,T]} = \max_{t\in[0,T]} |y(t) - w(t)|$ to denote the largest possible value of the difference $|y(t) - w(t)|$ between two functions defined on an interval $[0, T]$. In particular, when quantifying scale invariance error, w will be the output when the input is scaled.

Proposition 1. *Consider solutions $(x_i^\varepsilon(t), y_i^\varepsilon(t))$ of the following two initial value problems:*

$$\begin{array}{rclcrcl} \dot{x}_1 &=& u^* - x_1, \quad x_1(0) = u_0 & & \dot{x}_2 &=& u^* - x_2, \quad x_2(0) = pu_0 \\ \varepsilon\dot{y}_1 &=& x_1 - u^* y_1, \quad y_1(0) = \bar{y} & & \varepsilon\dot{y}_2 &=& x_2 - pu^* y_2, \quad y_2(0) = \bar{y}\,, \end{array} \tag{3.5}$$

where ε, u^*, u_0, and p are nonzero positive numbers, and we assume that $p \neq 1$, $u_0 \neq u^*$. Define $M = M(u^*, u_0, p) > 0$ by:

$$M := \left| \bar{y} - \frac{u_0}{u^*} \right| p^{\frac{p}{1-p}} \, |1 - p| \,. \tag{3.6}$$

Then, for any $0 < M' < M < M''$, there exist two numbers $\varepsilon_0 = \varepsilon_0(u^*, u_0, p, M', M'')$, and $\delta = \delta(u^*, u_0, p, M', M'') > 0$, such that:

$$M' \;\leq\; \|y_1^\varepsilon - y_2^\varepsilon\|_{[0,\delta]} \;\leq\; M'' \qquad \forall\, 0 < \varepsilon \leq \varepsilon_0 \,. \tag{3.7}$$

Since M' and M'' can be taken arbitrarily close to M, this result tells us, in particular, that $\|y_1^\varepsilon - y_2^\varepsilon\|_{[0,\delta]} \approx M$ for all $0 < \varepsilon \ll 1$, and δ small. In other words, the positive number given in (3.6), which does not depend on ε, provides a fundamentally irreducible error as $\varepsilon \to 0$, for any nontrivial scaling ($p \neq 1$) and any nontrivial step input ($u_0 \neq u^*$).

Proof of Proposition 1

We start with a number of technical results leading to the proof of Proposition 1.

Lemma 2. *For any nonzero positive numbers u^*, u_0, p such that $p \neq 1$ and $u_0 \neq u^*$, define $M = M(u^*, u_0, p) > 0$ and $T = T(p, u^*) > 0$ by:*

$$M := \left| \bar{y} - \frac{u_0}{u^*} \right| p^{\frac{p}{1-p}} \, |1 - p| \,, \qquad T := \frac{\ln p}{(p-1)u^*} \,.$$

Consider the initial value problems:

$$\begin{aligned} \varepsilon \dot{w}_1 &= u_0 - u^* w_1, \qquad w_1(0) = \bar{y}, \\ \varepsilon \dot{w}_2 &= p u_0 - p u^* w_2, \quad w_2(0) = \bar{y}, \end{aligned} \tag{3.8}$$

Then,

$$\|w_1 - w_2\|_\infty \;=\; |w_1(\varepsilon T) - w_2(\varepsilon T)| \;=\; M\,. \tag{3.9}$$

Proof. The solutions of equations (3.8) can be found in an explicit form as:

$$w_1(t) \;=\; \frac{u_0}{u^*} + \left(\bar{y} - \frac{u_0}{u^*}\right) e^{-u^* t/\varepsilon}\,, \quad w_2(t) \;=\; \frac{u_0}{u^*} + \left(\bar{y} - \frac{u_0}{u^*}\right) e^{-p u^* t/\varepsilon}\,. \tag{3.10}$$

Using (3.10), we obtain

$$|w_1(t) - w_2(t)| = \left|1 - \frac{u_0}{u^*}\right| \cdot |\varphi(t;\varepsilon,p)|\,, \tag{3.11}$$

where

$$\varphi(t;\varepsilon,p) = e^{-u^* t/\varepsilon} - e^{-p u^* t/\varepsilon}. \tag{3.12}$$

We see that $\varphi(0;\varepsilon,p) = 0$ and $\varphi(t;\varepsilon,p) \to 0$ as $t \to \infty$. Then it follows that $\varphi(t;\varepsilon,p)$ has its absolute extrema at $0 < t^* < \infty$ which can be found using the derivative tests, $\varphi'(t^*;\varepsilon,p) = 0$, and $\varphi''(t^*;\varepsilon,p) \neq 0$.

From the first derivative test $\varphi'(t;\varepsilon,p) = 0$ we obtain

$$\varphi'(t;\varepsilon,p) \;=\; -\frac{u^*}{\varepsilon} e^{-u^* t/\varepsilon} + \frac{p u^*}{\varepsilon} e^{-p u^* t/\varepsilon} \;=\; 0, \tag{3.13}$$

$$t^* = \varepsilon \frac{\ln p}{(p-1)u^*} = \varepsilon T.$$

Using the value for t^* in (3.12) we obtain

$$\varphi(t^*;\varepsilon,p) \;=\; p^{\frac{p}{1-p}} \cdot (p-1). \tag{3.14}$$

Using the second derivative test, we obtain

$$\varphi''(t^*;\varepsilon,p) \;=\; \Big(\frac{u^*}{\varepsilon}\Big)^2 p^{\frac{1}{1-p}} \cdot (1-p). \tag{3.15}$$

From (3.15), it follows that $\varphi''(t^*;\varepsilon,p) > 0$ if $p < 1$, and $\varphi''(t^*;\varepsilon,p) < 0$ if $p > 1$, which correspond respectively to the absolute minimum, $\varphi(t^*;\varepsilon,p) < 0$, and the absolute maximum, $\varphi(t^*;\varepsilon,p) > 0$, of the function $\varphi(t;\varepsilon,p)$. In both cases, $|\varphi(t^*;\varepsilon,p)|$ is the absolute maximum of $\varphi(t;\varepsilon,p)$. □

The following two results allow one to obtain tighter bounds, for the special example of the IFFL in Proposition 1, and also for generalizations in which the scalar x_1 subsystem is replaced by a generic linear system, than those assured by Theorem 1.

Proposition 2. *Consider a system*

$$\begin{aligned} \dot{x} \;&=\; qAx + qBv, \quad x(0) = 0 \\ y \;&=\; Cx, \end{aligned} \tag{3.16}$$

where $A \in \mathbb{R}^{n\times n}$ is Hurwitz, $B \in \mathbb{R}^{n\times r}$, $C \in \mathbb{R}^{p\times n}$, $q > 0$, $S > 0$, and $|v(t)| \le \bar{\Delta}$ for all $t \in [0, S]$. Then, there exists a $c > 0$ independent of q such that

$$\max_{t\in[0,S]} |y(t)| \le \bar{\Delta} \cdot c. \tag{3.17}$$

In fact, we may pick $c = \displaystyle\int_0^\infty \left\|Ce^{As}B\right\| ds$.

Proof. From (3.16)

$$|y(t)| \le \bar{\Delta} \int_0^t \left\|Ce^{qA(t-\tau)}B\right\| q d\tau\,,\ \forall t \in [0, S].$$

Introducing the change of variables $s = q(t-\tau)$, the previous expression becomes:

$$|y(t)| \le \bar{\Delta} \int_0^{qt} \left\|Ce^{As}B\right\| ds \le \bar{\Delta} \int_0^\infty \|K(s)\|\, ds = \bar{\Delta} \cdot \|K\|_1\,.$$

Define $c = \|K\|_1 < \infty$. Then,

$$\sup_{t\in[0,S]} |y(t)| \leq \bar{\Delta} \cdot c,$$

as desired. □

Proposition 3. *For any nonzero positive numbers u^*, u_0, r, p such that $r < 1$, $p < 1$, and $u_0 \neq u^*$, let $M = M(u^*, u_0, p) > 0$ and $T = T(p, u^*) > 0$ be as defined as earlier, and let $\delta = \delta(u^*, u_0, p, r) > 0$ be given by:*

$$\delta \;:=\; \begin{cases} \min\left\{\ln\left(\dfrac{2\,|u^*-u_0|}{2\,|u^*-u_0| - M(1-r)u^*}\right), \dfrac{\ln p}{p-1}\right\}, & \text{if } \dfrac{M(1-r)u^*}{2\,|u^*-u_0|} < 1, \\ \dfrac{\ln p}{p-1}, & \text{otherwise.} \end{cases} \tag{3.18}$$

Finally, define $\varepsilon_0 = \varepsilon_0(u^*, u_0, p, r) > 0$ by:

$$\varepsilon_0 \;:=\; \delta/T\,.$$

Consider any solution $(x(t), y_1(t), y_2(t))$, $t \geq 0$, of the following initial-value system of three differential equations:

$$\begin{aligned} \dot{x} &= -x + u^*, & x(0) &= u_0, \\ \varepsilon\dot{y}_1 &= x - u^* y_1, & y_1(0) &= \bar{y}, \\ \varepsilon\dot{y}_2 &= px - pu^* y_2, & y_2(0) &= \bar{y}, \end{aligned} \tag{3.19}$$

where $0 < \varepsilon \leq \varepsilon_0$. Then,

$$rM \;\leq\; \|y_1 - y_2\|_{[0,\delta]} \;\leq\; (2-r)M\,.$$

Proof. Consider the following equations:

$$\begin{aligned} \varepsilon\dot{w}_1 &= u_0 - u^* w_1, & w_1(0) &= \bar{y}, \\ \varepsilon\dot{w}_2 &= pu_0 - pu^* w_2, & w_2(0) &= \bar{y}. \end{aligned}$$

By Lemma 2, $\|w_1 - w_2\|_\infty = \|w_1 - w_2\|_{[0,\varepsilon T]} = M$, and, since $\varepsilon T \leq \varepsilon_0 T = \delta$, this implies that

$$\|w_1 - w_2\|_{[0,\delta]} = M \tag{3.20}$$

as well. Let $\Delta(t) := x(t) - x(0) = x(t) - u_0$ on the interval $t \in [0, \delta]$, and $\bar{\Delta} := \|\Delta\|_{[0,\delta]}$. Defining $e_1(t) := y_1(t) - w_1(t)$, we have that

$$\varepsilon \dot{e}_1(t) = \varepsilon \dot{y}_1(t) - \varepsilon \dot{w}_1(t) = -u^* e_1(t) + \Delta(t)$$

or, equivalently:

$$\dot{e}_1(t) = -\frac{u^*}{\varepsilon} e_1(t) + \frac{\Delta(t)}{\varepsilon}\,.$$

Applying Proposition 2 with $A = -u^*$, $B = 1$, $C = 1$, $S = \delta$, and $q = 1/\varepsilon$, we obtain: $|e_1(t)| \leq \bar{\Delta}/u^*$ for $t \in [0, \delta_r]$, and thus:

$$\|y_1 - w_1\|_{[0,\delta]} \leq \frac{\bar{\Delta}}{u^*}\,. \tag{3.21}$$

Similarly, to determine $|y_2(t) - w_2(t)|$ we apply Proposition 2 with the same matrices A, B and C, and $q = p/\varepsilon$, and obtain:

$$\|y_2 - w_2\|_{[0,\delta]} \leq \frac{\bar{\Delta}}{u^*}\,. \tag{3.22}$$

By the triangle inequality for norms,

$$\|w_1 - w_2\|_{[0,\delta]} \leq \|w_1 - y_1\|_{[0,\delta]} + \|y_1 - y_2\|_{[0,\delta]} + \|y_2 - w_2\|_{[0,\delta]}$$

and therefore, using (3.20), (3.21), and (3.22), we conclude

$$\|y_1 - y_2\|_{[0,\delta]} \geq M - \frac{2\bar{\Delta}}{u^*}\,. \tag{3.23}$$

Similarly, from

$$\|y_1 - y_2\|_{[0,\delta]} \leq \|y_1 - w_1\|_{[0,\delta]} + \|w_1 - w_2\|_{[0,\delta]} + \|w_2 - y_2\|_{[0,\delta]}$$

we obtain that

$$\|y_1 - y_2\|_{[0,\delta]} \;\leq\; M + \frac{2\bar{\Delta}}{u^*}\,. \tag{3.24}$$

We next show that:

$$\bar{\Delta} \;\leq\; \frac{M(1-r)u^*}{2}\,, \tag{3.25}$$

which will imply that

$$rM \;=\; M - M(1-r) \;\leq\; \|y_1 - y_2\|_{[0,\delta]} \;\leq\; M + M(1-r) = (2-r)M\,,$$

which is what the proposition asserts. To estimate $\bar{\Delta}$, we compute the explicit solution $x(t) = u^* + (u_0 - u^*)e^{-t}$, so that $\Delta(t) = x(t) - u_0 = (u^* - u_0)(1 - e^{-t})$. This means that:

$$|\Delta(t)| = |u^* - u_0|\,(1 - e^{-t})\,.$$

As $|\Delta(t)|$ is an increasing function on $[0, \delta]$, showing that (3.25) is the same as showing that

$$\Delta(\delta) \;=\; |u^* - u_0|\,(1 - e^{-\delta}) \;\leq\; \frac{M(1-r)u^*}{2}\,, \tag{3.26}$$

so we prove this last statement.

To prove (3.26), we first look at the case where $\delta = \frac{\ln p}{p-1}$, under the condition

$$\frac{M(1-r)u^*}{2\,|u^* - u_0|} \;\geq\; 1. \tag{3.27}$$

Since $1 - p^{\frac{1}{1-p}} < 1$, indeed from (3.27) we have that

$$\frac{M(1-r)u^*}{2} \geq |u^* - u_0| \;\geq\; |u^* - u_0|\left(1 - p^{\frac{1}{1-p}}\right) \;=\; |u^* - u_0|\,(1 - e^{-\delta})\,.$$

Next we consider the two cases for

$$\frac{M(1-r)u^*}{2\,|u^* - u_0|} \;<\; 1\,. \tag{3.28}$$

depending on what the minimum between

$$\ln\left(\frac{2\left|u^*-u_0\right|}{2\left|u^*-u_0\right|-M(1-r)u^*}\right)$$

and

$$\frac{\ln p}{p-1}$$

is. (Observe that (3.28) only plays a role in guaranteeing that the expresision inside the logarithm is positive, and hence, the logarithm is well-defined.) Consider first the case

$$\frac{\ln p}{p-1} \leq \ln\left(\frac{2\left|u^*-u_0\right|}{2\left|u^*-u_0\right|-M(1-r)u^*}\right). \tag{3.29}$$

With δ selected as a minimum of these two expressions, we again have that $\Delta(\delta) = |u^*-u_0|\left(1-p^{\frac{1}{1-p}}\right)$. Working with the condition given by (3.29) we have that

$$\begin{aligned} -\frac{\ln p}{p-1} &\geq \ln\left(\frac{2\left|u^*-u_0\right|-M(1-r)u^*}{2\left|u^*-u_0\right|}\right), \\ p^{\frac{1}{1-p}} &\geq 1-\frac{M(1-r)u^*}{2\left|u^*-u_0\right|}, \\ \left|u^*-u_0\right|\left(1-p^{\frac{1}{1-p}}\right) &\leq \frac{M(1-r)u^*}{2}, \end{aligned} \tag{3.30}$$

which is exactly what we were supposed to prove. Finally, consider the case when

$$\ln\left(\frac{2\left|u^*-u_0\right|}{2\left|u^*-u_0\right|-M(1-r)u^*}\right) < \frac{\ln p}{p-1}. \tag{3.31}$$

In this case

$$\begin{aligned} \left|\Delta(\delta_r)\right| &= \left|u^*-u_0\right|\left(1-e^{-\ln\left(\frac{2|u^*-u_0|}{2|u^*-u_0|-M(1-r)u^*}\right)}\right) \\ &= \left|u^*-u_0\right|\left(1-\frac{2\left|u^*-u_0\right|-M(1-r)u^*}{2\left|u^*-u_0\right|}\right) \\ &= \left|u^*-u_0\right|\left(\frac{M(1-r)u^*}{2\left|u^*-u_0\right|}\right) = \frac{M(1-r)u^*}{2}, \end{aligned}$$

which proves the claim asserted in (3.26). This completes the proof of the proposition.

□

We can now use the above results to prove the main Proposition 1.

Proof of Proposition 1

Proof. Without loss of generality, we may take $p < 1$. Indeed, if $p > 1$, we simply exchange the roles of y_1 and y_2, and the result is the same. Pick any $r \in (0,1)$ such that $M' < rM$ and $(2-r)M < M''$. Such an r can be found because $2 - r \to 1$ as $r \to 1$. and define $\varepsilon_0(u^*, u_0, p, r)$ as in Proposition 3. Fixing any $0 < \varepsilon \leq \varepsilon_0$, we have that $x_1^\varepsilon = x$ and $x_2^\varepsilon = px$ in that Proposition, so $y_1^\varepsilon = y_1$ and $y_2^\varepsilon = y_2$ are as there. It follows that

$$rM \;\leq\; \|y_1 - y_2\|_{[0,\delta]} \;\leq\; (2-r)M\,.$$

Thus, $\|y_1 - y_2\|_{[0,\delta]} \geq rM \geq M'$ and $\|y_1^\varepsilon - y_2^\varepsilon\|_{[0,\delta]} \leq (2-r)M < M''$, as desired. □

3.4 A general comparison theorem

We now formulate a general comparison theorem that generalizes Proposition 1 to arbitary systems. The bounds obtained are not as explicit as with the example, yet they again show the existence of a positive number M that lower-bounds the difference between outputs under scaling of inputs.

To achieve the greatest possible generality, our theorem will be formulated and proved for two arbitrary singularly-perturbed non-autonomous initial-value problems (IVPs), as follows:

$$(S_1)\begin{cases} \dot{x}_1 \;=\; f_1(x_1, y_1, t),\; x_1(0) = \xi_1, \\ \varepsilon\dot{y}_1 \;=\; g_1(x_1, y_1, t),\; y_1(0) = \kappa_1, \end{cases} \qquad (S_2)\begin{cases} \dot{x}_2 \;= f_2(x_2, y_2, t),\; x_2(0) = \xi_2, \\ \varepsilon\dot{y}_2 = g_2(x_2, y_2, t),\; y_2(0) = \kappa_2. \end{cases} \tag{3.32}$$

Here, (x_i, y_i), $(\xi_i, \kappa_i) \in X \times Y$, where X and Y are open sets, $X \subseteq \mathbb{R}^n$ and $Y \subseteq \mathbb{R}^s$. The functions f_i and g_i are of class C^1 with respect to x, y, and t, $i = 1, 2$.

The main result will be that a minimal difference exists between y_1 and y_2, independently of $\varepsilon > 0$, provided only that the following two associated ODE systems:

$$(A_1)\ Y_1' = g_1(\xi_1, Y_1, 0),\ Y_1(0) = \kappa_1, \quad (A_2)\ Y_2' = g_2(\xi_2, Y_2, 0),\ Y_2(0) = \kappa_2, \qquad (3.33)$$

have different solutions. These are the systems obtained when ε is ignored but x_1 and x_2 are replaced by their initial values ξ_2 and ξ_1 in S_1 and S_2, respectively. (We use primes $'$ instead of dots to indicate time derivatives, for reasons to be clear below.) We now explain how we can apply the theorem to scale invariance.

Suppose given a system of the generic form

$$\begin{aligned} \dot{x} &= f(x, y, u), \\ \varepsilon \dot{y} &= g(x, y, u)\,, \end{aligned}$$

where, generally speaking, the input as well as the state vector (x, y) are of arbitrary dimensions. We think of the components of y as an output, and want to compare the outputs associated to two inputs $u(t)$ and $pu(t)$, for $t > 0$, when initial states might themselves depend on the values of $u(t)$ and $pu(t)$ for $t < 0$. This latter dependence is encapsulated in the initial states (ξ_1, κ_1) and (ξ_2, κ_2) respectively. To apply the theorem, we let $f_1(x_1, y_1, t) := f(x_1, y_1, u(t))$, $g_1(x_1, y_1, t) := g(x_1, y_1, u(t))$, $f_2(x_2, y_2, t) := f(x_2, y_2, pu(t))$, and $g_2(x_2, y_2, t) := g(x_2, y_2, pu(t))$. The systems considered are quite arbitary, and allow for feedback and not merely feedforward structures, as will be evident when we study examples.

Our analysis starts from the observation that the transient scale invariance error occurs within a thin boundary layer adjacent to the perturbation moment $t = 0$, as can be seen in the example shown in Fig. 3.4. To analyze nonlinear effects occurring within small time intervals, it is convenient to use the stretched time $\tau = t/\varepsilon$. Substituting

$t = \varepsilon\tau$ into (3.32), we obtain

$$(R_1)\begin{cases} X_1' \;=\; \varepsilon f_1(X_1, Y_1, \varepsilon\tau),\; X_1(0) = \xi_1, \\ Y_1' \;=\; g_1(X_1, Y_1, \varepsilon\tau), \quad Y_1(0) = \kappa_1, \end{cases} \qquad (R_2)\begin{cases} X_2' \;=\; \varepsilon f(X_2, Y_2, \varepsilon\tau),\; X(0) = \xi_2, \\ Y_2' \;=\; g(X_2, Y_2, \varepsilon\tau), \quad Y(0) = \kappa_2, \end{cases} \tag{3.34}$$

where $(\cdot)' = d(\cdot)/d\tau$, and all functions are continuously-differentiable with respect to the variables, the initial conditions and the parameter $\varepsilon > 0$ as discussed above.

In contrast to the *singularly*-perturbed systems (S_1) and (S_2), both systems (R_1) and (R_2) are *regularly*-perturbed with respect to ε. It follows that the scale invariance error should be already detected at $\varepsilon = 0$ in which case the systems (R_1) and (R_2) can be further reduced to the associated systems described by (3.33). Observe that the system (A_i) is obtained from (R_i), where X_i is replaced by its initial condition ξ_i, using the reference IVP $X_i' = 0$, $X(0) = \xi_i$ at $\varepsilon = 0$, $i = 1, 2$. We will denote the solutions of the systems (R_i) by $X_i^\varepsilon(\tau)$ and $Y_i^\varepsilon(\tau)$, $i = 1, 2$.

Theorem 1. *Assume that the solution $(x_i^\varepsilon(t), y_i^\varepsilon(t))$ of the system (S_i) is defined on $[0, \infty)$ for all $\varepsilon \in (0, \varepsilon_0]$ with some $\varepsilon_0 > 0$, $i = 1, 2$. Let $Y_i^0(t)$ be the solution of the associated system (A_i), $i = 1, 2$. Then, for each $\varepsilon \in (0, \varepsilon_0]$ and each $0 \le \tau_0 < \infty$, we have:*

$$M_{\tau_0} - \varepsilon N_{\tau_0} \;\le\; \|y_1^\varepsilon - y_2^\varepsilon\|_{[0,\varepsilon\tau_0]} \;\le\; M_{\tau_0} + \varepsilon N_{\tau_0}, \tag{3.35}$$

where M_{τ_0} and N_{τ_0} are defined as follows:

$$M_{\tau_0} \;=\; \left|Y_2^0(\tau_0) - Y_1^0(\tau_0)\right|, \quad N_{\tau_0} = \max_{0\le\varepsilon\le\varepsilon_0} \left\| \frac{\partial Y_1^\varepsilon(\cdot)}{\partial\varepsilon} \right\|_{[0,\tau_0]} + \max_{0\le\varepsilon\le\varepsilon_0} \left\| \frac{\partial Y_2^\varepsilon(\cdot)}{\partial\varepsilon} \right\|_{[0,\tau_0]}. \tag{3.36}$$

Proof of the comparison theorem

Let $(X_i^0(\tau), Y_i^0(\tau))$ be the solution of the system (R_i) in (3.34) at $\varepsilon = 0$. Then, obviously, $Y_i^0(\tau)$ is the solution of the associated system (A_i) in (3.33). The following lemma, which will be used to prove Theorem 1, relates the solution of the associated system (A_i) with the solution of the regularly-perturbed system (R_i), $i = 1, 2$.

Lemma 3. *Consider the solution* $(X_i^\varepsilon(\tau), Y_i^\varepsilon(\tau))$ *of the system* (R_i) *in* (3.34) *on a closed interval* $[0, \tau_0]$ *for some fixed* $\tau_0 > 0$. *Let* $(X_i^\varepsilon(\tau), Y_i^\varepsilon(\tau))$ *be continuously-differentiable with respect to the parameter* $\varepsilon \in [0, \varepsilon_0]$, $\varepsilon_0 > 0$. *Then,*

$$\|Y_i^\varepsilon - Y_i^0\|_{[0,\tau_0]} \;\leq\; N_{\tau_0,i}\,\varepsilon\,, \tag{3.37}$$

where

$$N_{\tau_0,i} \;:=\; \max_{0\leq\varepsilon\leq\varepsilon_0} \left\| \frac{\partial Y_i^\varepsilon(\cdot)}{\partial \varepsilon} \right\|_{[0,\tau_0]} \tag{3.38}$$

for all $\varepsilon \in [0, \varepsilon_0]$ *and* $i = 1, 2$.

Proof. The statement is an immediate consequence of the differentiability of solutions with respect to parameters, as a function with values in the space of continuous functions with supremum norm, which in turn follows from the Lagrange form of the Mean Value Theorem, see for example Theorem 1 in [95]. We here provide the details. Fix any $\varepsilon_0 > 0$. Because the system (R_i) is of class C^1 with respect to x, y, ε, and t, the solution of the system (R_i) is also of class C^1 with respect to ε, see for instance [32]. We have:

$$Y_i^\varepsilon(\tau) - Y_i^0(\tau) \;=\; \left(\int_0^1 \frac{\partial Y_i^{\theta\varepsilon}(\tau)}{\partial \varepsilon} d\theta \right) \varepsilon\,. \tag{3.39}$$

Taking norms, and using that $\theta\varepsilon \in [0, \varepsilon_0]$ when $0 < \theta < 1$,

$$\left| \frac{\partial Y_i^\varepsilon(\cdot)}{\partial \varepsilon} \right| \;\leq\; N_{\tau_0,i}\,,$$

(3.39) yields (3.37). □

Using Lemma 3, Theorem 1 can now be proved as follows.

Proof. Consider solutions $(X_i^\varepsilon(\tau), Y_i^\varepsilon(\tau))$ of the system (R_i), and the corresponding solutions $Y_1^0(\tau)$ and $Y_2^0(\tau)$ of the associated systems (A_i). Fix τ_0 and $\varepsilon_0 > 0$, and pick $N_{\tau_0,i}$, $i = 1, 2$, as in Lemma 3. Let $N_{\tau_0} = N_{\tau_0,1} + N_{\tau_0,2}$. Then, it follows from (3.37)

that

$$\|Y_1^\varepsilon - Y_2^\varepsilon\|_{[0,\tau_0]} \geq \|Y_1^0 - Y_2^0\|_{[0,\tau_0]} - \|Y_1^\varepsilon - Y_1^0\|_{[0,\tau_0]} - \|Y_2^\varepsilon - Y_2^0\|_{[0,\tau_0]} \geq M_{\tau_0} - N_{\tau_0}\varepsilon \quad (3.40)$$

and also

$$\|Y_1^\varepsilon - Y_2^\varepsilon\|_{[0,\tau_0]} \leq \|Y_1^0 - Y_2^0\|_{[0,\tau_0]} + \|Y_1^\varepsilon - Y_1^0\|_{[0,\tau_0]} + \|Y_2^\varepsilon + Y_2^0\|_{[0,\tau_0]} \leq M_{\tau_0} + N_{\tau_0}\varepsilon \quad (3.41)$$

for all $0 < \varepsilon \leq \varepsilon_0$. Let $\tau = t/\varepsilon$, and let $(x_i^\varepsilon(t), y_i^\varepsilon(t)) = (X_i^\varepsilon(t/\varepsilon), Y_i^\varepsilon(t/\varepsilon))$, where $t \in [0, \varepsilon\tau_0]$. By uniqueness of solutions, we immediately obtain that $(x_i^\varepsilon(t), y_i^\varepsilon(t))$ is the solution of the singularly-perturbed problem (S_i) on the time interval $[0, \varepsilon\tau_0]$ for all $\varepsilon \in (0, \varepsilon_0]$, so $\|y_2^\varepsilon - y_1^\varepsilon\|_{[0,\varepsilon\tau_0]} = \|Y_2^\varepsilon - Y_1^\varepsilon\|_{[0,\tau_0]}$. It follows from (3.40) and (3.41) that

$$M_{\tau_0} - N_{\tau_0}\varepsilon \;\leq\; \|y_2^\varepsilon - y_1^\varepsilon\|_{[0,\varepsilon\tau_0]} \;\leq\; M_{\tau_0} + \varepsilon N_{\tau_0} \quad (3.42)$$

for all $\varepsilon \in (0, \varepsilon_0]$. □

3.5 Examples

To illustrate Theorem 1, we consider three examples of increasing complexity: first, we revisit the example of an incoherent feedforward loop, then study a more complicated system in which there is feedback, and finally we look at a published model of the chemotaxis signaling pathway of *Dictyostelium discoideum*.

3.5.1 Applying the general theorem to the IFFL

We first apply the results of Theorem 1 to the input-induced degradation IFFL circuit under time-scale separation described in (3.3). To emphasize the value of the scaling p, we shall denote the solution of the p-scaled system by $(x_p(t), y_p(t))$. The systems (S_1)

and (S_2) from (3.32) become, in this example:

$$(S_1)\begin{cases} \dot{x}_1 = u^* - x_1, & x_1(0) = u_0, \\ \varepsilon\dot{y}_1 = x_1 - u^* y_1, & y_1(0) = 1, \end{cases} \quad (S_2)\begin{cases} \dot{x}_p &= pu^* - x_p, & x_p(0) = pu_0, \\ \varepsilon\dot{y}_p &= x_p - pu^* y_p, & y_p(0) = 1. \end{cases} \tag{3.43}$$

Here, $u_0 = u(0^-)$ and $u^* = u(0^+) = u(t)$, $t \geq 0$. The associated systems (A_1) and (A_2) in (3.33) are:

$$(A_1)\ Y_1' = u_0 - u^* Y_1,\ Y_1(0) = 1, \qquad (A_2)\ Y_p' = p(u_0 - u^* Y_p),\ Y_p(0) = 1. \tag{3.44}$$

In what follows we will apply Theorem 1 to the systems (R_1) and (R_2) in (3.34) with the fixed values for ε_0 and τ_0 given by:

$$\varepsilon_0 = \min\{u^*, u^* p\}/2\,, \quad \tau_0 = \frac{\ln p}{(p-1)u^*}. \tag{3.45}$$

The constants M_{τ_0} and N_{τ_0} in (3.36) guaranteed by Theorem 1 satisfy, for these choices of ε_0 and τ_0:

$$M_{\tau_0} = \left|1 - \frac{u_0}{u^*}\right| |p-1|\, p^{\frac{p}{1-p}}, \tag{3.46a}$$

$$N_{\tau_0} \leq \tilde{N}_{\tau_0} = \frac{4}{u^*}\left|1 - \frac{u_0}{u^*}\right| \Big(\frac{2(p+1)}{p} + \frac{\ln p}{p-1}\Big). \tag{3.46b}$$

The expression for M_{τ_0} in (3.46a) is obtained in Lemma 2. Next we compute N_{τ_0}, using the fact that, for this example, where the dynamics are linear, each system (R_i) in (3.34) can be solved analytically.

Denote by $(x_1(t;\varepsilon), y_1(t;\varepsilon))$ and $(x_p(t;\varepsilon,p), y_p(t;\varepsilon,p))$ the solutions of the systems (S_1) and (S_2), respectively. We can find the solutions of (R_i) as:

$$X_1^\varepsilon(\tau) = u^* + (u_0 - u^*)e^{-\varepsilon\tau}\,, \quad Y_1^\varepsilon(\tau) \,=\, 1 + \frac{(u_0 - u^*)}{u^* - \varepsilon}\Big(e^{-u^*\tau} - e^{-\varepsilon\tau}\Big), \tag{3.47a}$$

$$X_2^\varepsilon(\tau) = p\Big(u^* + (u_0 - u^*)e^{-\varepsilon\tau}\Big)\,, \quad Y_2^\varepsilon(\tau) \,=\, 1 + \frac{p(u_0 - u^*)}{pu^* - \varepsilon}\Big(e^{-pu^*\tau} - e^{-\varepsilon\tau}\Big). \tag{3.47b}$$

Differentiating $Y_2^\varepsilon(\tau)$ by ε yields

$$\frac{\partial Y_2^\varepsilon(\tau)}{\partial \varepsilon} \;=\; \frac{p(u_0-u^*)}{pu^*-\varepsilon}\Big(\frac{e^{-pu^*\tau}-e^{-\varepsilon\tau}}{pu^*-\varepsilon}+\tau e^{-\varepsilon\tau}\Big), \tag{3.48}$$

and hence when $p=1$ we have:

$$\frac{\partial Y_1^\varepsilon(\tau)}{\partial \varepsilon} \;=\; \frac{(u_0-u^*)}{u^*-\varepsilon}\Big(\frac{e^{-u^*\tau}-e^{-\varepsilon\tau}}{u^*-\varepsilon}+\tau e^{-\varepsilon\tau}\Big). \tag{3.49}$$

Observe that

$$\Big\|\frac{\partial Y_1^\varepsilon(\tau)}{\partial \varepsilon}\Big\|_{[0,\tau_0]} \;\le\; \frac{|1-u_0/u^*|}{1-\varepsilon/u^*}\Big(\frac{2}{u^*(1-\varepsilon/u^*)}+\tau_0\Big), \tag{3.50a}$$

$$\Big\|\frac{\partial Y_2^\varepsilon(\tau)}{\partial \varepsilon}\Big\|_{[0,\tau_0]} \;\le\; \frac{|1-u_0/u^*|}{1-\varepsilon/(pu^*)}\Big(\frac{2}{pu^*(1-\varepsilon/(pu^*))}+\tau_0\Big). \tag{3.50b}$$

Since ε_0 is fixed according to (3.45), then, for all $0\le\varepsilon\le\varepsilon_0$, we obtain $1-\varepsilon/u^*\le 1/2$ and $1-\varepsilon/(pu^*)\le 1/2$, and, hence, the estimates (3.50) can be simplified as

$$\Big\|\frac{\partial Y_1^\varepsilon(\tau)}{\partial \varepsilon}\Big\|_{[0,\tau_0]} \;\le\; 2\Big|1-\frac{u_0}{u^*}\Big|\Big(\frac{4}{u^*}+\tau_0\Big), \tag{3.51a}$$

$$\Big\|\frac{\partial Y_2^\varepsilon(\tau)}{\partial \varepsilon}\Big\|_{[0,\tau_0]} \;\le\; 2\Big|1-\frac{u_0}{u^*}\Big|\Big(\frac{4}{pu^*}+\tau_0\Big). \tag{3.51b}$$

Finally, we can use the sum of the right hand sides from (3.51) to obtain $\tilde{N}_{\tau_0}$ as:

$$N_{\tau_0}\le\tilde{N}_{\tau_0}:=4\Big|1-\frac{u_0}{u^*}\Big|\Big(\frac{2}{u^*}\frac{(p+1)}{p}+\tau_0\Big). \tag{3.52}$$

Using (3.45) in (3.52) followed by simple algebraic rearrangements, we obtain (3.46b). Note that Theorem 1 gives $\|y_1^\varepsilon-y_2^\varepsilon\|_\infty\ge M_{\tau_0}-\varepsilon N_{\tau_0}\ge M_{\tau_0}-\varepsilon\tilde{N}_{\tau_0}$.

Let us next analyze this example numerically, to see how tight the estimate from the theorem is. With the values of u_0 and u^* used in Fig. 3.3, we have:

$$\begin{aligned} &M_{\tau_0}=0.2 \quad\text{and}\quad \tilde{N}_{\tau_0}=23.636, \quad\text{for}\quad p=2,\\ &M_{\tau_0}=0.64914 \quad\text{and}\quad \tilde{N}_{\tau_0}=13.169, \quad\text{for}\quad p=20. \end{aligned} \tag{3.53}$$

Tables 3.1 and 3.2 show numerically computed estimates of maximal error obtained by simulation of the system. This numerically computed magnitude of the scale invariance error belongs to the interval

$$M_{\tau_0} - \varepsilon \tilde{N}_{\tau_0} \leq E_\varepsilon \leq M_{\tau_0}\,, \tag{3.54}$$

where E_ε is the magnitude of the scale invariance error, that is, $E_\varepsilon = \|y_1^\varepsilon - y_2^\varepsilon\|_{[0,T]}$ on a short time interval. We see that $E_\varepsilon = M_{\tau_0} + \mathcal{O}(\varepsilon)$. The theoretical predicition is seen numerically to be very tight.

ε	E_ε	$M - N\varepsilon$
10^{-2}	0.19803	-0.03636
10^{-3}	0.199800	0.176364
10^{-4}	0.199980	0.197636
10^{-5}	0.199997	0.199763
10^{-6}	0.199999	0.199976

Table 3.1: A numerical estimation of the magnitude E_ε of the scale invariance error, as a function of the parameter ε, and its comparison with the theoretical prediction lower bound $M_{\tau_0} - \varepsilon N_{\tau_0}$, where the values of M_{τ_0} and N_{τ_0} are given in (3.53). The scaling is $p = 2$.

ε	E_ε	$M - N\varepsilon$
10^{-2}	0.647580	0.517450
10^{-3}	0.648983	0.635971
10^{-4}	0.649124	0.647823
10^{-5}	0.649138	0.649008
10^{-6}	0.649139	0.649126

Table 3.2: A numerical estimation of the magnitude E_ε of the scale invariance error, as a function of the parameter ε, and its comparison with the theoretical prediction lower bound $M_{\tau_0} - \varepsilon N_{\tau_0}$, where the values of M_{τ_0} and N_{τ_0} are given in (3.53). The parameter p is selected as $p = 20$.

3.5.2 A simple feedback system

The next example is the nonlinear system (3.55) obtained by adding a feedback term to the IFFL already analyzed, in the form of a y-dependent degradation of x:

$$\dot{x} = -xy + u^*, \quad x(0) = u_0, \tag{3.55a}$$

$$\varepsilon\dot{y} = x - u^* y, \quad y(0) = 1. \tag{3.55b}$$

Since an analytical solution cannot be obtained for the nonlinear system (3.55), we perform a numerical study. Remarks on how one would proceed to analyze the solution of this system using the boundary function method from [111] are given in Section 3.6, and this example will be revisited in Section 3.6.4. Here, we wish to compute the scale invariance error as a function of the parameter ε at the given fixed value of the scaling factor p. Because the scale invariance error is a function of two equally important parameters ε and p, the values of ε and p have been sampled in the ranges $[0.0005, 0.002]$ and $[0.5, 3.5]$, respectively. The corresponding 2D and 3D plots are presented in Fig. 3.7.

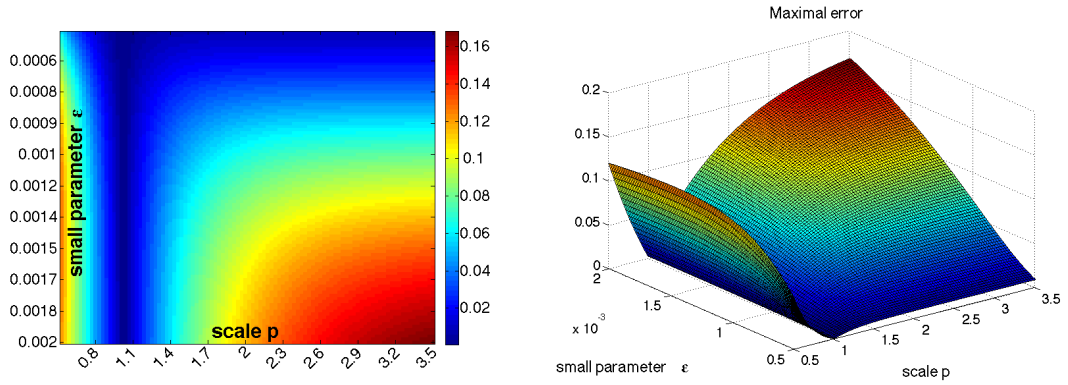

(a) (b)

Figure 3.7: Heatmap and a 3D plot representing the largest absolute value of the difference between the two outputs $y_2(t)$ and $y_1(t)$. The parameter ε was sampled in the range $[0.0005, 0.002]$ and p was sampled in the range $[0.5, 3.5]$. 100 different parameters for each were selected.

We observe from Fig. 3.7 that independently of the value of the parameter ε, the magnitude of the scale invariance error remains finite as $\varepsilon \to 0$, as predicted by the

Theorem.

3.5.3 A chemotaxis signaling pathway of *D. discoideum*

The analysis of the approximate scale invariance property can also be carried out for a more complex mathematical model describing the adaptation kinetics in a eukaryotic chemotaxis signaling pathway of *Dictyostelium discoideum* [102]. The system has been previously introduced in Chapter 2. Conceptually, and ignoring intermediates, we may think of this signaling pathway as an incoherent feedforward loop as shown in Fig. 3.8.

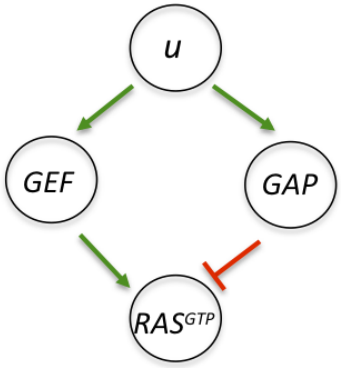

Figure 3.8: A simplified representation of the adaptation signaling pathway for *D. discoideum*.

As the parameter ε is not explicitly given, we sampled parameters k_{RAS} and k_{-RAS} in the range $[100, 5000]$ sec^{-1}, and simulated the six-dimensional system when using a step from 1 to 2 nM of cAMP, and also when stepping from 2 to 4 nM. For the sampled parameters we computed $|y_1(t) - y_2(t)|$, where $y_1(t)$ is a response of Ras^{GTP} when stepping from 1 to 2 nM and $y_2(t)$ stepping from 2 to 4 nM (scale factor $p = 2$). The numerical results are shown on Figures 3.9 and 3.10. Observe that, as expected from theory, there is a minimal value of the error, for each fixed p, as $\varepsilon \to 0$.

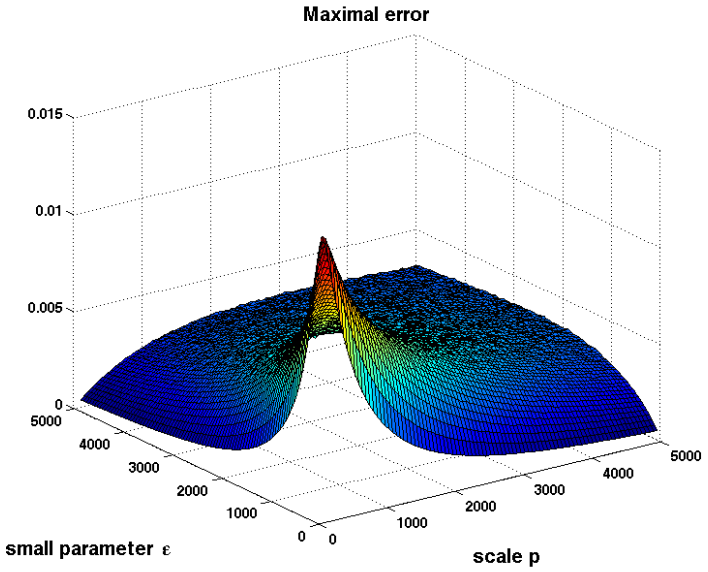

Figure 3.9: 3D plot representing the largest absolute value of the difference between the two outputs $y_1(t)$ and $y_2(t)$. The parameters k_{RAS} and k_{-RAS} were each sampled in a manner described in Fig. 3.10.

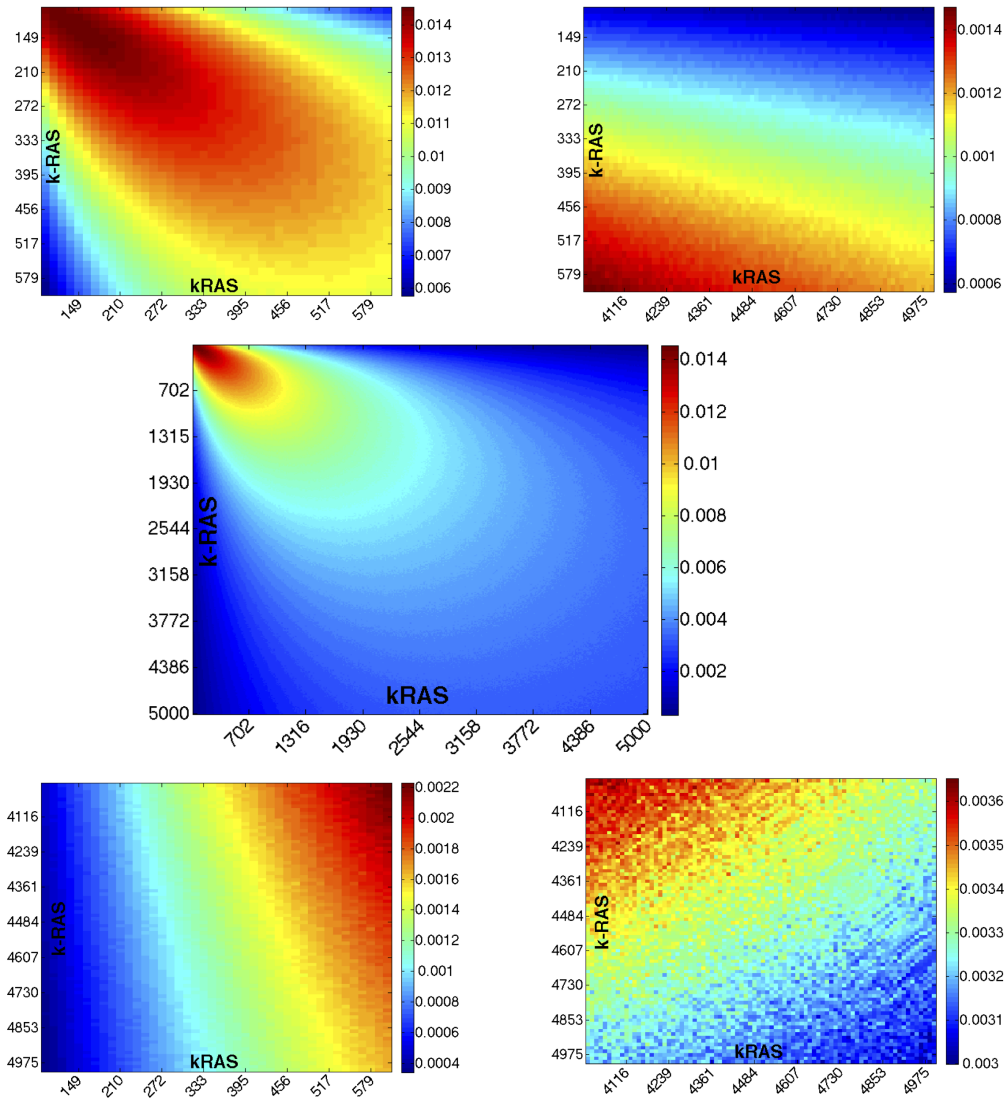

Figure 3.10: Heatmap representing the largest absolute value of the difference between the two outputs $y_1(t)$ and $y_2(t)$ (middle panel). Top and bottom corners were plotted separately to demonstrate the effect of no-zero scale invariance error. The parameters k_{RAS} and k_{-RAS} were each sampled in the range $[100, 5000]$, with a sampling rate $\frac{5000-100}{400}$.

3.6 Asymptotic expansions

The previous analysis is useful when one can compute explicitly solutions to both the original and the $p-$scaled system. We next sketch briefly how one may obtain estimates through the use of tools from singular perturbation theory.

Consider solutions $(x(t;\varepsilon), y(t;\varepsilon))$ and $(z(t;\varepsilon,p), w(t;\varepsilon,p))$ of the following two initial

value problems:

$$\begin{aligned} \dot{x} &= f(x, y, u(t)), \quad x(0) = \sigma_1(u_0), \\ \varepsilon\dot{y} &= g(x, y, u(t)), \quad y(0) = \sigma_2(u_0), \end{aligned} \tag{3.56}$$

and

$$\begin{aligned} \dot{z} &= f(z, w, pu(t)), \quad z(0) = \sigma_1(pu_0), \\ \varepsilon\dot{w} &= g(z, w, pu(t)), \quad w(0) = \sigma_2(pu_0). \end{aligned} \tag{3.57}$$

where the assumptions are the same as before, and $\sigma_1(u_0)$ and $\sigma_2(u_0)$ are the pre-adapted steady states for x and y, when an input u_0 has been applied. Similarly, for z and w. As before, our goal is to investigate the behavior of the scale-invariance error function $E(t; \varepsilon, p)$ defined as:

$$E(t; \varepsilon, p) = w(t; \varepsilon, p) - y(t; \varepsilon) \tag{3.58}$$

on t, p, and ε as $\varepsilon \to 0+$. More precisely, our objective will be to obtain accurate asymptotic series for the difference $E(t; \varepsilon)$ in the small parameter ε.

As in [87], we study the class of systems which satisfy the following homogeneity properties:

$$\begin{aligned} &\sigma(pu) = p\sigma(u), \\ &f(px, y, pu) = pf(x, y, u), \\ &g(px, y, pu) = pg(x, y, u). \end{aligned} \tag{3.59}$$

Then (3.57) can be rewritten in the form:

$$\begin{aligned} \dot{z} &= f(z, w, pu(t)), \quad z(0) = p\sigma_1(u_0), \\ \varepsilon\dot{w} &= g(z, w, pu(t)), \quad w(0) = \sigma_2(u_0). \end{aligned} \tag{3.60}$$

To estimate a lower bound for the scale invariance error in cases where an analytical solution of the system of ODEs cannot be found, it is convenient to employ the theory of singular perturbations [72, 111, 45], and in particular, make use of the *method of boundary functions* [111]. We begin the analysis of the error by stating some basic results from this method, in Sections 3.6.2 and 3.6.3, and also we introduce results concerning the scaling relationship between solutions of the original and p-scaled systems in Section

3.6.1.

3.6.1 Scaling relationships between solutions in reference and p-fold perturbed systems

Since our objective will be to obtain accurate asymptotic series for the difference $E(t;\varepsilon)$ in the small parameter ε, we consider the original (or reference) system (3.56), where the parameter ε is replaced by a new p-scaled parameter $\varepsilon_p = \varepsilon/p$ for some $p > 0$.

Lemma 4. I. *Let $(x(t;\varepsilon), y(t;\varepsilon))$ be the solution of the original system* (3.56)*, depending continuously on the parameter ε, that is, $x(t;\varepsilon)$ and $y(t;\varepsilon)$ are continuous functions of two arguments, t and ε. Assume that we seek the solution $(z(t;\varepsilon), w(t;\varepsilon))$ of the p-scaled system* (3.57)*. Then $(z(t;\varepsilon), w(t;\varepsilon))$ can be found from the following scaling transformations applied simultaneously to the state variable x and the parameter ε,*

$$\begin{aligned} z(t;p,\varepsilon) &= px(t;p^{-1}\varepsilon), \\ w(t;p,\varepsilon) &= y(t;p^{-1}\varepsilon). \end{aligned} \tag{3.61}$$

II. *Conversely, given the solution $(z(t;\varepsilon), w(t;\varepsilon))$ of the p-scaled system* (3.57)*, the scaling relationships* (3.62) *can be used to find the corresponding solution $(x(t;\varepsilon), y(t;\varepsilon))$ of the original system* (3.56)*,*

$$\begin{aligned} x(t;\varepsilon) &= p^{-1}z(t;p\varepsilon), \\ y(t;\varepsilon) &= w(t;p\varepsilon). \end{aligned} \tag{3.62}$$

Proof. After differentiation of the first equality in (3.61) with respect to t, and then using both (3.56), where ε is replaced by ε/p, and (3.59), we obtain

$$\begin{aligned} \dot{z}(t;p,\varepsilon) &= p\dot{x}(t;p^{-1}\varepsilon) \\ &= pf(x(t;p^{-1}\varepsilon), y(t;p^{-1}\varepsilon), u(t)) \\ &= f(px(t;p^{-1}\varepsilon), y(t;p^{-1}\varepsilon), pu(t)) \\ &= f(z(t;\varepsilon), w(t;\varepsilon), pu(t)). \end{aligned} \tag{3.63}$$

We immediately conclude from (3.63) that $z(t;\varepsilon)$ satisfies the first equation in (3.60).

By analogy, after differentiation of the second equality of (3.61) with respect to t, we obtain

$$\begin{aligned} \dot{w}(t;p,\varepsilon) &= \dot{y}(t;p^{-1}\varepsilon) \\ &= g(x(t;p^{-1}\varepsilon), y(t;p^{-1}\varepsilon), u(t))/(\varepsilon/p) \\ &= \varepsilon^{-1} p g(x(t;p^{-1}\varepsilon), y(t;p^{-1}\varepsilon), u(t)) \\ &= \varepsilon^{-1} g(px(t;p^{-1}\varepsilon), y(t;p^{-1}\varepsilon), pu(t)) \\ &= \varepsilon^{-1} g(z(t;\varepsilon), w(t;\varepsilon), pu(t)). \end{aligned} \tag{3.64}$$

After multiplication of (3.64) with ε, we can immediately conclude that $w(t;\varepsilon)$ satisfies the second equation of the IVP (3.60). The proof of Lemma 4 follows. □

3.6.2 Asymptotic expansions

For any fixed integer $N > 0$, we seek asymptotic expansions in the standard form [111],

$$x_N(t;\varepsilon) = \sum_{k=0}^{N} \varepsilon^k \Big(\bar{x}_k(t) + \bar{X}_k(t/\varepsilon) \Big), \tag{3.65}$$

$$y_N(t;\varepsilon) = \sum_{k=0}^{N} \varepsilon^k \Big(\bar{y}_k(t) + \bar{Y}_k(t/\varepsilon) \Big). \tag{3.66}$$

Here, $\bar{x}_k(t)$ and $\bar{y}_k(t)$ are called *regular* terms. Let τ be a stretched time, $\tau = t/\varepsilon$. Then, $\bar{X}_k(\tau)$ and $\bar{Y}_k(\tau)$ are called *boundary functions* (or, *singular* terms). All terms are independent of ε.

Lemma 5. *A formal expansions in ε for the p-scaled system* (3.60) *can be obtained from* (3.65)-(3.66) *obtained for the original system* (3.56)*, using the change of variables* (3.61) *as defined in Lemma 4,*

$$z_N(t;p,\varepsilon) = \sum_{k=0}^{N} \Big(\frac{\varepsilon}{p}\Big)^k \Big(\bar{x}_k(t) + \bar{X}_k(pt/\varepsilon) \Big), \tag{3.67}$$

$$w_N(t;p,\varepsilon) = \sum_{k=0}^{N} \Big(\frac{\varepsilon}{p}\Big)^k \Big(\bar{y}_k(t) + \bar{Y}_k(pt/\varepsilon) \Big). \tag{3.68}$$

Proof. The proof follows immediately from (3.61), see Lemma 4. □

The theory of singular perturbations [111] provides conditions under which (3.65)-(3.66) and (3.67)-(3.68) approximate asymptotically the solution $(x(t;\varepsilon), y(t;\varepsilon))$ of (3.56) and $(z(t;p,\varepsilon), w(t;p,\varepsilon))$ of (3.60), respectively, with the accuracy $\mathcal{O}(\varepsilon^{N+1})$ as $\varepsilon \to 0$. Using the boundary function algorithm one can show that these are asymptotic series, under reasonable regularity assumptions on f and g. We will also assume that the equation $g(x,y,u) = 0$ has a unique solution $y = h(x,u)$ for all (x,u) in an open domain of interest.

3.6.3 The boundary function method

We customize the asymptotic expansion algorithm from [111, Sect.2.1.2, p.20] with the objective to derive all asymptotic estimates adapted to our problem explicitly. Additionally, we would like to obtain a lower bound for the scale invariance error, for both reference (3.56) and p-scaled (3.60) systems. To estimate a lower bound for the error, it is enough to compute the zeroth order terms:

$$\begin{aligned} x(t;\varepsilon) &\sim \bar{x}_0(t) + \bar{X}_0(t/\varepsilon) + \mathcal{O}(\varepsilon), \\ y(t;\varepsilon) &\sim \bar{y}_0(t) + \bar{Y}_0(t/\varepsilon) + \mathcal{O}(\varepsilon), \end{aligned} \tag{3.69}$$

where $\bar{x}_0(t)$ and $\bar{y}_0(t)$ are the zeroth-order regular terms, and $\bar{X}_0(\tau)$ and $\bar{Y}_0(\tau)$ are called boundary functions (or, singular terms). Similar considerations would apply to higher-order expansions. One can then show, using the homogeneity properties (3.59), that

$$\begin{aligned} z(t;\varepsilon,p) &\sim \bar{x}_0(t) + \bar{X}_0(pt/\varepsilon) + \mathcal{O}(\varepsilon), \\ w(t;\varepsilon,p) &\sim \bar{y}_0(t) + \bar{Y}_0(pt/\varepsilon) + \mathcal{O}(\varepsilon), \end{aligned} \tag{3.70}$$

We start from:

$$\begin{aligned} x_0(t;\varepsilon) &= \bar{x}_0(t) + \bar{X}_0(t/\varepsilon), \\ y_0(t;\varepsilon) &= \bar{y}_0(t) + \bar{Y}_0(t/\varepsilon). \end{aligned} \tag{3.71}$$

Because we seek singular boundary functions $\bar{X}_0(t/\varepsilon)$ and $\bar{Y}_0(t/\varepsilon)$ rapidly decaying as $t \to \infty$, the corresponding boundary conditions at infinity are required,

$$\bar{X}_0(\infty) = 0 \text{ and } \bar{Y}_0(\infty) = 0. \tag{3.72}$$

For simplicity, we separate slow and fast time scales in (3.71) explicitly by formally introducing the stretched time $\tau = t/\varepsilon$ for the singular terms in (3.71), and obtain

$$\begin{aligned} x_0(t;\tau) &= \bar{x}_0(t) + \bar{X}_0(\tau), \\ y_0(t;\tau) &= \bar{y}_0(t) + \bar{Y}_0(\tau). \end{aligned} \tag{3.73}$$

To compute $\bar{x}_0(t)$, $\bar{X}_0(\tau)$, $\bar{y}_0(t)$, and $\bar{Y}_0(\tau)$, we substitute (3.73) into (3.56),

$$\begin{aligned} \dot{\bar{x}}_0(t) + \varepsilon^{-1}\bar{X}_0'(\tau) &= f(\bar{x}_0(t) + \bar{X}_0(\tau), \bar{y}_0(t) + \bar{Y}_0(\tau, u(t)), \\ \varepsilon\dot{\bar{y}}_0(t) + \bar{Y}_0'(\tau) &= g(\bar{x}_0(t) + \bar{X}_0(\tau), \bar{y}_0(t) + \bar{Y}_0(\tau), u(t)). \end{aligned} \tag{3.74}$$

Here $\dot{(\cdot)} = d(\cdot)/dt$ and $(\cdot)' = d(\cdot)/d\tau$. Using (3.72), we additionally obtain

$$\begin{aligned} \bar{x}_0(0) + \bar{X}_0(0) = x_0, \quad \bar{X}_0(\infty) = 0, \\ \bar{y}_0(0) + \bar{Y}_0(0) = y_0, \quad \bar{Y}_0(\infty) = 0. \end{aligned} \tag{3.75}$$

Rewrite (3.74) in the equivalent form, see [111],

$$\begin{aligned} \dot{\bar{x}}_0(t) + \varepsilon^{-1}\bar{X}_0'(\tau) &= \bar{f}(t;\varepsilon) + \bar{F}(\tau;\varepsilon), \\ \varepsilon\dot{\bar{y}}_0(t) + \bar{Y}_0'(\tau) &= \bar{g}(t;\varepsilon) + \bar{G}(\tau;\varepsilon), \end{aligned} \tag{3.76}$$

$$\begin{aligned} \bar{f}(t;\varepsilon) &= f(\bar{x}_0(t), \bar{y}_0(t), u(t)), \\ \bar{F}(\tau;\varepsilon) &= f(\bar{x}_0(\varepsilon\tau) + \bar{X}_0(\tau), \bar{y}_0(\varepsilon\tau) + \bar{Y}_0(\tau), u(\varepsilon\tau)) \\ &\quad - f(\bar{x}_0(\varepsilon\tau), \bar{y}_0(\varepsilon\tau), u(\varepsilon\tau)), \end{aligned} \tag{3.77}$$

$$\begin{aligned} \bar{g}(t;\varepsilon) &= g(\bar{x}_0(t), \bar{y}_0(t), u(t)), \\ \bar{G}(\tau;\varepsilon) &= g(\bar{x}_0(\varepsilon\tau) + \bar{X}_0(\tau), \bar{y}_0(\varepsilon\tau) + \bar{Y}_0(\tau), u(\varepsilon\tau)) \\ &\quad - g(\bar{x}_0(\varepsilon\tau), \bar{y}_0(\varepsilon\tau), u(\varepsilon\tau)). \end{aligned} \tag{3.78}$$

We expand $\bar{f}(t;\varepsilon)$, $\bar{F}(\tau;\varepsilon)$, $\bar{g}(t;\varepsilon)$, and $\bar{G}(\tau;\varepsilon)$ into the corresponding Taylor series at $\varepsilon = 0$ in the right-hand sides of (3.76), and, then, equate coefficients at like powers of ε on both sides of (3.76), separately for the coefficients depending on t and τ.

It follows from (3.76) and (3.75) that $\bar{X}_0(\tau) \equiv 0$. For the regular leading terms $\bar{x}_0(t)$

and $\bar{y}_0(t)$, we obtain

$$\begin{aligned} \dot{\bar{x}}_0 &= f(\bar{x}_0, y_0, u(t)),\ \bar{x}_0(0) = x_0, \\ 0 &= g(\bar{x}_0, y_0, u(t)). \end{aligned} \tag{3.79}$$

Let $\bar{y}_0 = h(\bar{x}_0, u(t))$ be the unique root of the scalar algebraic equation in (3.79) .Using $\bar{y}_0 = h(\bar{x}_0, u(t))$ in the differential equation (3.79), we obtain the reduced system

$$\dot{\bar{x}}_0 = f(\bar{x}_0, h(\bar{x}_0, u(t)), u(t)),\ \bar{x}_0(0) = x_0,\ t \in [0, T]. \tag{3.80}$$

Let $\bar{x}_0(t)$ be the unique solution of the IVP (3.80). Then, $y_0(t) = h(\bar{x}_0(t), u(t))$.

After setting $\varepsilon = 0$ and equating terms depending on τ in the second equation of (3.76), we obtain

$$\bar{Y}_0' = g(x_0, y^* + \bar{Y}_0, u^*) - g(x_0, y^*, u^*),\ \bar{Y}_0(0) = y_0 - \bar{y}_0(0). \tag{3.81}$$

Recall that $\bar{y}_0(0) = h(x(0), u(0)) = h(x_0, u^*) = y^*$ and $u^* = u(0+)$. Hence, $\bar{Y}_0(0) = y_0 - y^* = \Delta y$ in (3.81). We know, in general, that y_0 is the preadapted initial condition, and hence obtained from $y_0 = h(x_0, u_0)$. To have (3.71), we need to replace τ by t, $\tau = t/\varepsilon$, in the solution of (3.81), that is, $\bar{Y}_0(\tau)$. Additionally, we obtain

$$\begin{aligned} \bar{z}_0(t; \varepsilon, p) &= p\bar{x}_0(t), \\ \bar{w}_0(t; \varepsilon, p) &= \bar{y}_0(t) + \bar{Y}_0(pt/\varepsilon). \end{aligned} \tag{3.82}$$

Using (3.69) and (3.70), and recalling the definition (3.58) of the SI-error $E(t; \varepsilon, p)$, we conclude that the zeroth-order approximation $E_0(t; \varepsilon, p)$ of $E(t; \varepsilon, p)$ is:

$$E_0(t; \varepsilon, p) \ = \ E_0(t/\varepsilon; p) \ = \ \bar{Y}_0(pt/\varepsilon) - \bar{Y}_0(t/\varepsilon). \tag{3.83}$$

Obviously, $E(t; \varepsilon, 1) \equiv E_0(t/\varepsilon) \equiv 0$ at $p = 1$. Under uniform stability assumptions on g, one can derive, using the theory of asymptotic expansions, an estimate of the following form:

$$\|E_0(\cdot; \varepsilon, p)\|_T \geq M_0, \tag{3.84}$$

where

$$M_0 = \sup_{\tau\in[0,\infty]} \left\|\bar{Y}_0(p\tau) - \bar{Y}_0(\tau)\right\|, \tag{3.85}$$

and

$$M_0 \;=\; \mathcal{O}\left(\phi(u_0,u^*)\left|\alpha p-1\right|(\alpha p)^{\alpha p/(1-\alpha p)}\right) \tag{3.86}$$

where α is a positive constant independent of ε and p, $\phi(u_0,u^*)$ is a factor that equals zero when $u_0 = u^*$. It follows that $E = E_0 + \mathcal{O}(\varepsilon)$ always satisfies an estimate similar to the one in our simple example (3.6). This is guaranteed also by our general Theorem 1 in Section 3.4.

3.6.4 Feedback example revisited

Consider a system given by:

$$\begin{aligned} \tfrac{dx}{dt} &= -xy + u, \\ \varepsilon\tfrac{dy}{dt} &= x - uy, \end{aligned} \tag{3.87}$$

with the initial conditions: $x(0) = u_0$, $y(0) = y^0$. For this example we will derive both the first- and the second-order terms in the expansions, to demonstrate the how complexity of the calculations increases drastically even for this simple example, and to point out the power of the application of our Thoerem 1 in estimating the irreducible error. The solutions of (3.87) can be represented in terms of expansions as:

$$\begin{aligned} x(t,\varepsilon) &= \bar{x}_0(t) + \varepsilon\bar{x}_0(t) + \bar{X}_0(\tfrac{t}{\varepsilon}) + \varepsilon\bar{X}_1(\tfrac{t}{\varepsilon}), \\ y(t,\varepsilon) &= \bar{y}_0(t) + \varepsilon\bar{y}_1(t) + \bar{Y}_0(\tfrac{t}{\varepsilon}) + \varepsilon\bar{Y}_1(\tfrac{t}{\varepsilon}). \end{aligned} \tag{3.88}$$

Applying the expansions (3.88) to (3.87), and denoting $\frac{t}{\varepsilon} = \tau$ we have

$$\begin{gathered} \dot{\bar{x}}_0(t) + \varepsilon\dot{\bar{x}}_1(t) + \tfrac{1}{\varepsilon}\dot{\bar{X}}_0(\tau) + \dot{\bar{X}}_1(\tau) \;= \\ -\Big(\bar{x}_0(t) + \varepsilon\bar{x}_1(t) + \bar{X}_0(\tau) + \varepsilon\bar{X}_1(\tau)\Big)\Big(\bar{y}_0(t) + \varepsilon\bar{y}_1(t) + \bar{Y}_0(\tau) + \varepsilon\bar{Y}_1(\tau)\Big) + u \;= \\ -\Big[\bar{y}_0(t)\bar{x}_0(t) + \varepsilon\bar{x}_1(t)\bar{y}_0(t) + \bar{y}_0(\varepsilon\tau)\bar{X}_0(\tau) + \varepsilon\bar{y}_0(\varepsilon\tau)\bar{X}_1(\tau) + \varepsilon\bar{y}_1(t)\bar{x}_0(t) + O(\varepsilon^2) \\ +\varepsilon\bar{y}_1(\varepsilon\tau)\bar{X}_0(\tau) + O(\varepsilon^2) + \bar{Y}_0(\tau)\bar{x}_0(\varepsilon\tau) + \varepsilon\bar{Y}_0(\tau)\bar{x}_1(\varepsilon\tau) + \bar{Y}_0(\tau)\bar{X}_0(\tau) + \varepsilon\bar{Y}_0(\tau)\bar{X}_1(\tau) \\ +\varepsilon\bar{Y}_1(\tau)\bar{x}_0(\varepsilon\tau) + O(\varepsilon^2) + \bar{Y}_1(\tau)\bar{X}_0(\tau) + O(\varepsilon^2)\Big] + u \end{gathered}$$

Clearly, $\frac{1}{\varepsilon}\dot{\bar{X}}_0(\tau) = 0$, and therefore:

$$\bar{X}_0(\tau) = 0. \tag{3.89}$$

The system simplifies to:

$$\begin{aligned}
\dot{\bar{x}}_0(t) + \varepsilon\dot{\bar{x}}_1(t) + \dot{\bar{X}}_1(\tau) = -\Big[\bar{y}_0(t)\bar{x}_0(t) + \varepsilon\bar{x}_1(t)\bar{y}_0(t) + \varepsilon\bar{y}_0(\varepsilon\tau)\bar{X}_1(\tau) + \varepsilon\bar{y}_1(t)\bar{x}_0(t) \\
+\bar{Y}_0(\tau)\bar{x}_0(\varepsilon\tau) + \varepsilon\bar{Y}_0(\tau)\bar{x}_1(\varepsilon\tau) + \varepsilon\bar{Y}_0(\tau)\bar{X}_1(\tau) + \varepsilon\bar{Y}_1(\tau)\bar{x}_0(\varepsilon\tau)\Big] + u = \\
-\Big[\bar{y}_0(t)\bar{x}_0(t) + \varepsilon\bar{x}_1(t)\bar{y}_0(t) + \varepsilon\bar{y}_0(0)\bar{X}_1(\tau) + \varepsilon\bar{y}_1(t)\bar{x}_0(t) + \bar{Y}_0(\tau)[\bar{x}_0(0) + \varepsilon\bar{x'}_0(0)] \\
+\varepsilon\bar{Y}_0(\tau)\bar{x}_1(0) + \varepsilon\bar{Y}_0(\tau)\bar{X}_1(\tau) + \varepsilon\bar{Y}_1(\tau)\bar{x}_0(0)\Big] + u
\end{aligned}$$

The previous equation is equivalent to the following set of ODEs:

$$\begin{aligned}
\dot{\bar{x}}_0(t) &= -\bar{y}_0(t)\bar{x}_0(t) + u, \\
\dot{\bar{x}}_1(t) &= -\bar{x}_1(t)\bar{y}_0(t) - \bar{y}_1(t)\bar{x}_0(t), \\
\dot{\bar{X}}_1(\tau) &= -\bar{x}_0(0)\bar{Y}_0(\tau).
\end{aligned} \tag{3.90}$$

Using the initial conditions for x we have:

$$\bar{x}_0(0) + \varepsilon\bar{x}_1(0) + \bar{X}_0(0) + \varepsilon\bar{X}_1(0) = u_0, \tag{3.91}$$

which decouples into:

$$\begin{aligned}
\bar{x}_0(0) + \bar{X}_0(0) = u_0, \\
\bar{x}_1(0) + \bar{X}_1(0) = 0.
\end{aligned}$$

Since we already know from (3.89) that $\bar{X}_0(0) = 0$ we have that:

$$\begin{aligned}
\bar{x}_0(0) = u_0, \\
\bar{X}_1(0) = -\bar{x}_1(0).
\end{aligned} \tag{3.92}$$

Now let's solve the set of equations for y :

$$\begin{aligned}
\varepsilon\dot{\bar{y}}_0(t) + \varepsilon^2\dot{\bar{y}}_1(t) + \dot{\bar{Y}}_0(\tau) + \varepsilon\dot{\bar{Y}}_1(\tau) = \\
\bar{x}_0(t) + \varepsilon\bar{x}_0(t) + \bar{X}_0(\tau) + \varepsilon\bar{X}_1(\tau) - u\bar{y}_0(t) - \varepsilon u\bar{y}_1(t) - u\bar{Y}_0(\tau) - \varepsilon u\bar{Y}_1(\tau)
\end{aligned}$$

Thus, we get the following set of differential equations:

$$\begin{aligned} \bar{x}_0(t) - u\bar{y}_0(t) &= 0\,, \quad \dot{\bar{y}}_0(t) = \bar{x}_1(t) - u\bar{y}_1(t), \\ \dot{\bar{Y}}_0(\tau) &= -u\bar{Y}_0(\tau)\,, \quad \dot{\bar{Y}}_1(\tau) = \bar{X}_1(\tau) - u\bar{Y}_1(\tau), \end{aligned} \tag{3.93}$$

which yield:

$$\begin{aligned} \bar{y}_0(t) &= \tfrac{\bar{x}_0(t)}{u}\,, \quad \bar{y}_1(t) = \tfrac{\bar{x}_1(t)-\dot{\bar{y}}_0(t)}{u}, \\ \bar{Y}_0(\tau) &= \bar{Y}_0(0)e^{-u\tau}. \end{aligned} \tag{3.94}$$

Using the initial conditions for y we have:

$$\bar{y}_0(0) + \varepsilon\bar{y}_1(0) + \bar{Y}_1(0) + \varepsilon\bar{Y}_1(0) = y^0,$$

which decouples into:

$$\bar{y}_0(0) + \bar{Y}_0(0) = y^0\,, \quad \bar{y}_1(0) + \bar{Y}_1(0) = 0.$$

Hence,

$$\bar{y}_0(0) + \bar{Y}_0(0) = y^0\,, \quad \bar{Y}_1(0) = -\bar{y}_1(0). \tag{3.95}$$

From (3.90) we have:

$$\begin{aligned} \dot{\bar{x}}_0(t) &= \tfrac{\bar{x}_0^2(t)}{u} + u = \tfrac{\bar{x}_0^2(t)+u^2}{u}, \\ \tfrac{d\bar{x}_0(t)}{u^2-\bar{x}_0^2(t)} = \tfrac{dt}{u} \quad &\Rightarrow \quad \int\limits_{\bar{x}_0(0)}^{\bar{x}_0(t)} \tfrac{d\bar{x}_0(t)}{(\bar{x}_0(t)-u)(\bar{x}_0(t)+u)} = \int\limits_0^t -\tfrac{dt}{u} \end{aligned}$$

Using that $\bar{x}_0(0) = u_0$,

$$\bar{x}_0(t) = \tfrac{u(e^{2t}+k)}{(e^{2t}-k)} = \tfrac{u(e^{2t}+\frac{u_0-u}{u_0+u})}{(e^{2t}-\frac{u_0-u}{u_0+u})}\,, \quad k = \tfrac{u_0-u}{u_0+u}. \tag{3.96}$$

Applying the second equation from (3.94) to (3.90) we obtain:

$$\dot{\bar{x}}_1(t) = -2\bar{y}_0(t)\bar{x}_1(t) + \tfrac{\bar{x}_0(t)\dot{\bar{x}}_0(t)}{u^2} \tag{3.97}$$

From (3.96),

$$\dot{\bar{x}}_0(t) = -\frac{4uke^{2t}}{(e^{2t}-k)^2} \quad \text{and} \quad \frac{\bar{x}_0(t)\dot{\bar{x}}_0(t)}{u^2} = -\frac{4ke^{2t}(e^{2t}+k)}{(e^{2t}-k)^3}$$

Substituting in (3.97), and using (3.94) and (3.96)

$$\begin{aligned} \dot{\bar{x}}_1(t) &= -\tfrac{2(e^{2t}+k)}{(e^{2t}-k)}\bar{x}_1(t) - \tfrac{4ke^{2t}(e^{2t}+k)}{(e^{2t}-k)^3} \\ \bar{x}_1(t) &= \tfrac{e^{2t}\left(\bar{x}_1(0)-2\bar{x}_1(0)k+4k\ln(1-k)+4kt+\bar{x}_1(0)k^2-4k\ln(e^{2t}-k)\right)}{(k-e^{2t})^2} \end{aligned} \tag{3.98}$$

From (3.94):

$$\bar{y}_1(t) = \tfrac{\bar{x}_1(t)+\frac{4ke^{2t}}{(e^{2t}-k)^2}}{u}$$

Using (3.98):

$$\bar{y}_1(t) = \tfrac{e^{2t}\left(\bar{x}_1(0)(1-k)^2+4kt+4k\ln(\frac{1-k}{e^{2t}-k})\right)+4ke^{2t}}{u(k-e^{2t})^2} \tag{3.99}$$

The initial condition for $\bar{y}_1$ and $\bar{y}_0$ can be expressed as:

$$\bar{y}_1(0) = \tfrac{\bar{x}_1(0)(1-k)^2+4k}{u(1-k)^2} = \tfrac{\bar{x}_1(0)}{u} + \tfrac{4k}{u(1-k)^2}\,, \quad \bar{y}_0(0) = \tfrac{\bar{x}_0(0)}{u} = \tfrac{u_0}{u} \tag{3.100}$$

Using (3.94), (3.95):

$$\bar{Y}_0(\tau) = \bar{Y}_0(0)e^{-u\tau} = (y^0 - \bar{y}_0(0))e^{-u\tau} = (y^0 - \tfrac{u_0}{u})e^{-u\tau} \tag{3.101}$$

$$\begin{aligned} \dot{\bar{X}}_1(\tau) &= -\bar{x}_0(0)\bar{Y}_0(\tau) = -u_0(y^0 - \tfrac{u_0}{u})e^{-u\tau}, \\ \bar{X}_1(\tau) &= -\bar{x}_1(0) + \tfrac{u_0}{u}(y^0 - \tfrac{u_0}{u})(e^{-u\tau} - 1). \end{aligned} \tag{3.102}$$

Combining (3.93) and (3.102)

$$\dot{\bar{Y}}_1(\tau) = k_3 + k_2e^{-u\tau} - u\bar{Y}_1(\tau) \tag{3.103}$$

where $k_2 = \frac{u_0}{u}(y^0 - \frac{u_0}{u})$ and $k_3 = -\bar{x}_1(0) - k_2$. The solution is given by:

$$\bar{Y}_1(\tau) = \bar{Y}_1(0)e^{-u\tau} + \tfrac{\bar{x}_1(0)+k_2}{u}e^{-u\tau} + k_2\tau e^{-u\tau} - \tfrac{\bar{x}_1(0)+k_2}{u} \tag{3.104}$$

From (3.95):

$$\bar{Y}_1(0) \;=\; -\bar{y}_1(0) \;=\; -\tfrac{\bar{x}_1(0)}{u} - \tfrac{4k}{u(1-k)^2} \tag{3.105}$$

Next, in order to find the missing initial condition $\bar{x}_1(0)$ we need to take into account that the boundary functions vanish as $\tau \to \infty$. For $\bar{Y}_1(\tau)$ from (3.104) we have $\bar{Y}_1(\infty) = -\frac{\bar{x}_1(0)+k_2}{u} = 0$. Hence,

$$\bar{x}_1(0) = -k_2 = \tfrac{u_0}{u}(\tfrac{u_0}{u} - y^0). \tag{3.106}$$

Similarly, if we require $\bar{X}_1(\infty) = 0$ the same result follows. From (3.106), and the expressions for k, k_2 and k_3, the complete solution of the problem can be written as:

$$\begin{aligned}
\bar{y}_0(t) &= \tfrac{(u_0+u)e^{2t}+u_0-u}{(u_0+u)e^{2t}-(u_0-u)}\,, \quad \bar{Y}_0(\tfrac{t}{\varepsilon}) = (y^0 - \tfrac{u_0}{u})e^{-\frac{ut}{\varepsilon}}, \\
\bar{y}_1(t) &= \frac{4e^{2t}\Big[u_0u(\frac{u_0}{u}-y^0)+((u_0)^2-u^2)\Big\{t+ln\Big(\frac{2u}{(u_0+u)e^{2t}-(u_0-u)}\Big)+1\Big\}\Big]}{u((u_0+u)e^{2t}-(u_0-u))^2}, \\
\bar{Y}_1(\tfrac{t}{\varepsilon}) &= \Big(-\tfrac{u_0}{u^2}(\tfrac{u_0}{u}-y^0) - \tfrac{(u_0-u)(u_0+u)}{u^3}\Big)e^{-\frac{ut}{\varepsilon}} + \tfrac{u_0}{u}(y^0-\tfrac{u_0}{u})\tfrac{t}{\varepsilon}e^{-\frac{ut}{\varepsilon}}.
\end{aligned} \tag{3.107}$$

Applying Lemma (5) we additionally obtain

$$\bar{z}(t;p,\varepsilon) = p\bar{x}_0(t) + \frac{\varepsilon}{p}\Big(\bar{x}_1(t) + \bar{X}_1(pt/\varepsilon)\Big), \tag{3.108}$$

$$\bar{w}(t;p,\varepsilon) = \bar{y}_0(t) + \bar{Y}_0(pt/\varepsilon) + \frac{\varepsilon}{p}\Big(\bar{y}_1(t) + \bar{Y}_1(pt/\varepsilon)\Big). \tag{3.109}$$

Ignoring the first order terms, we

$$\begin{aligned}
&\bar{y}_0(t) = \frac{(u_0+u)e^{2t}+u_0-u}{(u_0+u)e^{2t}-(u_0-u)}\,, \quad \bar{x}_0(t) = u\bar{y}_0(t)\,, \\
&\bar{Y}_0(\frac{t}{\varepsilon}) = (y^0 - \frac{u_0}{u})e^{-\frac{ut}{\varepsilon}}\,, \\
&\bar{z}(t;p,\varepsilon) = p\bar{x}_0(t)\,, \quad \bar{w}(t;p,\varepsilon) = \bar{y}_0(t) + \bar{Y}_0(pt/\varepsilon).
\end{aligned}$$

Chapter 4

Estimation of a rate function of a nonhomogeneous Poisson process (NHPP)

It is of great importance to quantify adaptation and scale-invariance properties for an arbitrary class of experimentally controlled stimuli, to help us understand the molecular mechanisms which these properties entail, [65]. Novel experimental methods based on microfluidics devices provide powerful tools to design a controlled experiment where a behavior of individual cells and a population of cells can be assayed.

Hence, motivated by experimental challenges, and the current work we are pursuing with our experimental collaborators in the design of microfluidic devices that will allow the same (designed) inputs to be fed to a population of chemotactic bacteria, we use microscope-based observations of tumbling events for estimation of the tumbling rate (which is a function of chemotactic protein concentrations). In the case of bacteria *E. coli*, the schematic representing the estimation problem we are posing here is given on Fig. 1.5, where we are interested in estimating the concentration of $CheY - P$, and consequently due to linear relationship between them, the concentration of active kinease $CheA$, $a(t)$, in the model (1.4). Unlike in the example for *E. coli*, where direct input/output relationship has already been established through experiments based on FRET, for many bacterial species of interest FRET experiments which require extensive genetic modifications are not available, and alternative methods for assessing their behavior must be used.

In this chapter we are looking at the estimation problem arising from modeling such biological phenomena in which discrete measurements such as "spikes" or "tumbles" are measured, and the objective is to estimate the underlying rate of a nonhomogeneous Poisson process (NHPP) that describes these events.

In our applications, a small number of realizations is available, through single-cell measurements of a population of bacteria. Current microfluidic technology, described in Chapter 1, allows us to assume that internal variables (protein concentrations) in the system behave reasonably identically, so that the only source of randomness is in a jump process driven by these internal variables. Superficially analogous problems have been studied in various disciplines.

In the statistics and signal processing literature, this problem has been studied for certain special classes of signals. We will discuss several groups of commonly used methods from the literature, divided into subgroups: methods using the cumulative intensity function (nonparametric methods), parametric models, and methods from neuroscience which use a Bayesian framework.

Parametric models for the rate of a nonhomogeneous Poisson process, $\lambda(t)$, have been very frequently assumed in the literature. In that case, one could look for a maximum likelihood (ML) estimate of parameters. This amounts essentially to a maximum a posteriori (MAP) estimate with a uniform distribution on parameters as prior [46]. However, there is no natural probabilistic structure in our applications to suggest the most natural prior; even a conjugate prior to the given Poisson model would not be necessarily justified.

On the other hand, often the ultimate objective is control, in which case estimates of current states (and specifically of the current $\lambda(t)$) are more important than estimates of the entire history. This suggests the use of observers, or more generally Kalman filters, as done routinely in control theory, to obtain estimates that asymptotically improve.

A problem in which a diffusion (stochastic differential equation) describes the evolution of internal parameters and a NHPP is observed, is analyzed in [110], [13]. Our problem is substantially different, because no randomness is assumed in the internal variables, but repeated realizations are observed.

In the next subsections, we highlight most commonly used approaches, and indicate the reasons why we could not adapt them for our purposes.

4.1 Methods used in the literature

4.1.1 Maximum likelihood results

In statistics literature, (see for instance [50]) the unknown rate function $\lambda(t)$ of a NHPP is modeled as an exponential-polynomial-trigonometric function with multiple periodicities. Long term evolutionary trends are represented by polynomial terms, and potential periodic effects are introduced by the appropriate number of harmonics of the corresponding phases, frequencies and magnitudes. The positivity condition of is guaranteed by taking an exponential of it; i.e.

$$\begin{aligned} \lambda(t) &= e^{h(t;m,p,\Theta)}, \\ h(t;m,p,\Theta) &= \sum_{i=0}^{m} \alpha_i t^i + \sum_{j=1}^{p} \gamma_k \sin(\omega_k t + \phi_k) \end{aligned} \tag{4.1}$$

with $\Theta = [\alpha_0, \alpha_1, \cdots, \alpha_m, \gamma_1, \cdots \gamma_p, \phi_1, \cdots \phi_p, \omega_1, \cdots \omega_p]$. Then one looks for log-likelihood function of Θ, given $N(T) = n$, total number of event by time T, and $\mathbf{t} = (t_1, t_2, \cdots t_n)$, event (arrival) times.

$$\mathcal{L}(\Theta|n, \mathbf{t}) = \sum_{i=0}^{m} \alpha_i T^i + \sum_{k=1}^{p} \sum_{j=1}^{n} \gamma_k \sin(\omega_k t + \phi_k) - \int_0^T e^{h(z;m,p,\Theta)} dz$$

The authors in [50, 48, 49] provide a method for the inference of the initial parameter estimates; initial estimates for (γ's and ϕ's) were found using Fourier analysis, moment matching procedure were used for identifying the polynomial coefficients, and a likelihood ratio test is used to decide on the number of polynomial terms. The importance of good choice of initial guesses lies in the fact that Newton-Raphson method can be unstable when it is applied to the system of likelihood equations outside a small neighborhood of the optimal solution. However, the methods applied in [50] do not guarantee that the initial estimates will converge to a global extremum of the log-likelihood function.

In the communications literature, the problem of estimating the rate function of a

NHPP arises in problems of modeling call arrival processes based on hundreds of millions of calls, which is of great importance for dynamic resource allocation, and minimization of call blocking probability [63, 3]. Similarly to [50, 48, 49] the authors propose a parametric form of the rate function $\lambda(t)$, specifically the one that describes Poisson regression model, with the positivity condition satisfied by taking the logarithm. Call arrival data are aggregated into m non overlapping time intervals of a predefined duration in seconds. Assuming that total number of calls within each time interval are denoted by $n_1, n_2, \cdots, n_m$, where the intervals $(a_1, a_2], (a_2, a_3], \cdots, (a_{m-1}, a_m)$, then the likelihood, and the log-likelihood functions are given by

$$\begin{aligned} \mathcal{L} &= exp\left\{-\sum_{i=1}^{m}\int_{a_i}^{a_{i+1}}\lambda(t)dt\right\}\prod_{i=1}^{m}\frac{(\int_{a_i}^{a_{i+1}}\lambda(t)dt)^{n_i}}{n_i!}, \\ l &= \sum_{i=1}^{m} n_i \log\int_{a_i}^{a_{i+1}}\lambda(t)dt - \sum_{i=1}^{m}\int_{a_i}^{a_{i+1}}\lambda(t)dt \end{aligned} \tag{4.2}$$

4.1.2 Methods that use cumulative intensity function of NHPP

Numerous papers, see for example [54, 7, 53] propose nonparametric techniques for estimating the cumulative intensity function of a NHPP, $\Lambda(t) = \int_0^t \lambda(s)ds$, on the time interval $[0, T]$, as a variable of interest. In [53] the authors propose the piecewise-linear estimator of the cumulative intensity function between the time values $t_{(1)}, t_{(2)}, \cdots, t_{(n)}$, which represent the order statistics of the superposition of the k realizations, as

$$\tilde{\Lambda}(t) = \frac{i}{k} + \frac{t - t_{(i)}}{k(t_{(i+1)} - t_{(i)})},$$

where $\lambda(t) > 0, \forall t \in (0, T]$, and $\lambda(t)$ continuous for almost all $t \in (0, T]$. The cumulative intensity function $\Lambda(t)$ is estimated from k (overlapping or non-overlapping) realizations on $(0, T]$, with n_i $i = 1, 2, \cdots k$ being the number of observations in the $i-$th realization, and $n = \sum_{i=1}^{k} n_i$ being the total number of observations. For this estimator, a strong consistency result and an asymptotically valid $100(1-\alpha)\%$ confidence

interval for $\Lambda(t), \forall t \in (0, T]$ were shown, as

$$\tilde{\Lambda}(t) \to \Lambda(t),$$

with probability one as $k \to \infty, \forall t \in (0, T]$, and

$$\hat{\Lambda}(t) - z_{\alpha/2}\sqrt{\frac{\hat{\Lambda}(t)}{k}} < \Lambda(t) < \hat{\Lambda}(t) + z_{\alpha/2}\sqrt{\frac{\hat{\Lambda}(t)}{k}},$$

where $z_{\alpha/2}$ is the $1 - \alpha/2$ fractile of the standard normal distribution. However these methods fail to provide good estimates of the derivative of $\Lambda(t)$, shown on the right panel of Fig. 4.1. Our interest, recall, is on $\lambda(t)$, computed as $\frac{1}{k(t_{(i+1)} - t_{(i)})}$. Similar

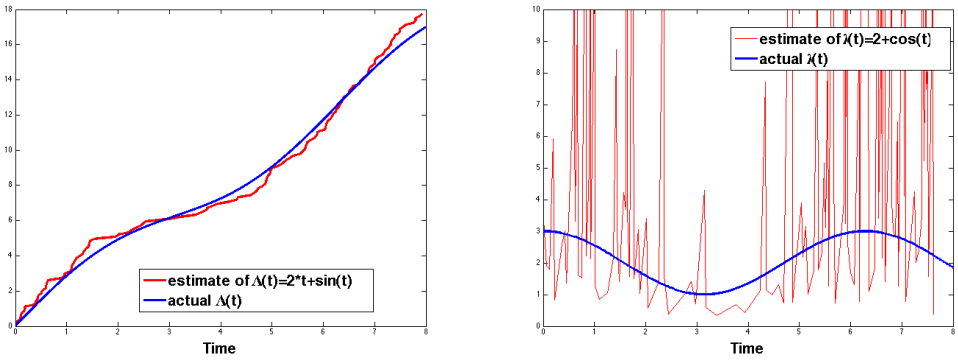

(a) Cumulative Intensity function

(b) Rate of a Poisson Process

Figure 4.1: Piecewise linear estimator of the Cumulative Intensity function that uses k=8 realizations. mesh size= 10^{-4},$n = 143$, i.e $n_i = \{16, 22, 23, 16, 19, 20, 15, 12\}$, $i = 1, \cdots, 8$

results, that we have initially attempted, can be obtained by finely sampling the time axis, and for every time point on the grid, find the closest spike, and compute the average wait time until a spike occurs across all realizations. Then the rate $\lambda(t)$ can be found for every time point on the grid by computing the inverse of the average wait time at that time point, shown on Fig. 4.2a.

The method developed in [63] deals with the estimation of an arrival rate function $\lambda(t) = a + bt$, $t \in [0, T]$ by dividing the entire time interval into M equispaced subintervals (bins), and observing an average number of events in each. The authors propose several

methods for finding the estimates $\hat{a}$ and $\hat{b}$, namely, ordinary least squares, iterative weighted least squares and maximum likelihood method, and elaborate on the effect of the time interval length T, and number of measurement subintervals M, but do not provide the optimal length of the subinterval. This method works well for slowly changing $\lambda(t)$, however it fails in cases of fast-varying signals and would not be a good starting choice, especially in cases where we have some prior information about the signal we are estimating. Another possibility, we have developed, is to use what we

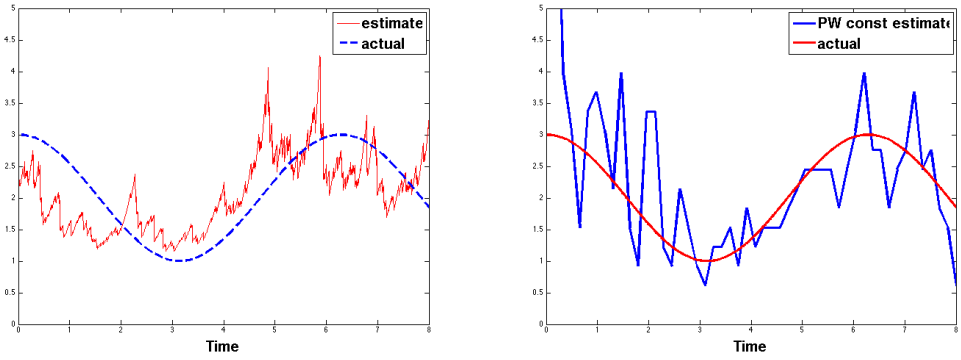

(a) (b)

Figure 4.2: Modified piecewise-linear method, $k = 20$ realizations (a), and Naive (piecewise constant) method, $k = 20$, $M = 50$ (b)

will call "the naive method," in which one observes the average number of events r in a bin containing a time t, and estimate $\lambda(t)$ as $\frac{r}{bt}$, where b is a predetermined bin size. As an example of an application of this method, we obtain an estimate shown in Fig. 4.2b. In general, finding an optimal bin size is a difficult problem (see [85]). Estimation of the mean-value function of NHPP with the rate parametrized as (4.1) has also been analyzed in [48]. The mean-value function of NHPP, $\mu(t)$ represents the expected number of arrivals of the Poisson Process for all $t \geq 0$,

$$\mu(t) = E[N(t)] = \int_0^t \lambda(s)ds.$$

A weighted least square method was used, i.e. $\mu(\tau_i;\Theta) = E[\mu(\tau_i;\Theta)] + \varepsilon_i\,, \quad i = 1, 2, \cdots$ where τ_i are random arrival times, and ε_i random errors, and assumed identically distributed, and independent, standard method of minimization of the error of the

weighted sum of squares can be applied to find the underlying parameters, namely

$$SS_E(\hat{\Theta}) = \varepsilon^T(\hat{\Theta})V^{-1}\varepsilon(\hat{\Theta})$$

with

$$\varepsilon_i(\hat{\Theta}) = \mu(\tau_i;\hat{\Theta}) - E[\mu(\tau_i;\hat{\Theta})]\,, \quad i = 1, 2, \cdots, N(T).$$

Denoting by $u(\hat{\Theta}) = V^{-1/2}\varepsilon(\hat{\Theta})$ the vector of transformed residuals, the weighted least-square estimate of the NHPP parameter vector Θ is given by:

$$\hat{\Theta}_{WLS} = \arg\min_{\hat{\Theta}} \sum_{i=1}^{N(T)} u_i^2(\hat{\Theta}).$$

Looking at the $i-$th and the last transformed residual

$$\begin{aligned} u_i(\hat{\Theta}) &= \mu(\tau_i;\hat{\Theta})\sqrt{\frac{i+1}{i}} - \mu(\tau_{i+1};\hat{\Theta})\sqrt{\frac{i}{i+1}}\,, \\ u_{N(T)}(\hat{\Theta}) &= \sqrt{\frac{1}{N(T)}}\left(\mu(\tau_{N(T)};\hat{\Theta}) - N(\tau_{N(T)}\right)\,, \end{aligned} \tag{4.3}$$

we see that all the information about the discrepancy between the empirical and the and the fitted mean-value of the is completely eliminated from the first $N(T)-1$. The error in the estimate was demonstrated on examples. The proposed method is based on ordinary least squares and variance stabilizing transformations. The variance-stabilized OLS estimate is

$$\hat{\Theta}_{OLS} = \arg\min_{\hat{\Theta}} \sum_{i=1}^{N(T)} \left(\sqrt{\mu(\tau_i;\Theta)} - \sqrt{i - \frac{1}{4}}\right)^2.$$

Again, looking for the numerical MLE estimate can be a tedious procedure leading to potentially incorrect estimates. Also, looking for the integral of the obtained quantity, which is our ultimate goal, introduces noise, so this method is also inadequate for the purpose of our application.

4.1.3 Methods from the neuroscience literature

Linear Nonlinear Poisson (LNP) method

In the literature on sensory systems in neuroscience, the ultimate goal is to construct a model for neural response, by measuring the spike rate for a period during and after stimulation (where stimulus is a vector of dimension k) [20, 83]. A class of solutions commonly used is "spike triggered analysis". The assumptions of these models are that the probability of a neuron eliciting a spike is governed only by the recent stimuli, the response model is a Poisson process whose rate is a function of a stimuli presented during a recent temporal window of fixed duration. In a forward neural response model, the stimuli are mapped to a scalar value that determines the instantaneous firing rate of a Poisson spike generator. Based on the available data, a backward approach is more plausible: from the stimuli that elicited spikes, the goal is to estimate the firing rate function. Assumptions these papers are making are that the response of a neuron is modeled with a small set of linear filters whose outputs are combined nonlinearly to generate the instantaneous firing rate The linear filter may be estimated by computing the spike triggered average stimulus (the mean stimulus that elicited a spike), then using experimental data determine the nonlinearity. This model is called LNP (Linear-Nonlinear-Poisson Model). A typical experiment in the field of neural science is represented on Fig. 4.3.

4.1.4 Bayesian decoding and particle filtering

In [14] the authors consider the reconstruction of signals coming from multiple neurons, and propose a recursive Bayesian algorithm for determining the firing rate of a neuron. This method consists of a state model for a process v_t, which is the state we are trying to estimate and an observation model, specifying the probability distribution of the data y_t given the underlying state v_t, $p(y_t|v_t)$. The objective is to find, for each time t, the distributions of the unobserved signal v_t, given observations $\{y_1, y_2, \cdots y_t\}$. y_t represents vectors of spike counts during the respective time bins. After defining the state and the observation model, one implements the particle filter to estimate the unobserved

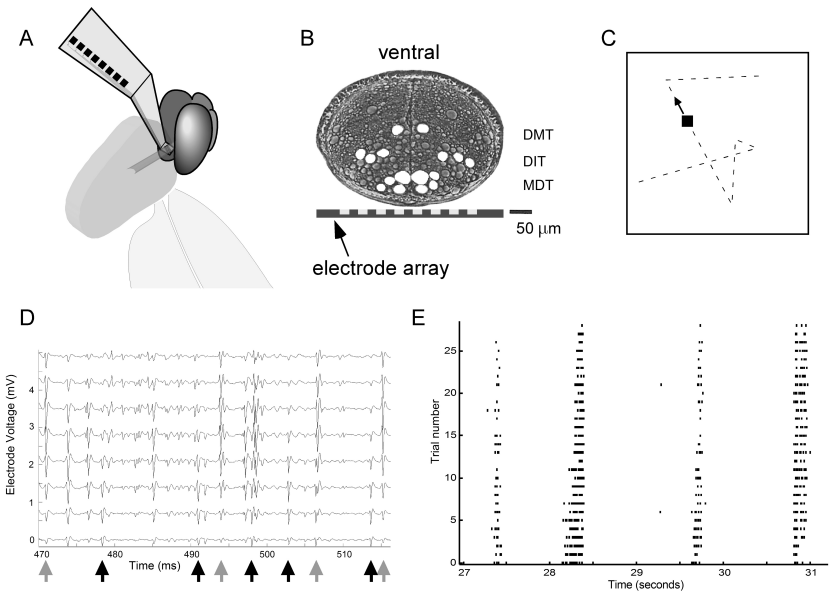

Figure 4.3: (A) An eight-channel electrode array positioned under the nerve cord for measurement. (B) The cross-section of the ventral nerve cord. (C) The stimulus.Trajectory consisting of connected 0.25 s segments within which the spot moves at constant velocity (D) A short section of the recording from the electrode array. (E) The response plot to the repeated stimuli for cell A. The stimulus is repeated 30 times, and the spike times are indicated.Adapted from [1]

sequence v_t. Typically, given v_t, v_{t+1} has a Gaussian distribution with mean v_t and covariance matrix Σ given by

$$p(v_{t+1}|v_t)^{-\dim(v_t)/2}\det\Sigma^{-1/2}\exp\left(-\left(v_{t+1}-v_t\right)^T\Sigma^{-1}\left(v_{t+1}-v_t\right)/2\right).$$

To construct the covariance matrix Σ one constructs a number of "typical paths" for the unobserved signal, computes the sample covariance matrix of all the steps $(v_{t+1}-v_t)$ in all the paths, and uses this as Σ. The initial distribution $p(v_0)$ must also be specified. In many cases, v_0 is unknown, and this distribution is chosen to represent an initial guess of the signal.

The additional assumptions are that in a time bin, a neuron generates a Poisson distributed spike count, with mean specified by the number of spikes in that bin, and the spike counts are independent of each other. Hence,

$$p(y_t|v_t) = \Pi_{i=1}^{N}\frac{e^{-\lambda_i(v_t)}[\lambda_i(v_t)]^{y_t^{(i)}}}{y_t(i)!}$$

where $\lambda_i(v_t)$ is the rate for the $i-$th neuron, evaluated with state v_t, and $y_t^{(i)}$ represents the spike count for the $i-$th neuron, in the $t-$th time bin. The set of posterior distributions, for $t = 1, 2, \cdots$ is determined by

$$\begin{aligned} p\left(v_t|y_1, y_2, \cdots y_t\right) &\propto p(y_t|v_t)p(v_t|y_1, y_2, \cdots y_{t-1}) \\ p\left(v_t|y_1, y_2, \cdots y_{t-1}\right) &= \int p(v_t|v_{t-1})p(v_{t-1}|y_1, y_2, \cdots y_t)dv_{t-1} \end{aligned} \tag{4.4}$$

The two recursive equations cannot be solved analytically, and one has to resort to usually very slow numerical methods to approximate these integrals. The PF algorithm computes numerical approximations to the distributions in the recursions (4.4).

4.2 Problem formulation using observers and Kalman filters

As an alternative we propose observer based methods, that we summarize in the subsequent sections.

Let N_t be a counting process with rate $\lambda(t)$, i.e N_t is a Poisson random variable with rate $y(t) = \int_0^t \lambda(s)ds$. The probability of having j events until time t is

$$P_{y(t)}(N_t = j) = P(j \text{ events on } [0, t]) = \frac{y(t)^j e^{-y(t)}}{j!}.$$

Observe that, $E[N_t] = \text{var}[N_t] = y(t)$.

Fix an integer $k > 0$, which denotes the number of realizations of a counting process N_t and consider k IID N's. For a fixed t, each N_i^t, $i = 1 \ldots k$, is an IID random variable with rate $y(t)$ that gives the number of events until time t for a realization i. Let

$$N_k(t) := \frac{1}{k}(N_1^t + N_2^t + N_3^t + \cdots + N_k^t),$$

be the average number of events (across all realizations) until the time t. Then

$$E[N_k(t)] = y(t),$$

$$\text{var}[N_k(t)] = \frac{1}{k^2}\text{var}(N_1^t + N_2^t + N_3^t + \cdots + N_k^t) = \frac{y(t)}{k}.$$

The random variables, $N_k(t)$, are computed from the data, and we can rewrite them in the form

$$N_k(t) = y(t) + (N_k(t) - y(t)),$$

and our goal is to find an estimate of $\lambda(t)$. The schematic representation of the problem is shown on Fig. 4.4.

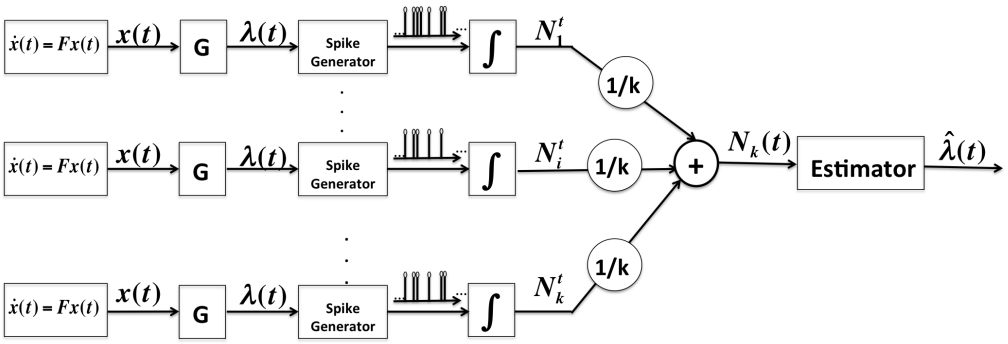

Figure 4.4: The schematic representation of the problem formulation

Denote

$$\Delta_k(t) := N_k(t) - y(t),$$

so that

$$N_k(t) = y(t) + \Delta_k(t),$$

which is represented in Fig. 4.5.

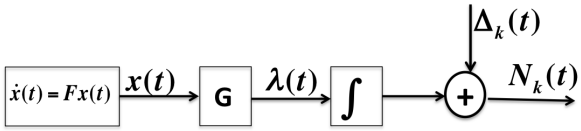

Figure 4.5: Exact problem formulation in terms of key system variables. $\Delta_k(t) := N_k(t) - \int_0^t \lambda(s)ds$

By the central limit theorem, for large k, $\Delta_k(t) \sim N(0, \frac{y(t)}{k})$. Due to the independent increments in N, and the fact that N_i are IID, it follows that Δ_k is approximately a

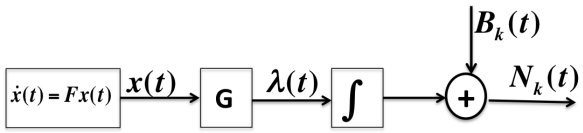

Figure 4.6: Problem formulation using an approximation of $\Delta_k(t)$ with Brownian motion, in case when k is sufficiently large

Brownian motion, $\Delta_k \approx B_k$ (Fig. 4.6). Purely formally, we define

$$\xi_k(t) := \frac{dB_k(t)}{dt},$$

and think of $\xi_k(t)$ as a white noise, normally distributed with zero mean and variance, $\text{var}[\xi(t)] = \frac{\text{var}[N_k(t)]}{t} = \frac{y(t)}{kt}$. Thus,

$$N_k(t) = y(t) + \Delta_k(t) \approx y(t) + B_k(t),$$
$$\dot{N}_k(t) \approx \lambda(t) + \xi_k(t).$$

See Fig. 4.7.

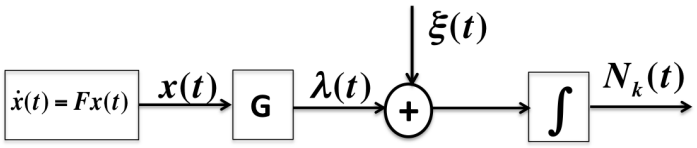

Figure 4.7: Formally writing $\xi_k(t) = \frac{dB_k(t)}{dt}$, where B_k was introduced on Fig. 4.6.

Suppose now that we have a deterministic system,

$$\dot{x} = f(x),$$

which we will at first assume is linear

$$\dot{x} = Fx.$$

The observation that is available for estimation is a non-homogeneous Poisson random process N_t, whose rate is $\lambda(t) = h(x(t)) = Gx$. We assume that $\lambda(t)$ is always positive.

This will be guaranteed if the matrix F is Metzler, $G > 0$, and $x(0)$ has positive coordinates. The objective is to obtain an estimate of the state x, or more specifically, of the rate $\lambda(t)$.

Assume next that we have access to k realizations of the process, with the same $x(0)$, so that the rate of the process, $\lambda(t)$ is the same in every realization.

Let's rewrite the full state-space model for the approximate system on Fig. 4.7 as:

$$\begin{aligned} \frac{dx}{dt} &= Fx, \\ \dot{N}_k(t) &= Gx + \xi, \end{aligned} \tag{4.5}$$

with unknown initial condition $x(0)$. Notice that if we estimate (x, N_k), we will have in particular an estimate of $\lambda(t) = Gx(t)$. In order to more compactly describe the extended system (4.5), we introduce the state $z_1 = \begin{bmatrix} x \\ N_k \end{bmatrix}$, with the output y being equal to the last variable $N_k(t)$. Since $N_k(t)$ will typically be very noisy, we do not want our estimator to compute numerical derivatives, so the output that we would like to feed as the input to the state estimator is $N_k(t)$, which contains colored noise.

The extended system can be written in the form:

$$\frac{dz_1}{dt} = F_1 z_1 + G_1 \xi\,, \quad \text{with} \quad F_1 = \begin{bmatrix} F & 0 \\ G & 0 \end{bmatrix} \in \mathbb{R}^{(n+1)\times(n+1)}\,,\ G_1 = \begin{bmatrix} 0_n \\ 1 \end{bmatrix}. \tag{4.6}$$

The output of this system corresponds to the last state of (4.6), namely

$$y_1(t) = H z_1(t)\,, \quad \text{with } H = \begin{bmatrix} 0_n & 1 \end{bmatrix}. \tag{4.7}$$

If we would attempt to build a Kalman filter for the estimation of the state z_1, in (4.6), we would encounter a singular problem with zero output noise covariance matrix. To avoid this case, we apply the method developed in [15, 16, 69] and look for the derivative of y_1

$$\dot{y}_1 = H_1 z_1(t) + v_1(t),$$

where H_1=HF_1, $v_1(t)$=$HG_1\xi$, and $E[v_1(t)v_1^T(t)] = HG_1m(t)G_1^TH^T$ with $\text{cov}[\xi(t)\xi^T(t)] = m(t)$. Now the estimate of $z_1(t)$ is $\hat{z}_1$ obtained as

$$\dot{\hat{z}}_1 = F_1\hat{z}_1 + L(t)(\dot{y}_1 - \dot{\hat{y}}_1) = F_1\hat{z}_1 + L(t)(\dot{y}_1 - H_1\hat{z}_1), \tag{4.8}$$

where $L = L(t)$ is time varying gain. Since differentiation introduces the noise in the filtering problem, introduce the following change of variables

$$g(t) = \hat{z}_1 - Ly_1. \tag{4.9}$$

If we differentiate g

$$\begin{aligned} \dot{g} &= \dot{\hat{z}}_1 - L\dot{y}_1 - \dot{L}y_1 \\ \dot{g} &= (F_1 - L(t)H_1)g(t) + [F_1L(t) - L(t)H_1L(t) - \dot{L}(t)]y_1(t) \end{aligned} \tag{4.10}$$

from where we can find $\hat{z}_1(t) = g(t) + L(t)y_1(t)$.

In order to find the time-varying gain $L(t)$ we now solve a routine Kalman filtering problem for (4.8).

Define the observation error as $e(t) = z(t) - \hat{z}(t)$, so its derivative is

$$\dot{e}(t) = \dot{z}_1(t) - \dot{\hat{z}}_1 = F_1z_1 + G_1\xi - F_1\hat{z}_1 - L\dot{y}_1 + L\dot{\hat{y}}_1,$$

Therefore,

$$\dot{e}(t) = (F_1 - LHF_1)e(t) - (LHG_1 - G_1)\xi(t) \tag{4.11}$$

where $\dot{\hat{y}}_1$=$HF_1\hat{z}_1$. Denote the covariance of $e(t)$ by Σ:=$E[e(t)e^T(t)]$, and $\text{Var}[e(t)] = E[(e(t)-\bar{e}(t))(e(t)-\bar{e}(t))^T]$, with $\bar{e}(t) = E[e(t)]$. Also, $\text{cov}[\xi(t)\xi^T(t)] = m(t)$, where $\xi(t)$ is the white noise, $E[\xi(t)] = 0$. The covariance matrix Σ satisfies the Riccati equation:

$$\dot{\Sigma} = (F_1 - LHF_1)\Sigma + \Sigma(F_1 - LHF_1)^T + (LHG_1 - G_1)m(t)(LHG_1 - G_1)^T \tag{4.12}$$

with

$$L_{opt} = [\Sigma F_1^T H^T + G_1 G_1^T H^T m(t)](HG_1 G_1^T H^T)^{-1} m(t)^{-1} \tag{4.13}$$

$$\dot{L}_{opt} = \dot{\Sigma} F_1^T H^T (HG_1 G_1^T H^T)^{-1} m(t)^{-1} - \Sigma F_1^T H^T (HG_1 G_1^T H^T)^{-1} \Big(\frac{\dot{m}(t)}{m^2(t)}\Big) \tag{4.14}$$

In the computation of the optimal gain $L(t)$ from the Riccati equation we use $m(t)$, which we will estimate from the sample variance, which, in turn is estimated from the data. However in the expression (4.10), the derivative of $m(t)$ will appear through the term $\dot{L}(t)$, but this numerical derivative does not affect the estimate directly.

The complexity of the filter led us to study an alternative approach, where we simply look for any stabilizing, not necessarily optimal, gains; in other words, we studied the use of Luenberger observers. We now turn to this approach, based on picking a suitable constant stabilizing L, and show that results also look satisfactory. For the Luenberger observer design we observe the system defined by (4.6) and (4.7), and ignore the noise, ξ.

4.3 Examples

4.3.1 Periodic input-periodic based estimator

In this section we will demonstrate the advantage of model based methods in cases where we have some prior information about the system or about the inputs acting upon the system. Consider an output $\lambda(t)$ generated by the following system with a known frequency ω_0 :

$$\begin{aligned}
\dot{x}_0 &= 0\,, \qquad x_0(0) = 2.5,\\
\dot{x}_1(t) &= x_2\,, \qquad x_1(0) = 0.15,\\
\dot{x}_2(t) &= -\omega_0^2 x_1\,,\ x_2(0) = 0.25,\\
\lambda(t) &= x_0(t) + x_2(t),
\end{aligned}$$

where the initial conditions are such that $\lambda(t) > 0$ $(\forall t)$, and $\omega_0 = 10$. If we use the prior information of the frequency, an oscillatory estimator for this system can be represented

as

$$\begin{aligned}
\dot{x} &= \begin{bmatrix} \dot{x}_0 & \dot{x}_1 & \dot{x}_2 \end{bmatrix}^T = Fx\,, \quad F = \begin{bmatrix} 0 & 0 & 0 \\ 0 & 0 & 1 \\ 0 & -w_0^2 & 0 \end{bmatrix}, \\
\lambda(t) &= Gx\,, \quad G = \begin{bmatrix} 1 & 0 & 1 \end{bmatrix}, \\
\dot{N} &= Gx,
\end{aligned} \tag{4.15}$$

where we introduced another state, N, to represent the counting process. The extended system is now

$$\dot{z}_1 = \begin{bmatrix} \dot{x}_0 & \dot{x}_1 & \dot{x}_2 & \dot{N} \end{bmatrix}^T = F_1 z_1\,,$$

$$F_1 = \begin{bmatrix} F & 0 \\ G & 0 \end{bmatrix} = \begin{bmatrix} 0 & 0 & 0 & 0 \\ 0 & 0 & 1 & 0 \\ 0 & -w_0^2 & 0 & 0 \\ 1 & 0 & 1 & 0 \end{bmatrix},$$

with the output

$$\dot{y}_1 = Hz_1\,, \quad H = \begin{bmatrix} 0 & 0 & 0 & 1 \end{bmatrix}.$$

Thus, we can build an observer for the system as

$$\frac{d\hat{z}_1}{dt} = \quad F_1\hat{z}_1 + L(y_1 - H\hat{z}_1). \tag{4.16}$$

We picked the observer gains L so that the observer poles are arbitrarily chosen as $-10, -9, -8$ and -7. The simulation results and comparison with the piecewise constant estimator are shown on Fig. 4.8. We have challenged the "naive method" by increasing and decreasing the bin size, b, while keeping the same number of realizations k as in our model-based approach, and the simulation results do not indicate any improvement of the naive, piecewise constant method, in comparison to the

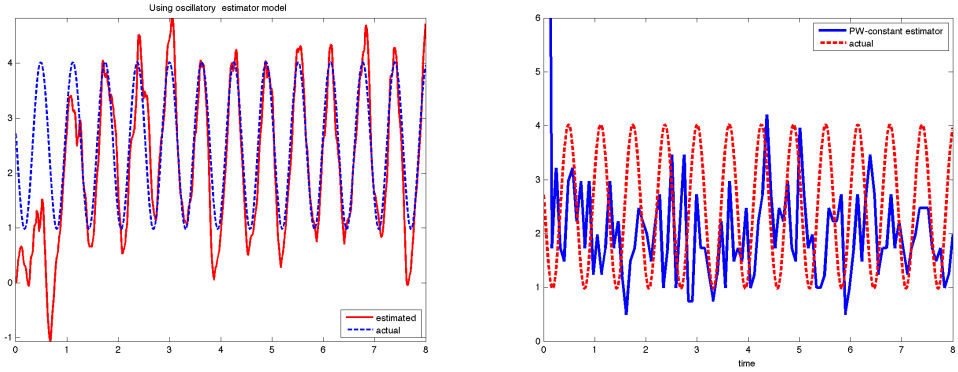

(a) Observer Method, $k = 50$

(b) Naive method, k=50 M=100

Figure 4.8: Comparison of estimates obtained using piecewise constant estimator and a model-based oscillatory observer

4.4 A biological example

This work was motivated by current work we are pursuing with experimental collaborators in the design of microfluidics devices that will allow the same inputs to be fed to a population of chemotactic bacteria, and microscope-based observations of tumbling events will be used for estimation of the tumbling rate (a function of chemotactic protein concentrations). Since these data are not available yet, we use here experimental data from the paper [52], which measured the actual rates through FRET techniques for a particular strain of *E. coli* bacteria. Since FRET measurements are very noisy, we first low-pass filtered this data in order to simulate $\lambda(t)$ and generate artificial events, see Fig. 4.9. There are numerous methods for the generation of a NHPP known in the literature [74]. In our work, we use the following modified method of inversion. Suppose y is a given function and we want to generate the Poisson process with rate $y(t)$. We pick a small step size h, and on each time ih generate a spike with probability $P = F(ih)h + o(h)$. We will briefly remark on the other methods for generation in Section 4.4.3.

We see from Fig. 4.10 that a simple observer-based method recovers the FRET measurement with roughly the same amount of noise. Of course, if FRET data is available,

there would be no need for our observers. The goal, however, is to study similar questions for other bacterial species for which FRET measurements, which require extensive genetic modifications, are not available. Note that since we did not have a priori information about the nature of the output, we have tested the zeroth-order observer, which is essentially an observer designed to estimate constant signals, and also a first-order or linear observer which would be optimal for linear or piecewise linear signals. We see an improvement of our proposed method compared to the "naive" method, shown on Fig. 4.11.

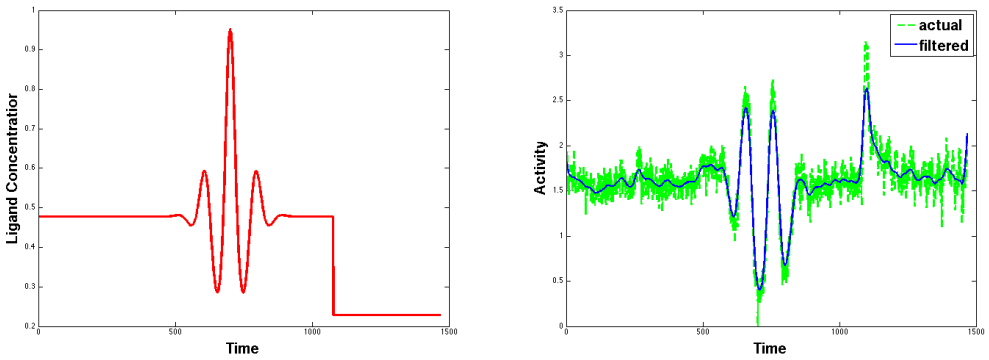

(a) (b)

Figure 4.9: (a) Input (ligand concentration) and (b) Measured output and a filtered output used for the estimation process

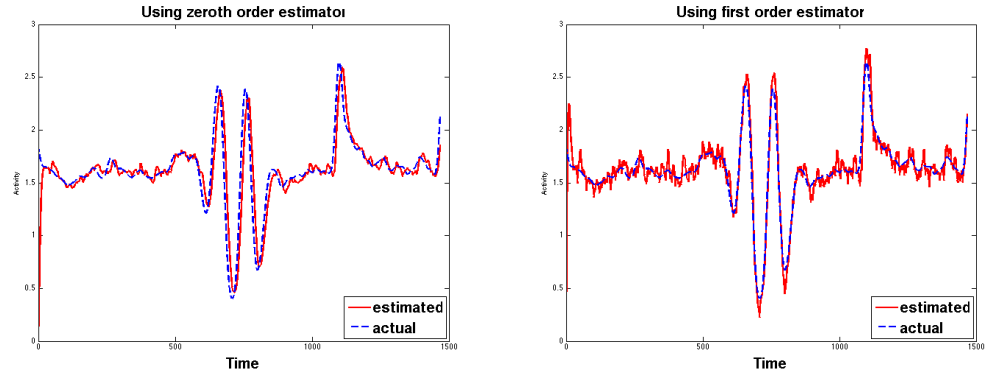

(a) (b)

Figure 4.10: Estimation using the observer method of zeroth order (i.e. constant estimator) (a) and first order (i.e. linear estimator) (b) $k = 50$

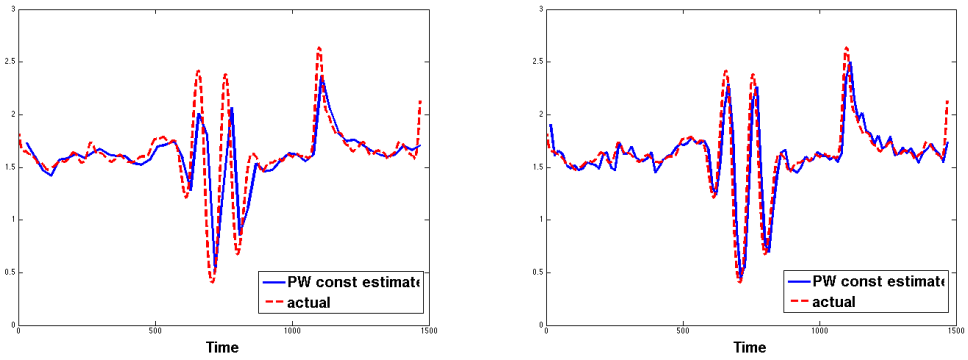

(a) $M = 50$ (b) $M = 100$

Figure 4.11: Naive piece-wise constant estimator with subinterval width M

4.4.1 Estimation using SPECS model for *E. Coli* chemotaxis

As an alternative example, we use model from [86] to generate the spike data, introduced in Chapter 1, which we repeat here for convenience:

$$\begin{aligned} \frac{dm(t)}{dt} &= k_R(1-a) - k_B a\,, \\ a(t) &= \left(1+\exp\left(N\left[\alpha(m_0-m) - \ln\left(\frac{1+L/K_A}{1+L/K_I}\right)\right]\right)\right)^{-1}, \end{aligned} \tag{4.17}$$

with $K_I = 18.2$, $K_A = 3000$, $N = 6$, $\alpha = 1.7$, $m_0 = 1$, $K_R = 0.005$, $K_B = K_R$. The state $m(t)$ represents the methylation of the receptors, the output is the activity of the kinease $CheY - P$, and the input to the system, $L(t)$ is the ligand concentration. It is known from the literature that the FCD regime can be expected for inputs in the range $K_I < L(t) < K_A$.

We test if the system (4.17) exhibits scale invariance, by applying several plausible input signals, and their scaled versions. We show the results of the experiments from the model simulations, and also from our estimation procedure, where we again used the model to generate the artificial experiments, "spikes", that we feed to our observer. In addition to reconstructing the rate of the NHPP that underlies the "spike" or tumble data, we also show its integral as well. If the objective is to test only whether or not the system exhibits scale invariance behavior the integral would have been sufficient

to estimate. However for the modeling purposes of distinguishing between the models of various species, input-output data are necessary, and hence the intensity function is required.

First, we test for the response to constant inputs, in which the system is preadapted to a constant input L_0, and then presented to a new input L^*. Then one repeats the experiment using the p-scaled inputs, where the scale factor p was picked to be 2, 5 and 15, to cover both the scale invariance and the non-scale invariance regime. The values for L_0, and L^* were fixed to 200 and 400, respectively.

Figures 4.12 and 4.13 show estimation result for scale invariant case, where scaling factor $p = 2$. Three estimators were presented: zeroth ("piecewise constant"), first ("piecewise linear"), and second ("quadratic") oder. As expected, zeroth order estimator in this case performs the best, given that the signal we are estimating is piecewise constant. The estimator for the integral of the rate function is more robust to number of realizations, whereas the rate function itself is better estimated with a higher number of samples, $N = 100$. Figures 4.14 and 4.15 show estimation result for non- scale invariant case, with $p = 5$. The loss of scale-invariance is even more striking when scale is chosen to be $p = 15$, and it can be seen on Figures 4.16, 4.17 and 4.18.

Additionally, we tested for the response to oscillatory inputs. In these experiments,the system is preadapted to the ligand concentration $L_0(t) = 200$, and then presented to $L^*(t) = 200 + 100\sin(0.1\pi t)$ or $L^*(t) = 200 + 100\sin(5t)$. Two different scaling parameters were tested; $p = 3$, which should yield the scale-invariance property, and $p = 20$ which should not, based on the experimental results and previous modeling efforts. On examples we demonstrate the application of the oscillatory, model-based estimator (periodic input-periodic model estimator), and its advantage in cases where one has prior information about the inputs to the system. The frequency content of the estimated output is matched to that of the input, and this assumption is justified by looking at the amplitude spectrum of the output, and recognizing that its spectrum is matched to the input one. We demonstrate that the oscillatory observer is superior to the other methods, for instance we will compare it with the "naive" estimator, and

the second-order, high-gain model based observer.

Figure 4.19 shows the expected scale invariant behavior from the model, and the frequency content of the actual output. The input signal is given by $L^*(t) = 200 + 100\sin(0.1\pi t)$, and the scaling factor is $p = 3$. Figures 4.20 and 4.21 show the advantageous results of the oscillatory estimator for different number of realizations. Figure 4.22 shows the loss of scale invariant behavior, when the scaling factor is $p = 20$. Oscillatory observer also "sees" the loss of scale invariance.

We demonstrate the advantage of the oscillatory based observer to second order estimator and the "naive" estimator on an example of fast-varying signal. The system is preadapted to the ligand concentration $L_0(t) = 200$, and then presented to $L^*(t) = 200 + 100\sin(5t)$. Two different scaling parameters were tested; $p = 3$, which should yield the scale-invariance property, and $p = 20$ which should not.

Figures 4.23 (c) and (d) show the advantageous results of the oscillatory observer, and Fig. 4.24 shows the failure to estimate the fast-varying output of the "naive" method. Figures 4.25, 4.26, and 4.27 show poor performance of the quadratic, first and zeroth order observer. Finally for $p = 20$, the same example fails to exhibit scale invariant behavior, and our observer detects the loss of scale invariance as well (see Fig. 4.28.

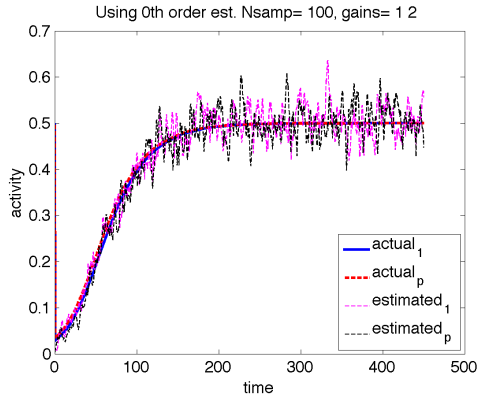

(a) Intensity function

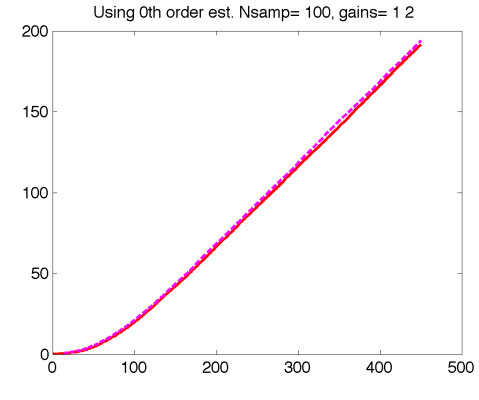

(b) Integral of the intensity function

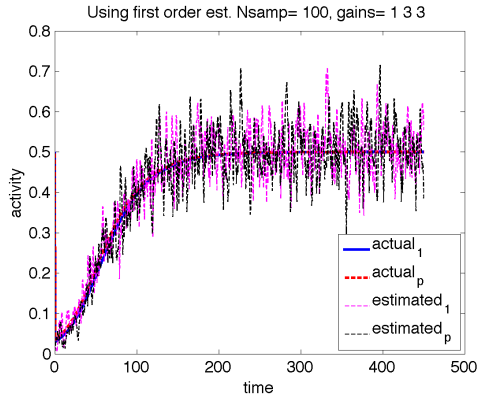

(c) Intensity function

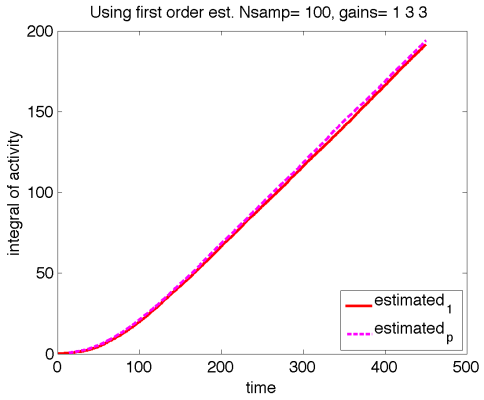

(d) Integral of the intensity function

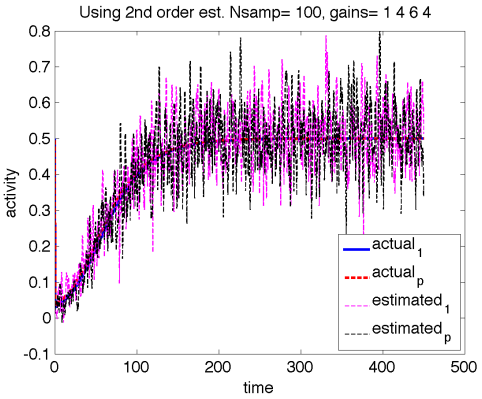

(e) Intensity function

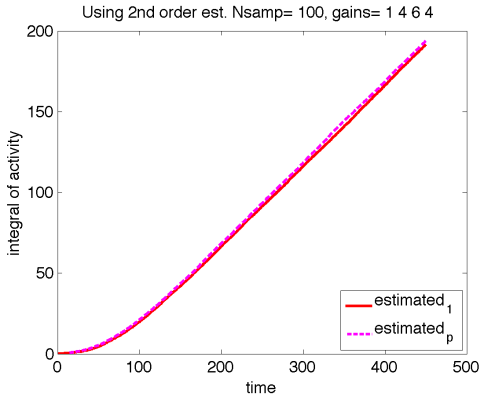

(f) Integral of the intensity function

Figure 4.12: Scale invariant system. Scaling factor is $p = 2$, $N = 100$ experiment repetitions were used for estimation of a NHPP arising from the model (4.17). The plots show the estimation results using the zeroth, first- and second-order estimators. The eigenvalues were selected to all be 1.

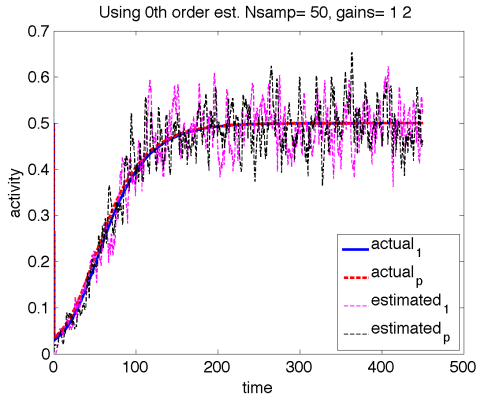

(a) Intensity function

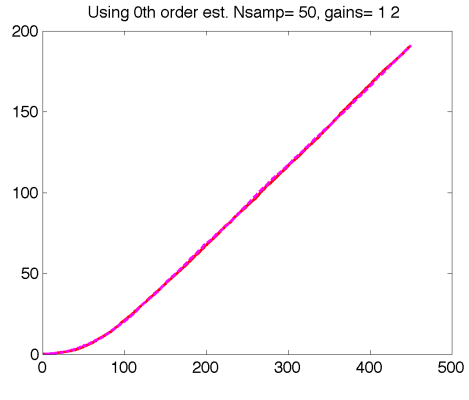

(b) Integral of the intensity function

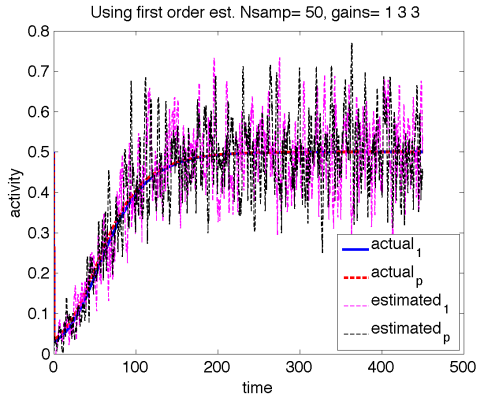

(c) Intensity fcn

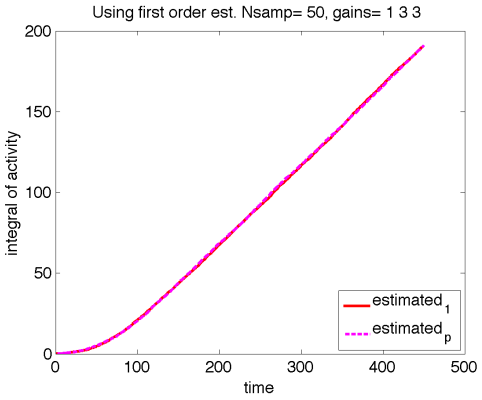

(d) Integral of the intensity function

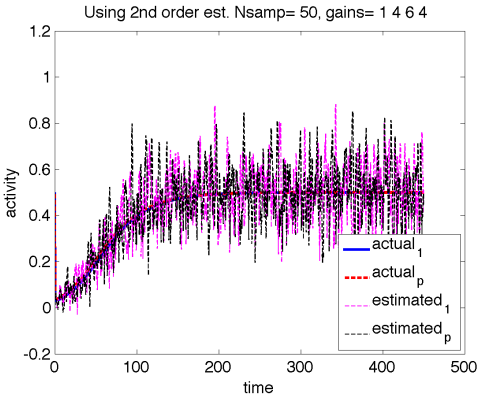

(e) Intensity fcn

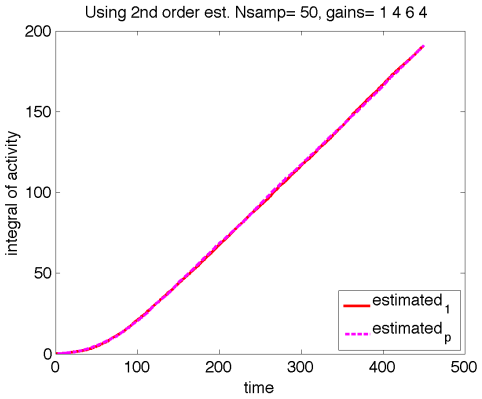

(f) Integral of the intensity function

Figure 4.13: Scale invariant system. Scaling factor is $p = 2$, $N = 50$ experiment repetitions were used for estimation of a NHPP arising from the model (4.17). The plots shows the estimation results using the zeroth, first- and second-order observer based estimators. The eigenvalues were selected to all be equal to 1.

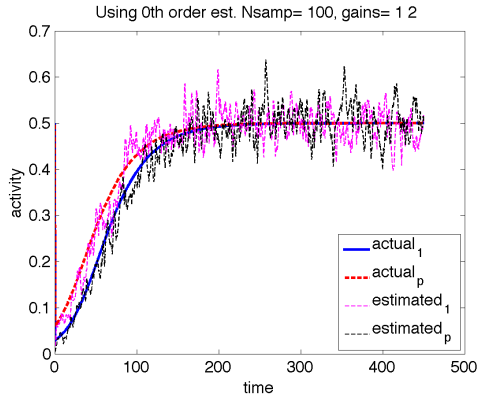

(a) Intensity function

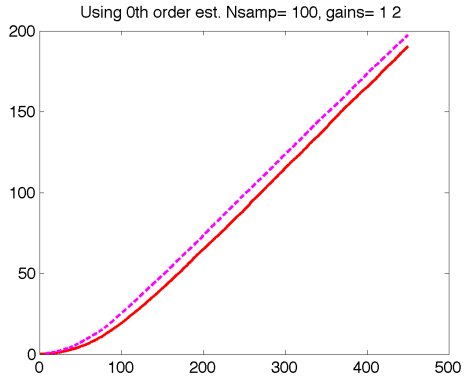

(b) Integral of the intensity function

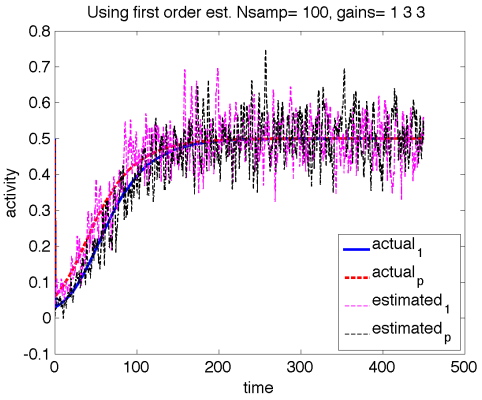

(c) Intensity function

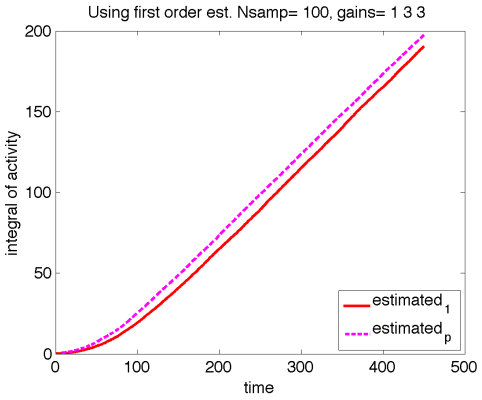

(d) Integral of the intensity function

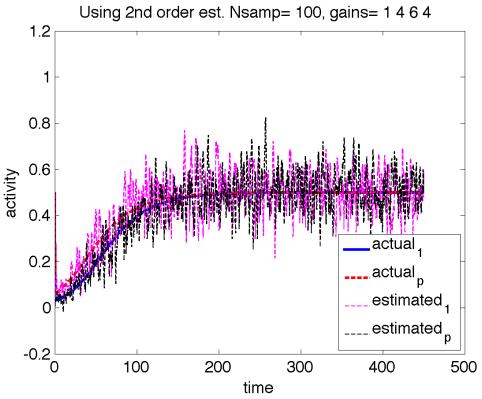

(e) Intensity function

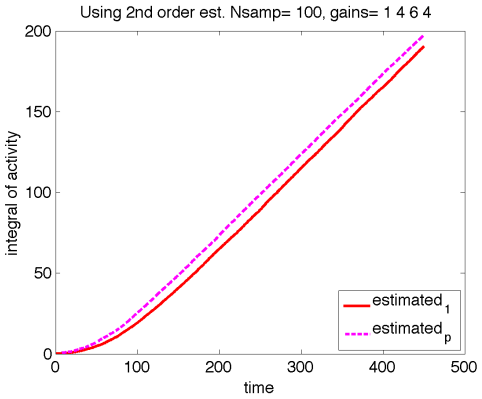

(f) Integral of the intensity function

Figure 4.14: Not a scale invariant system. Scaling factor is $p = 5$, $N = 100$ experiment repetitions were used for estimation of a NHPP arising from the model (4.17). The plots show the estimation results using the zeroth, first- and second-order observer based estimators. The eigenvalues were selected to all be equal to 1.

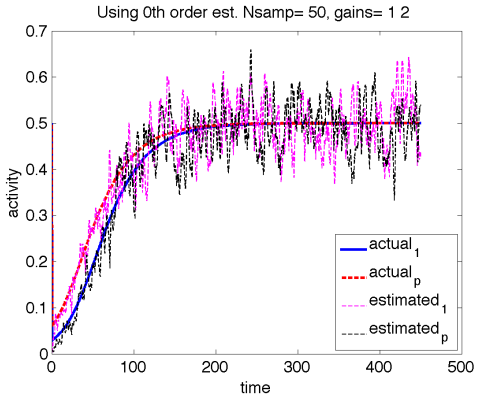

(a) Intensity function

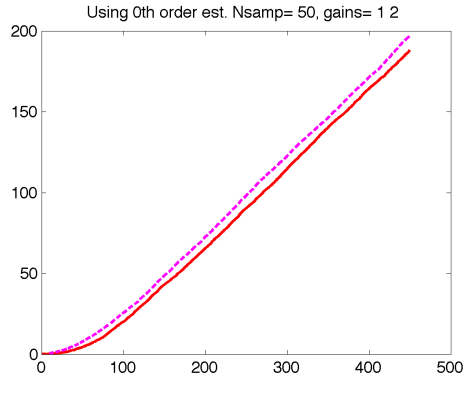

(b) Integral of the intensity function

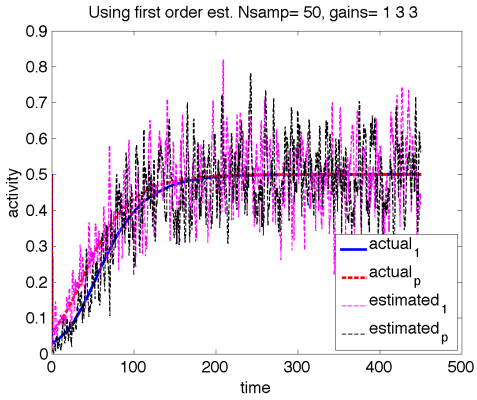

(c) Intensity function

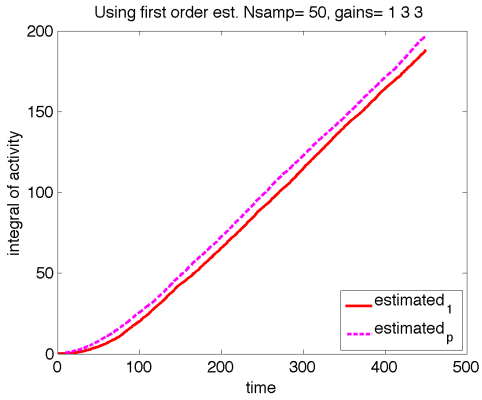

(d) Integral of the intensity function

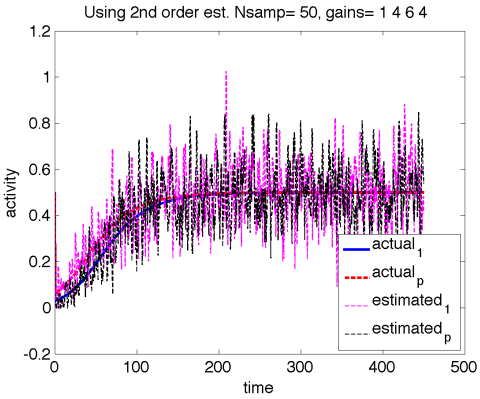

(e) Intensity function

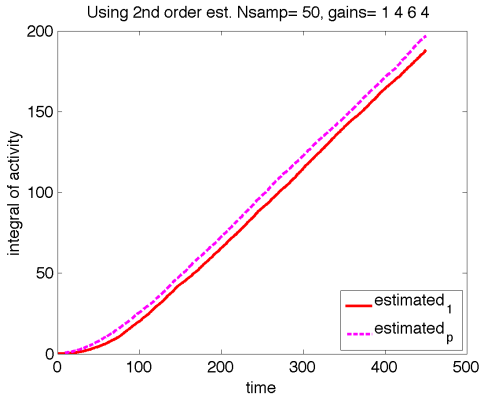

(f) Integral of the intensity function

Figure 4.15: Not a scale invariant system. Scaling factor is $p = 5$, $N = 50$ experiment repetitions were used for estimation of a NHPP arising from the model (4.17). The plots show the estimation results using the zeroth, first- and second-order observer based estimators. The eigenvalues were selected to all be equal to 1.

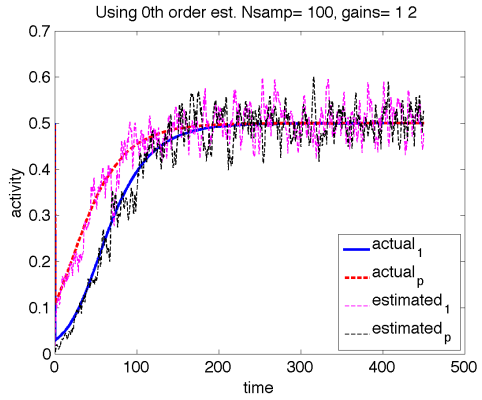

(a) Intensity function

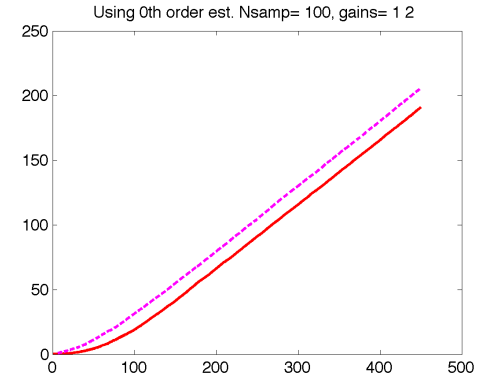

(b) Integral of intensity function

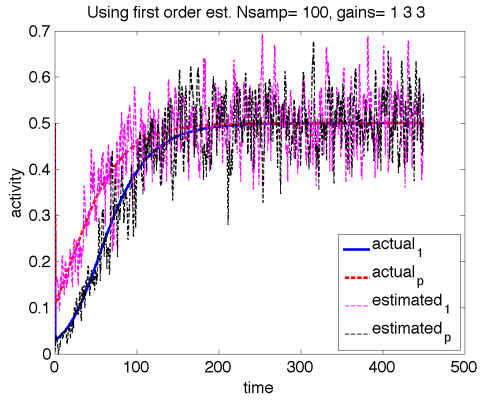

(c) Intensity function

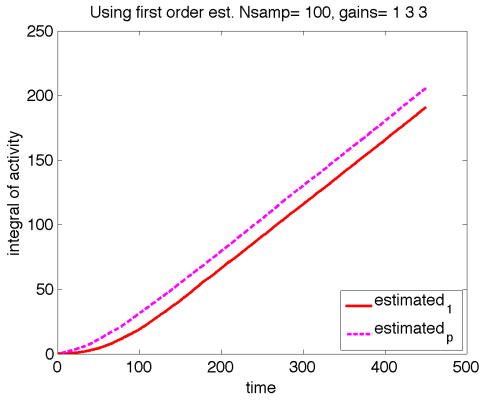

(d) Integral of intensity function

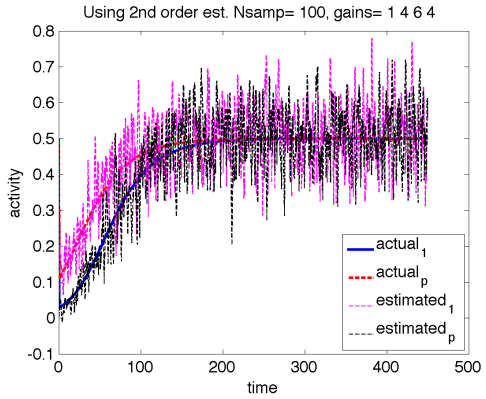

(e) Intensity function

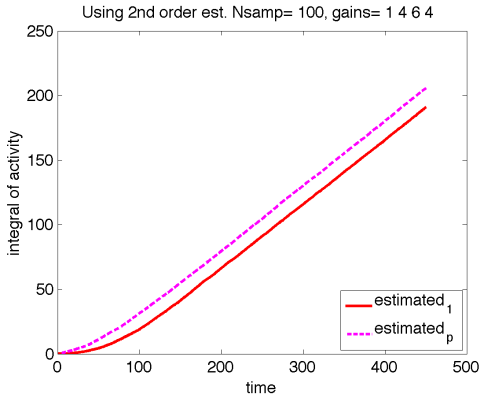

(f) Integral of intensity function

Figure 4.16: Not a scale invariant system. Scaling factor is $p = 15$, $N = 100$ experiment repetitions were used for estimation of a NHPP arising from the model (4.17). The plots depict the estimation results using the zeroth, first- and second-order observer based estimators. The eigenvalues were selected to all be equal to 1.

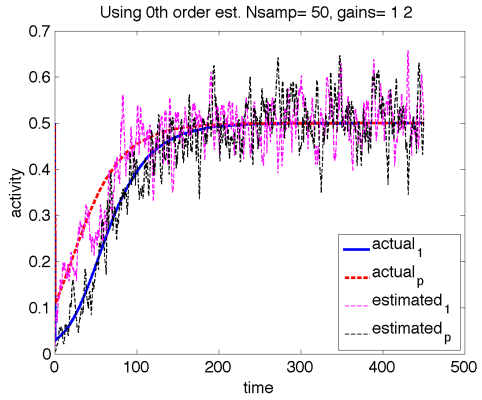

(a) Intensity function

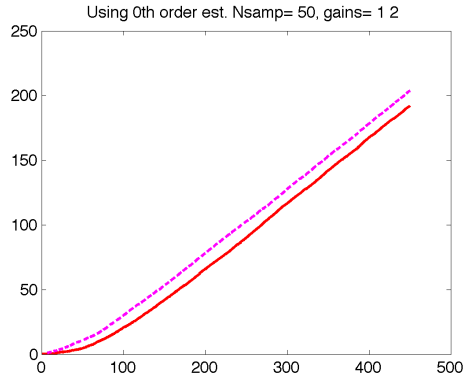

(b) Integral of intensity fcn

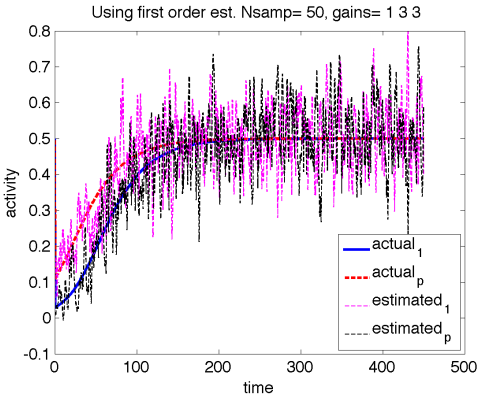

(c) Intensity function

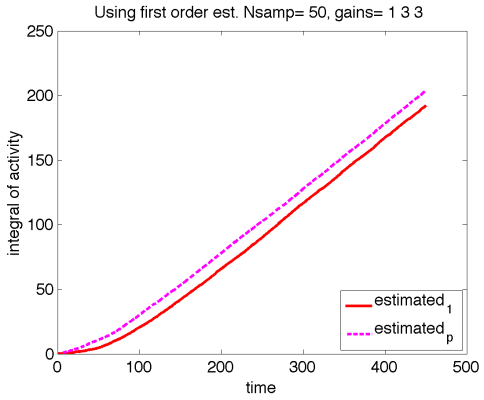

(d) Integral of intensity function

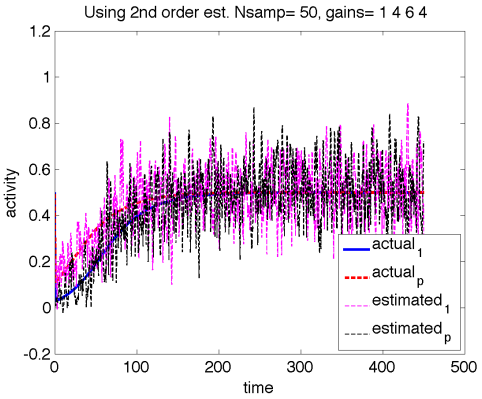

(e) Intensity function

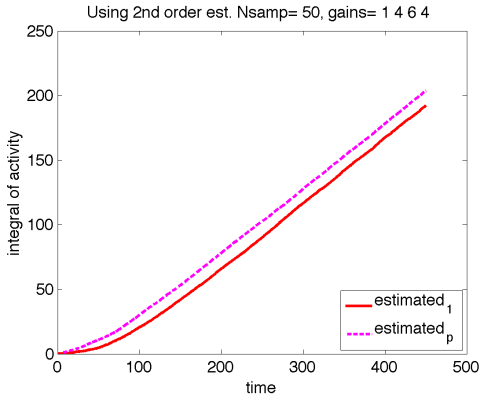

(f) Integral of intensity function

Figure 4.17: Not a scale invariant system. Scaling factor is $p = 15$, $N = 50$ experiment repetitions were used for estimation of a NHPP arising from the model (4.17). The plots show the estimation results using the zeroth, first- and second-order observer based estimators. The eigenvalues were selected to all be equal to 1.

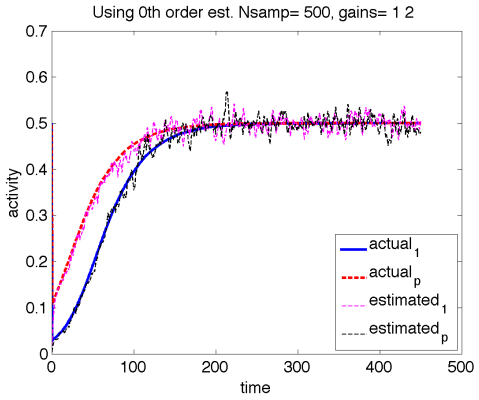

(a) Intensity function

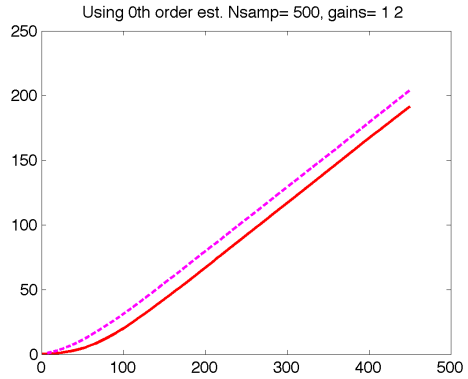

(b) Integral of intensity function

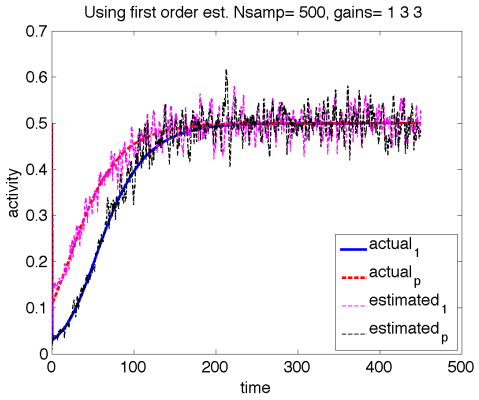

(c) Intensity function

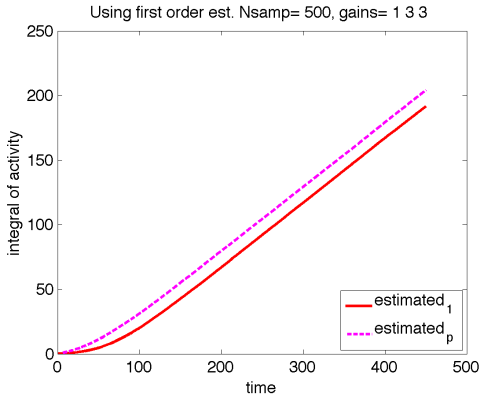

(d) Integral of intensity function

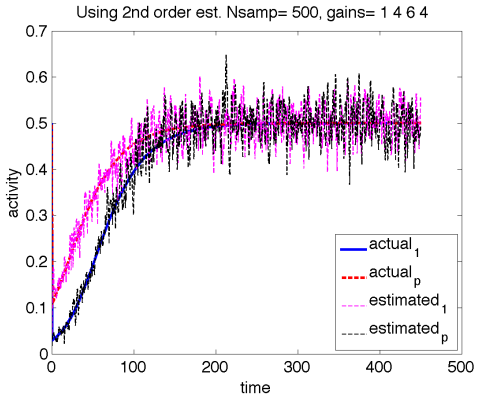

(e) Intensity function

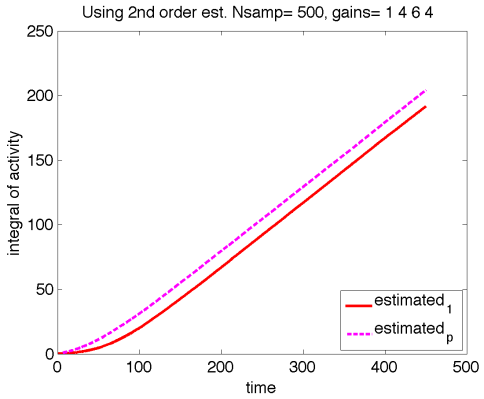

(f) Integral of intensity function

Figure 4.18: Not a scale invariant system. Scaling factor is $p = 15$, $N = 500$ experiment repetitions were used for estimation of a NHPP arising from the model (4.17). The plots show the estimation results using the zeroth, first- and second-order observer based estimators. The eigenvalues were selected to all be equal to 1.

Example 1.

In this example the input signal is periodic with frequency $f = 0.05Hz$. The systems exhibits scale invariant behavior when when comparing the output corresponding to $L^*(t) = 200 + 100\sin(0.1\pi t)$ (previously preadapted to $L_0(t) = 200$), and then is presented to $3L^*(t)$ $(p = 3)$.

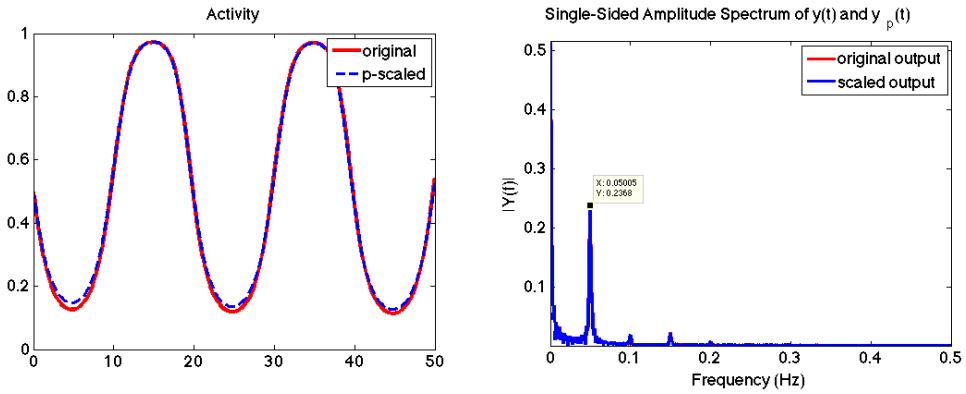

(a) (b)

Figure 4.19: Scale invariant system. (a) Original and p-scaled outputs and their corresponding spectra, (b). The input frequency is $f = 0.05Hz$.

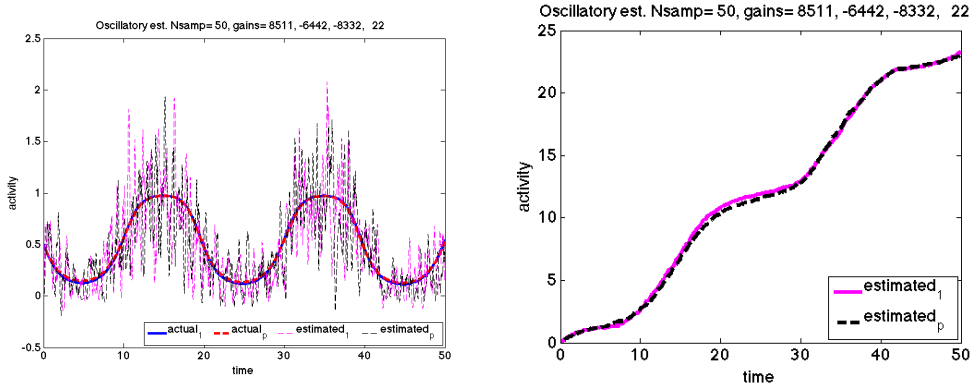

(a) Intensity function (b) Integral of the intensity function

Figure 4.20: Scale invariant system, $p = 3$, $N = 50$ repetitions. The plots depict the estimation results using oscillatory estimator. The observer gains are given in the figures.

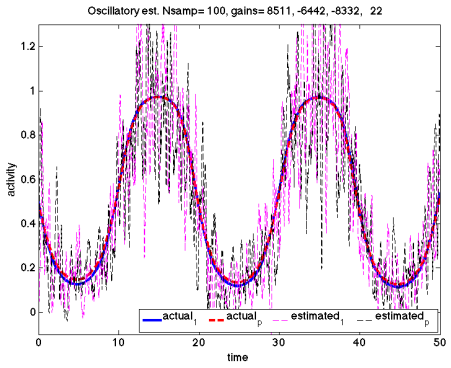

(a) Intensity function

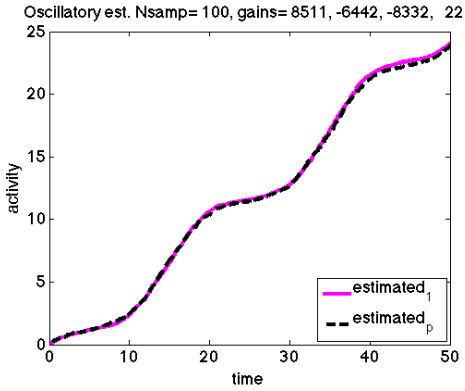

(b) Integral of the intensity function

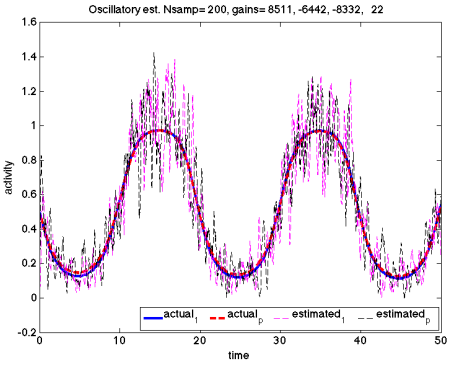

(c) Intensity function

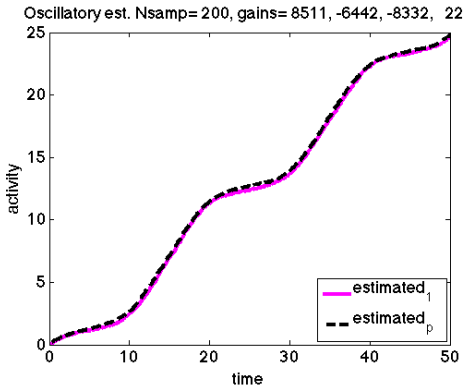

(d) Integral of the intensity function

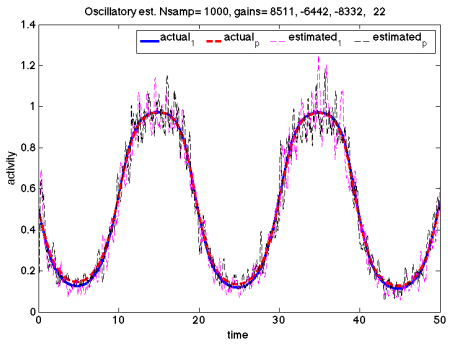

(e) Intensity function

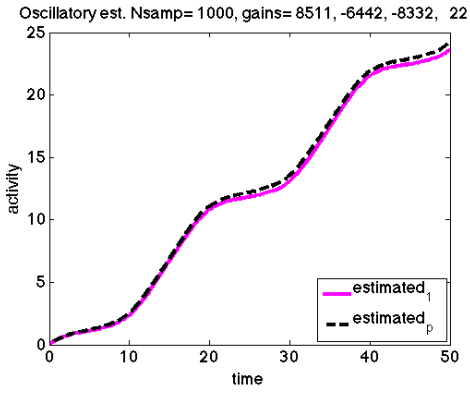

(f) Integral of the intensity function

Figure 4.21: Scale invariant system. Scaling factor is $p = 3$, $N = 100, 200, 1000$ experiment repetitions were used for estimation. The plots show the estimation results using oscillatory observer based estimator. The observer gains are given in the figures.

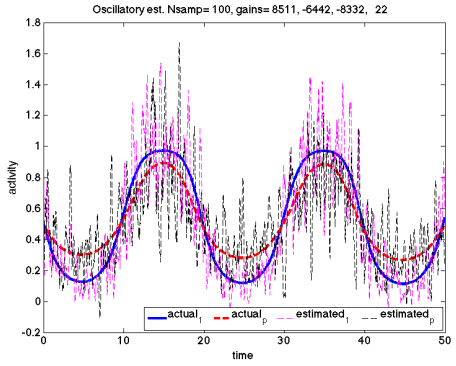

(a) Intensity function

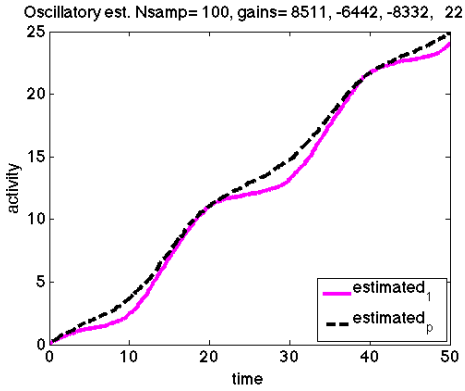

(b) Integral of the intensity function

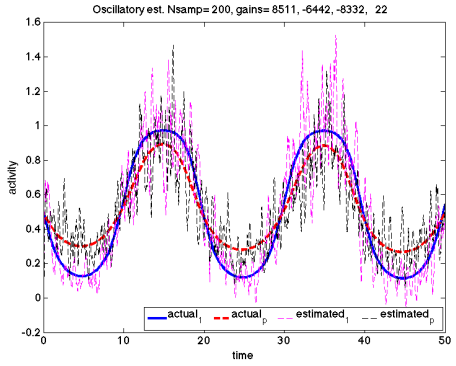

(c) Intensity function

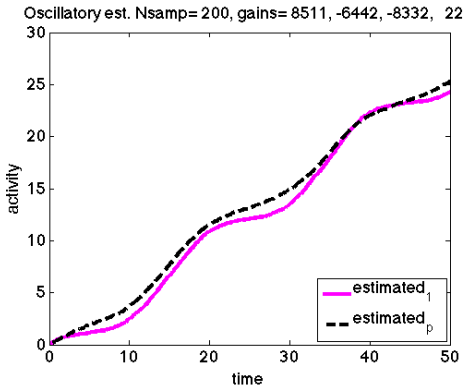

(d) Integral of the intensity function

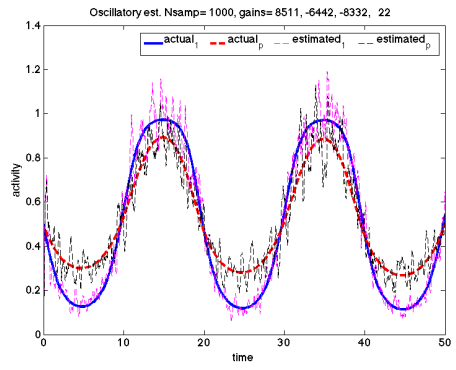

(e) Intensity function

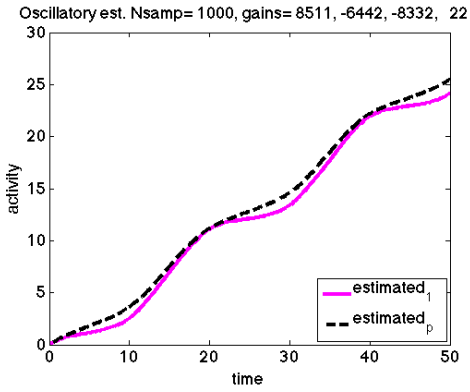

(f) Integral of the intensity function

Figure 4.22: A non-scale invariant system. Scaling factor is $p = 20$, $N = 100, 200, 1000$ experiment repetitions were used for estimation. The plots depict the estimation results using oscillatory observer based estimator. The observer gains are given in the figures.

Example 2.

In this example, the input signal is periodic with frequency $f = 0.8Hz$. The system exhibits scale invariant behavior when comparing the output corresponding to $L^*(t) = 200 + 100\sin(5t)$ (previously preadapted to $L_0(t) = 200$), and then is presented to $3L^*(t)$.

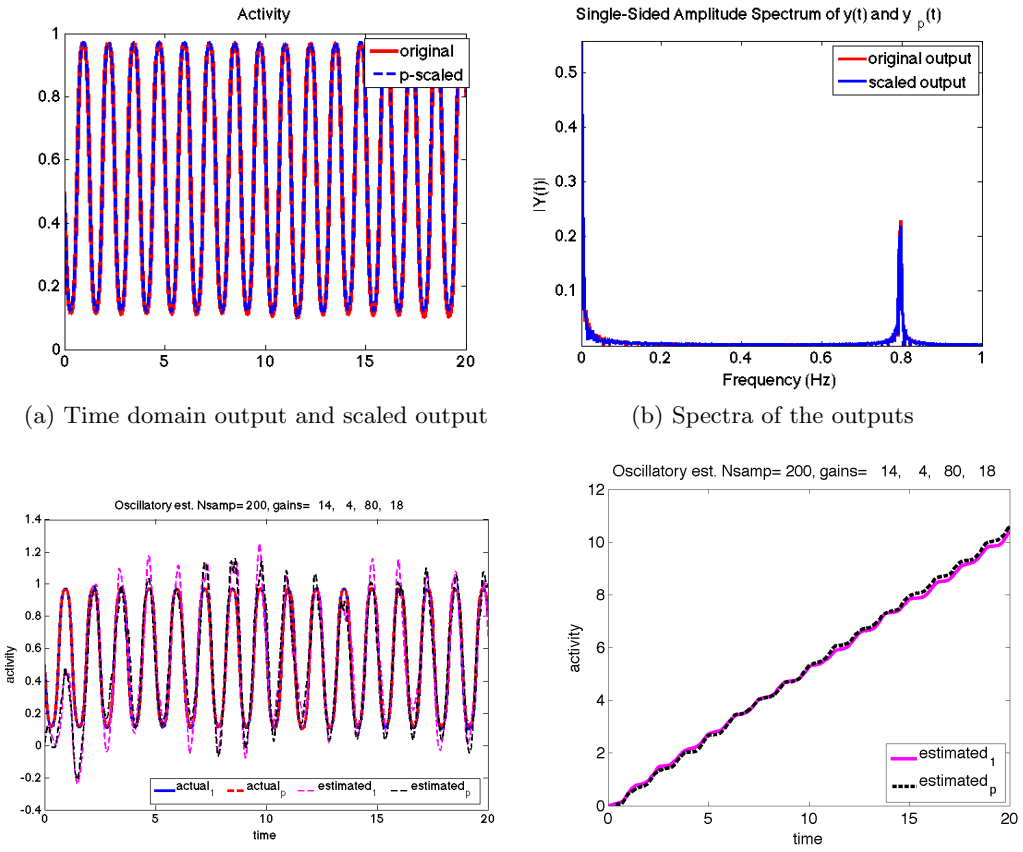

(a) Time domain output and scaled output

(b) Spectra of the outputs

(c) Integral of the intensity function

(d) Intensity fcn

Figure 4.23: SI system with the input containing frequency of 0.8Hz. Scaling factor is $p = 2$, $N = 200$ experiment repetitions were used for estimation. The plots depict the estimation results using oscillatory observer based estimator.

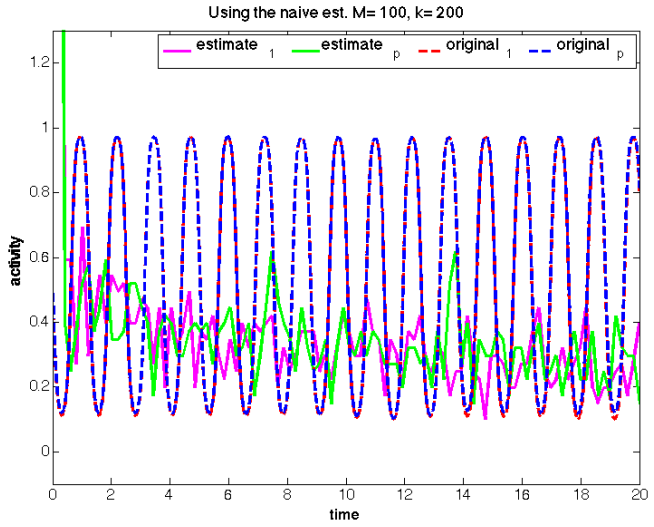

Figure 4.24: Application of the "naive method" to the estimation of a highly oscillating unknown output. In comparison, oscillatory method performs significantly better.

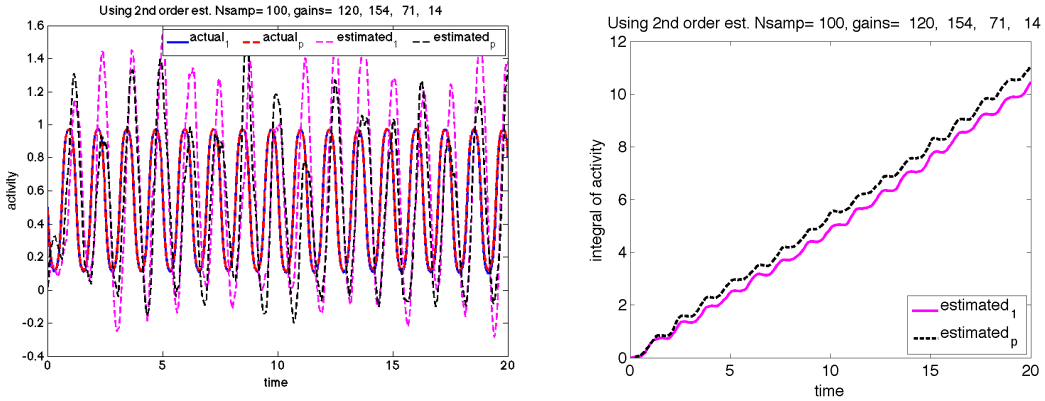

(a) Intensity function

(b) Integral of the intensity function

Figure 4.25: Scale invariant system. Scaling factor is $p = 2$, $N = 100$ experiment repetitions were used for estimation. The plots depict the estimation results using second-order observer estimator. The observer gains are given in the figures

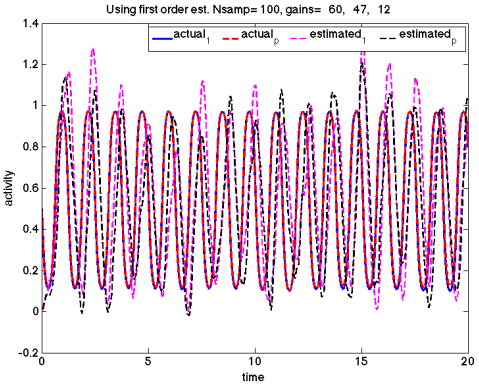

(a) Intensity function

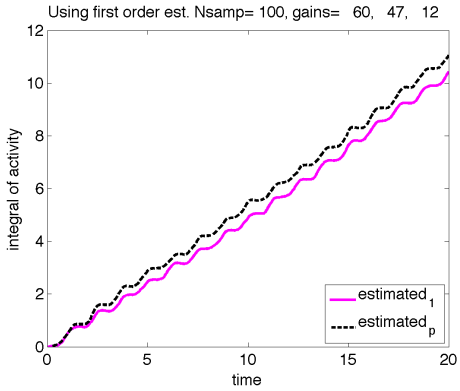

(b) Integral of the intensity function

Figure 4.26: Scale invariant system. Scaling factor is $p = 2$, $N = 100$ experiment repetitions were used for estimation. The plots depict the estimation results using first-order observer estimator. The observer gains are given in the figures

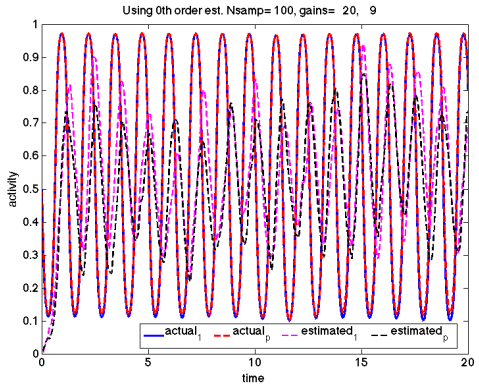

(a) Intensity function

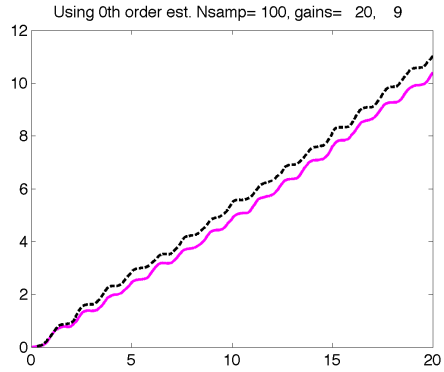

(b) Integral of the intensity function

Figure 4.27: Scale invariant system. Scaling factor is $p = 2$, $N = 100$ experiment repetitions were used for estimation. The plots depict the estimation results using zeroth-order observer estimator. The observer gains are given in the figures

A non scale invariant example, $p = 20$

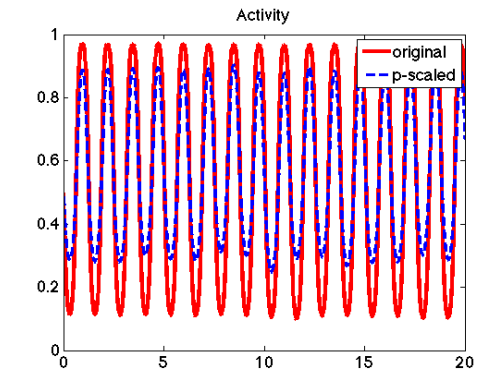

(a) Plot of the output and the p-scaled output

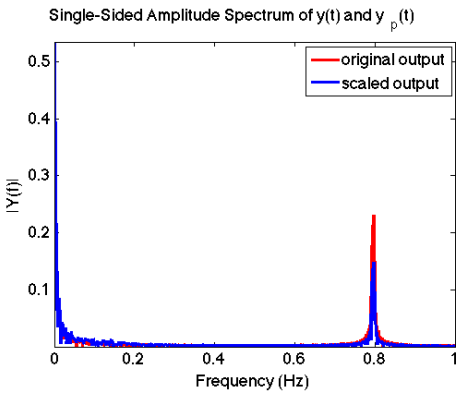

(b) Spectra of the output and p-scaled output

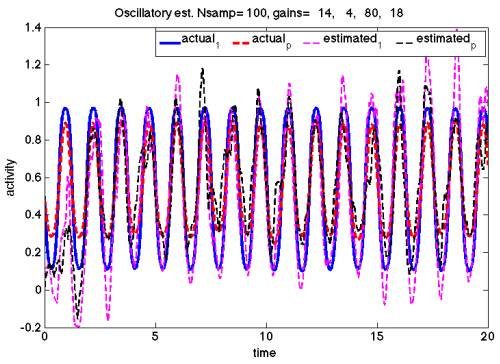

(c) Intensity function

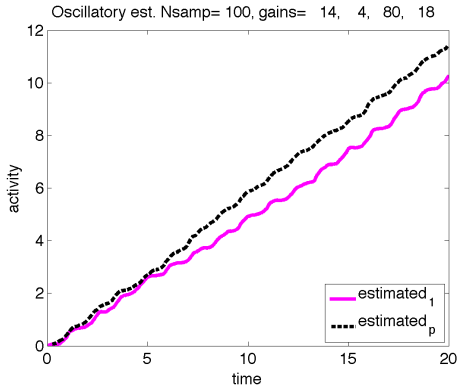

(d) Integral of the intensity function

Figure 4.28: A non-scale invariant system. Scaling factor is $p = 20$, $N = 100$ experiment repetitions were used for estimation. The plots depict the estimation results using oscillatory estimator. The observer gains are given on the figures. Obviously, both the plot for the intensity function and the plot for the integral of the intensity function, predict the loss of FCD.

4.4.2 A simple nonlinear observer model of an *E. coli* chemotactic pathway

As we have seen in the previous examples, the naive method does not take advantage of the known input signal. Consider a system given by

$$\begin{aligned} \dot{x} &= f(x,u), \\ y &= h(x,u), \end{aligned} \tag{4.18}$$

where $y(t) \in \mathbb{R}^1$ corresponds to the measured output ("activity") in a simple but realistic model of the *E. coli* chemotactic pathway, see for example [52], [86], [93], [88]. Here, $x(t) \in \mathbb{R}^n$ is the unknown internal state, and $u(t)$ is a known input signal. As before, we introduce the extended $(n+1)-$dimensional system that models the counting process by adding an integrator:

$$\begin{aligned} \dot{x} &= f(x,u), \\ \dot{z} &= h(x,u). \end{aligned} \tag{4.19}$$

Specifically, we take a simplified version of the model from [86], by picking the Hill coefficients in the model equal to 1, and all coefficients set to unity. Thus, we consider the following model:

$$\begin{aligned} \dot{x} &= \frac{1}{2} - \frac{1}{1+\frac{u}{x}} \\ \dot{z} &= \frac{1}{1+\frac{u}{x}}, \end{aligned} \tag{4.20}$$

with output z. An observer for this $n-$ dimensional system can be obtained as follows:

$$\begin{aligned} \dot{\hat{x}} &= \frac{1}{2} - \frac{1}{1+\frac{u}{\hat{x}}} \\ \dot{\hat{z}} &= \frac{1}{1+\frac{u}{\hat{x}}} - L(\hat{z}-z). \end{aligned} \tag{4.21}$$

Define the errors

$$\begin{aligned} e_1(t) &= \hat{x}(t) - x(t), \\ e_2(t) &= \hat{z}(t) - z(t). \end{aligned} \tag{4.22}$$

Then,

$$\dot{e}_1(t) = \dot{\hat{x}} - \dot{x}(t) = \frac{u(x-\hat{x})}{(x+u)(\hat{x}+u)} = \frac{-ue_1}{(x+u)(\hat{x}+u)}.$$
$$\dot{e}_2(t) = \dot{\hat{z}} - \dot{z}(t) = -\Big(\frac{1}{1+\frac{u}{x}} - \frac{1}{1+\frac{u}{\hat{x}}}\Big) - L(\hat{z}-z) \tag{4.23}$$
$$= \frac{e_1 u}{(x+u)(\hat{x}+u)} - Le_2.$$

It can be shown that if $0 < \alpha \leq u(t) \leq \beta \ \forall t$, then both $\hat{x}(t)$ and $x(t)$ are bounded, and $e_1(t) \to 0$ and $e_2(t) \to 0$ as $t \to \infty$.

For the system defined by (4.20) we have applied an input signal given by $u(t) = 2+\sin(5t)+0.5\sin(t)-0.2\cos(3t-20)$ and generated $k = 20$ realizations of the process, shown on left panel of Fig. 4.29. Then we applied the observer-based method described above to estimate the output of the process. We assumed that the model has an initial state $x_0 = 3$ and that the observer initial state was picked to be 0. The results indicate

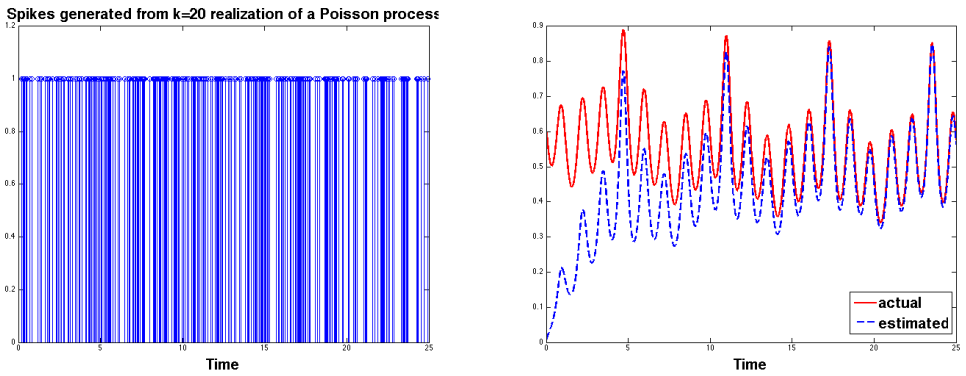

(a) (b)

Figure 4.29: Spikes (events) used as an input to the observer (a), and comparison between the true output and an estimate obtained by using a nonlinear observer (b). $k = 20$ realizations were used. L was picked to be 1.

that the observer performs extremely well.

4.4.3 Methods used for generation of a NHPP

There are numerous methods for the generation of a NHPP known in the literature. Most commonly used in the literature are generation by inversion, order statistics method, and acceptance-rejection method. A detailed overview of these methods can

be found in [74]. In our work, we use the following modified method of inversion. Suppose y is a given function and we want to generate the Poisson process with rate $y(t)$. We pick a small step size h, and on each time ih generate a spike with probability $P = F(ih)h + o(h)$.

Another method we will briefly describe is Monte Carlo based method. To explain this method, let is suppose that a spike happened at time t_0 and we wish to generate the time for the next spike. Let T be the random variable that gives the time t until the next spike, so that the spike will happen at time $t + t_0$. Then,

$$P(\text{next spike will happen at } t + t_0) = 1 - e^{-\int_{t_0}^{t} \lambda(\tau)d\tau}.$$

We write $y(t) := \int_{t_0}^{t} \lambda(\tau)d\tau$, as before.

The two methods are equivalent in the following sense:

Let X be the time of the next spike. Then,

$$F_X(t) = P(\text{first spike is at time } \leq t) = 1 - e^{-\int_0^t f(s)ds}$$

Proof. Let $G(t) = 1 - F(t) = P(\text{no spikes in } [0, t])$. Then,

$$G(t) = P(\text{no spikes in } [0, h])P(\text{no spikes in } [h, 2h]) \cdots P(\text{no spikes in } [(Nh - 1), Nh])$$

$$G(t) = [1 - f(0)h + o(h)][1 - f(h)h + o(h)] \cdots$$

$$\ln G(t) = \sum_{i=0}^{\frac{T}{h}-1} \ln(1 - f(ih) + o(h)) = \sum_{i=0}^{\frac{T}{h}-1} (-f(ih) + o(h))$$
$$= -\frac{T}{h} \sum f(ih) + N\frac{o(h)}{h}$$

Taking the limit of the expression above

$$\lim_{h \to 0} \ln G(t) = -e^{-\int_0^T f(s)ds}$$

□

Chapter 5

Remarks on stochastic adaptation and scale-invariance

Introduction

In the analysis of biochemical networks one can proceed with two modeling strategies, a deterministic and a stochastic one [108, 109]. In the deterministic approach, the reaction rate equations are ordinary differential equations, with states being the continuous variables representing the concentrations. A pathway is therefore decomposed into set of elementary reactions, and then the law of mass action is applied to each elementary reaction to obtain the ODEs. The incoherent feedforward motif presented in Chapter 2 and further analyzed in Chapter 3, and given by (3.3) was analyzed in a deterministic setting, and was shown to exhibit exact adaptation and an approximate scale invariance. However, deterministic models represent an aggregate (mean) behavior of the system, and are not accurate when the "copy numbers" of species (ions, atoms, molecules, individuals) are very small, which is sometimes the case in molecular biology at the single-cell level [97].

The occurrence of chemical reactions in the stochastic setting involves discrete and random events, and in order to predict the progress of chemical reactions in terms of observables such as copy number, $X(t)$, we consider a chemical reaction network consisting of m reactions which involve n species S_i, $i \in \{1, 2, \dots n\}$, [109]. We use notation as in [97] and here we provide the details to make the thesis self-contained.

The reactions $\mathcal{R}_j$, $j \in \{1, 2, \dots m\}$ are described by the combinations of reactants and products:

$$\mathcal{R}_j : \quad \sum_{i=1}^{n} a_{ij} S_i \to \sum_{i=1}^{n} b_{ij} S_i, \tag{5.1}$$

where a_{ij} and b_{ij} are nonnegative integers. Additionally, $\sum_{i=1}^{n} a_{ij}$ is the order of the

reaction $\mathcal{R}_j$.

From (5.1) the $n \times m$ stochiometry matrix $\Gamma = \{\gamma_{ij}\}$ of the network can be found, and it has entries that describe the net change in the number of units of species S_i each time the reaction R_j takes place; $\gamma_{ij} = b_{ij} - a_{ij}$, $i = 1, \dots n$, $j = 1, \dots m$. In addition to the stochiometry matrix, the rates at which various reactions take place are specified through propensity functions, ρ.

To illustrate the probabilistic aspect in this setting, we assume that starting at time $t = 0$ from an initial state $X(0)$, every sample path stays in state $X(0)$ for a random amount of time T_1, until an occurrence of a reaction takes the process to a new state $X(T_1)$. The process stays at this state for another random amount of time T_2, until the occurrence of another reaction takes the process to a new state $X(T_1 + T_2)$, and so on. Hence, the copy number X is a jump process, [109]. For the sake of notation, we write this process as $X{=}(X_1, X_2, \dots X_n)'$, indexed by time $t \geq 0$, and for each t, $X(t)$ is a random variable. The interest is to compute the probability that, at time t there are k_1 units of species S_1, k_2 units of species S_2, k_3 units of species S_3, and so forth:

$$p_k(t) = P[X(t) = k], \tag{5.2}$$

for each k. We call the vector k the state of the process. Abusing the notation we will denote the outcome of the random variable on a realization of the process for a species S_i as:

$$X_i(t) = \#\text{ of units of species } i \text{ at time } t. \tag{5.3}$$

A chemical master equation (CME) gives a system of linear differential equations for the p_k's in the following form:

$$\frac{dp_k}{dt} = \sum_{j=1}^{m} \rho_j(k - \gamma_j) p_{k-\gamma_j} - \sum_{j=1}^{m} \rho_j(k) p_k\,, \quad k \in \mathcal{Z}^n_{\geq 0}. \tag{5.4}$$

It can be seen from (5.4) that there is one equation for each state k, so this is an infinite system of linked equations. We assume that the initial probability vector $p(0)$ is given, and that there is a unique solution of (5.4) defined for all $t \geq 0$. We also introduce a

n-column vector:

$$f(k) := \sum_{j=1}^{m} \rho_j(k)\gamma_j = \Gamma R(k)\,, \quad k \in \mathcal{Z}^n_{\geq 0} \tag{5.5}$$

where $R(k) = (\rho_1(k), \cdots \rho_m(k))'$, and $\rho_j(k)h + o(h)$ is the probability that the reaction $\mathcal{R}_j$ takes place during an interval of length h, if the current state is k. When studying steady state properties we define the steady state distribution $\pi = (\pi_k)$ of the process X as any solution of the equations:

$$\sum_{j=1}^{m} \rho_j(k-\gamma_j)\pi_{k-\gamma_j} - \sum_{j=1}^{m} \rho_j(k)\pi_k = 0\,, \quad k \in \mathcal{Z}^n_{\geq 0}. \tag{5.6}$$

In order to solve the CME, one usually generates sample paths of the stochastic process $\{X(t)\}$, which is referred to as a stochastic simulation algorithm, SSA (for reference, see [26]). The algorithm addresses two questions: when is the next reaction going to occur, and what type of reaction will it be? The mean and the higher moments can be obtained by averaging the results of such stochastic simulations. Assuming that the probability density of $X(t)$ is given by (5.4), it can be shown that one can derive exact or approximate differential equations satisfied by the mean and the variance of $X(t)$. The expression for the mean satisfies:

$$\frac{d}{dt}\mathrm{E}[X(t)] = \mathrm{E}[f(X(t))], \tag{5.7}$$

where $f(k)$ is given by (5.5). If all reactions are mass-action of order zero or one, then (5.7) simplifies to:

$$\frac{d}{dt}\mathrm{E}[X(t)] = f(\mathrm{E}[X(t)]). \tag{5.8}$$

For reactions of order higher than one, one can prove the following expression

$$\begin{aligned} &\frac{d}{dt}\mathrm{E}[X(t)] = \mathrm{E}[f(X(t))] = f(\mathrm{E}[X(t)]) + G(t), \\ &G(t) = \mathrm{E}[g_{\mu(t)}(X(t) - \mu(t))], \\ &g^i_{\mu(t)}(x) = \frac{1}{2}(x-\mu(t))' H_i(\mu(t))(x-\mu(t)) + o(x-\mu(t)^2), \end{aligned} \tag{5.9}$$

where $x = X(t)$, $\mu(t) = \mathrm{E}[X(t)]$, $H_i(\mu(t))$ is the Hessian of the i-th component of the

vector field f. For the matrix of the second moments we first introduce the $n \times n$ diffusion matrix $B(k) = (B_{pq}(k))$ with entries as:

$$B_{pk}(k) = \sum_{j=1}^{m} \rho_j(k)\gamma_{pj}\gamma_{qj}\,, \quad p, q = 1, \ldots, n, \tag{5.10}$$

and then the second moment can be solved from

$$\frac{d}{dt}\mathrm{E}[X(t)X(t)'] = \mathrm{E}[X(t)f(X(t))'] + \mathrm{E}[f(X(t))X(t)'] + \mathrm{E}[B(X(t))]. \tag{5.11}$$

The expression for the variance can be obtained as:

$$\begin{aligned}
&\frac{d}{dt}\mathrm{Var}[X(t)] = \mathrm{E}[(X(t)-\mu(t))f(X(t))'] + \mathrm{E}[f(X(t))(X(t)-\mu(t))'] + \mathrm{E}[B(X(t))]\,,\\
&\mathrm{E}[B(X(t))] = \Gamma \mathrm{diag}\left(\mathrm{E}[\rho_1(X(t))], \ldots, \mathrm{E}[\rho_m(X(t))]\right)\Gamma'\,,\\
&f(X(t)) = f(\mu(t)) + J(\mu(t))(X(t)-\mu(t)) + g_{\mu(t)}(X(t)-\mu(t)),
\end{aligned} \tag{5.12}$$

where $J(x)$ is the Jacobian matrix of f evaluated at $x = \mu(t)$. Thus,

$$\begin{aligned}
&\frac{d}{dt}\mathrm{Var}[X(t)] = \mathrm{Var}[X(t)]J(\mu(t))' + J(\mu(t))\mathrm{Var}[X(t)] + \mathrm{E}[B(X(t))] + \alpha(t)\,,\\
&\alpha(t) = E[(X(t)-\mu(t))g_{\mu(t)}(X(t)-\mu(t))' + (X(t)-\mu(t))g_{\mu(t)}(X(t)-\mu(t))'].
\end{aligned} \tag{5.13}$$

Dropping the term $\alpha(t)$ one has the fluctuation-dissipation (FD) formula

$$\frac{d}{dt}\mathrm{Var}[X(t)] = \mathrm{Var}[X(t)]J(\mu(t))' + J(\mu(t))\mathrm{Var}[X(t)] + \mathrm{E}[B(X(t))]. \tag{5.14}$$

If the higher-order moments of $X(t)$ are small, then $\alpha(t) = o(X(t)-\mu(t)^2)$. For mass-action kinetics, and all reactions of order at most two, the fluctuation equation says that the mean $\mu(t) = \mathrm{E}[X(t)]$, and covariance matrix $\Sigma(t) = \mathrm{Var}[X(t)]$ satisfy:

$$\begin{aligned}
&\frac{d}{dt}\mu(t) = f(\mu) + L\Sigma,\\
&\frac{d}{dt}\Sigma \approx \Sigma J(\mu)' + J(\mu)\Sigma + H_0 + H_1\mu + H_2\Sigma.
\end{aligned} \tag{5.15}$$

The FD formula is exact for zero and first order mass-action reaction, because in that

case the Hessian, and therefore $g_{\mu(t)}$ are zero. Then the mean and the covariance matrix are the solutions of the coupled system of differential equations:

$$\begin{aligned} \frac{d}{dt}\mu(t) &= f(\mu), \\ \frac{d}{dt}\Sigma &= \Sigma J(\mu)' + J(\mu)\Sigma + B(\mu)\,, \end{aligned} \tag{5.16}$$

where

$$B(\mu) = \Gamma \mathrm{diag}\left(\rho_1(\mu), \ldots, \rho_m(\mu)\right)\Gamma'.$$

We explored a deterministic setting for analyzing and describing adaptation and scale invariance properties, and in particular we discussed a molecular representation for the model which gave rise to exact adaptation and an approximate scale invariance, (3.3). In addition, a structure in which the state degrades the output also possesses the same properties, as given by (3.4).

We next revisit these examples in the light of stochastic adaptation. The numerical study of effects of stochasticity for a minimal "two state protein scheme" was previously analyzed in [61]. In this Section we will give an analytical explanation of this example as well, and also revisit it in the light of adaptation of the mean and the higher order moments.

5.1 Adaptation of feedforward model

We study here the model represented by the following reactions:

$$\begin{aligned} &\emptyset \xrightarrow{u} X \xrightarrow{1} \emptyset \\ &X \xrightarrow{1/\varepsilon} X + Y\,, \qquad Y \xrightarrow{u/\varepsilon} \emptyset \end{aligned}$$

The set of ODEs for the deterministic setting are given by $\dot{x} = u - x$, and $\varepsilon\dot{y} = x - uy$, and was previously analyzed in Section 3.1. The state transition diagram corresponding to this circuit is given on Fig. 5.1.

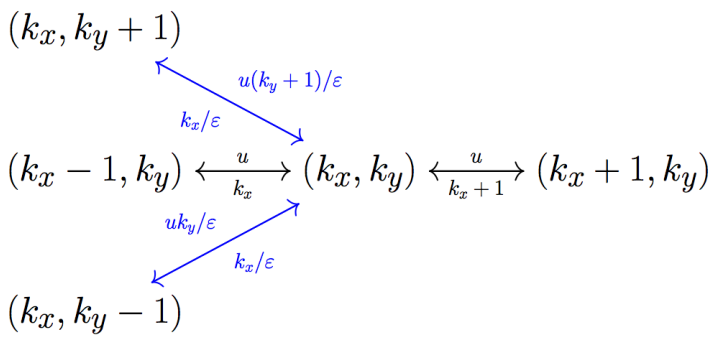

Figure 5.1: State transitions corresponding to an IFFL chemical reaction network

.

The stochiometry matrix for this system is given by $\Gamma = \begin{bmatrix} 1 & -1 & 0 & 0 \\ 0 & 0 & 1 & -1 \end{bmatrix}$, and the propensities for the four listed reactions are

$$\rho_1(k) = u\,, \quad \rho_2(k) = k_1\,, \quad \rho_3(k) = \frac{1}{\varepsilon}k_1\,, \quad \rho_4(k) = \frac{1}{\varepsilon}uk_2,$$

where we denote

$$R(k) = \begin{bmatrix} u & X & \frac{X}{\varepsilon} & \frac{1}{\varepsilon}uY \end{bmatrix}^T, \quad f(X,Y) = \Gamma R(k) = \begin{bmatrix} u - X \\ \frac{1}{\varepsilon}X - \frac{1}{\varepsilon}uY \end{bmatrix}.$$

The following equations for the means can be obtained:

$$\dot{\mu}_x(t) \;=\; u - \mu_x\,, \quad \dot{\mu}_y(t) \;=\; \frac{1}{\varepsilon}\mu_x - \frac{u}{\varepsilon}\mu_y. \tag{5.17}$$

Since all reactions are of order zero or one, first moments are the same as the deterministic ones. At the steady state $\mu_x^{ss} = u$, and $\mu_y^{ss} = 1$. Hence, moment of y (the output) adapts perfectly.

In order to find differential equations for the second moments we find the diffusion

$B(X)$ and $\mathrm{E}[B(X)]$:

$$E[B(X(t))] = \Gamma \cdot \mathrm{diag}\left\{u, E[X], \frac{1}{\varepsilon}E[X], \frac{u}{\varepsilon}E[Y]\right\} \cdot \Gamma^T = \begin{bmatrix} u+\mu_x & 0 \\ 0 & \frac{1}{\varepsilon}\mu_x + \frac{u}{\varepsilon}\mu_y \end{bmatrix}.$$

The linearization J is given by $J = \begin{bmatrix} -1 & 0 \\ \frac{1}{\varepsilon} & -\frac{u}{\varepsilon} \end{bmatrix}$.
Using (5) the following system of equations can be obtained:

$$\dot{\Sigma} = \begin{bmatrix} \dot{\Sigma}_{xx} & \dot{\Sigma}_{xy} \\ \dot{\Sigma}_{yx} & \dot{\Sigma}_{yy} \end{bmatrix} = \Sigma J^T + J\Sigma + B$$

$$\begin{aligned} \dot{\Sigma}_{xx} &= -2\Sigma_{xx} + u + \mu_x\,, \quad \dot{\Sigma}_{xy} = \frac{1}{\varepsilon}\Sigma_{xx} - \frac{u}{\varepsilon}\Sigma_{xy} - \Sigma_{xy}, \\ \dot{\Sigma}_{yy} &= \frac{2}{\varepsilon}\Sigma_{xy} - \frac{2u}{\varepsilon}\Sigma_{yy} + \frac{1}{\varepsilon}\mu_x + \frac{u}{\varepsilon}\mu_y. \end{aligned} \tag{5.18}$$

We denoted $\mathrm{cov}(X,Y)$ by Σ_{XY}. At the steady state we obtain that:

$$\begin{aligned} \Sigma^{ss}_{xx} = \frac{u+\mu^{ss}_x}{2} = u, \quad \Sigma^{ss}_{xy} = \frac{\frac{1}{\varepsilon}\Sigma^{ss}_{xx}}{\frac{u}{\varepsilon}+1} = \frac{u}{u+\varepsilon}, \\ \Sigma^{ss}_{yy} = \frac{1}{2u}\left(2\Sigma^{ss}_{xy} + \mu^{ss}_x + u\mu^{ss}_y\right) = 1 + \frac{1}{u+\varepsilon} \end{aligned} \tag{5.19}$$

From (5.19), we notice that for large u, $u \gg 1$, and small ε, $\Sigma^{ss}_{yy} \approx 1$, which is independent of u. Morever, for $\varepsilon \ll 1$ the system (with output y) also shows approximate scale invariance. To show that this is true, we suppose that $(\mu_x(t), \mu_y(t))$ is any solution corresponding to the input $u(t)$, for the system described by (5.17). Then, $(p\mu_x(t), \mu_y(t))$ is a solution corresponding to the input $pu(t)$:

$$\begin{aligned} \dot{\mu}_x &= u - \mu_x \quad &\Rightarrow \quad (p\dot{\mu}_x) &= (pu) - (p\mu_x), \\ \varepsilon\dot{\mu}_y &= \mu_x - u\mu_y\,, & & \\ \varepsilon &\approx 0 \quad &\Rightarrow \quad \mu_y &= \frac{\not{p}\mu_x}{\not{p}u}\,. \end{aligned} \tag{5.20}$$

Hence the scaling $\mu_x \mapsto p\mu_x$ and $u \mapsto pu$ leaves the μ_y equation (approximately)

invariant. Similarly, from (5.18),

$$\begin{aligned}
\dot{\Sigma}_{xx} &= -2\Sigma_{xx} + u + \mu_x \quad \Rightarrow \quad (p\dot{\Sigma}_{xx}) = -2(p\Sigma_{xx}) + (pu) + (p\mu_x), \\
\varepsilon\dot{\Sigma}_{xy} &= \Sigma_{xx} - u\Sigma_{xy} - \varepsilon\Sigma_{xy} \quad \Rightarrow \quad \varepsilon\dot{\Sigma}_{xy} = p\Sigma_{xx} - (pu)\Sigma_{xy} - \varepsilon\Sigma_{xy}\,, \\
\varepsilon\dot{\Sigma}_{yy} &= 2\Sigma_{xy} - 2u\Sigma_{yy} + \mu_x + u\mu_y \quad \Rightarrow \quad \varepsilon\dot{\Sigma}_{yy} = 2\Sigma_{xy} - 2(pu)\Sigma_{yy} + (p\mu_x) + (pu)\mu_y\,.
\end{aligned} \tag{5.21}$$

The last two expressions in (5.21) can be solved by using their quasi-steady state approximation as:

$$\begin{aligned}
\varepsilon \approx 0 \;&\Rightarrow\; \Sigma_{xy} \approx \tfrac{p\Sigma_{xx}}{pu} = \tfrac{\Sigma_{xx}}{u}, \\
\varepsilon \approx 0 \;&\Rightarrow\; \Sigma_{yy} \approx \tfrac{\Sigma_{xx}}{pu^2} + \tfrac{1}{2u}\mu_x + \tfrac{1}{2}\mu_y\,.
\end{aligned} \tag{5.22}$$

For large u, the first two terms in the second expression of (5.22) are negligible, so we finally obtain that under these assumptions the variance of the output y does not depend on the scale p, and the approximate scale invariance (of the mean and the variance of y) can be obtained.

5.2 Another feedforward model (IFFL2)

We also consider the following feedforward model in which the state degrades the output (IFFL2), for which an approximate scale invariance can also be shown in the deterministic setting. The chemical reactions underlying this model are given by:

$$\emptyset \xrightarrow{u} X \xrightarrow{1} \emptyset\,, \qquad \emptyset \xrightarrow{u/\varepsilon} Y$$
$$X + Y \xrightarrow{1/\varepsilon} X$$

In the deterministic setting the model is described by the following ODEs: $\dot{x} = u - x$, $\varepsilon\dot{y} = u - xy$, given in Chapter 3. The state transition diagram corresponding this circuit is given on Fig. 5.2, and the CME for this case is given by (5.23).

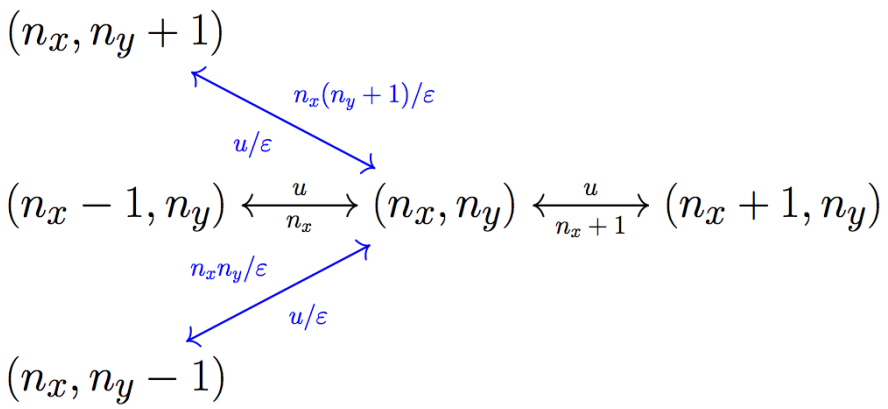

Figure 5.2: State transitions corresponding to an negative feedback chemical reaction network

.

$$\begin{aligned}\frac{\partial}{\partial t}P(n_x,n_y,t) &= -\frac{1}{\varepsilon}P(n_x,n_y,t) + \frac{1}{\varepsilon}(n_y+1)n_xP(n_x,n_y+1,t)\\ &+ uP(n_x-1,n_y,t) - n_xP(n_x,n_y,t) - uP(n_x,n_y,t) + (n_x+1)P(n_x+1,n_y,t)\\ &- \frac{1}{\varepsilon}n_xn_yP(n_x,n_y,t) + \frac{1}{\varepsilon}uP(n_x,n_y-1,t)\end{aligned} \tag{5.23}$$

The stochiometry matrix for this system is given by $\Gamma = \begin{bmatrix} 1 & -1 & 0 & 0 \\ 0 & 0 & 1 & -1 \end{bmatrix}$ with the propensities:

$$\rho_1(k) = u\,, \quad \rho_2(k) = k_1\,, \quad \rho_3(k) = \frac{u}{\varepsilon}\,, \quad \rho_4(k) = \frac{1}{\varepsilon}k_1k_2.$$

We denote

$$R(k) = \begin{bmatrix} u & X & \frac{u}{\varepsilon} & \frac{1}{\varepsilon}XY \end{bmatrix}^T, \quad f(X,Y) = \Gamma R(k) = \begin{bmatrix} u - X \\ \frac{1}{\varepsilon}u - \frac{1}{\varepsilon}XY \end{bmatrix}.$$

The following moment equations can be obtained:

$$\dot{\mu}_x(t) \;=\; u - \mu_x\,, \qquad \dot{\mu}_y(t) \;=\; \frac{1}{\varepsilon}u - \frac{1}{\varepsilon}\Sigma_{XY} - \frac{1}{\varepsilon}\mu_x\mu_y, \tag{5.24}$$

where we use the notation $\mathrm{cov}(X,Y) = \Sigma_{XY}$. It can be seen from (5.24) that the equation for the first moment of the output y does not match the corresponding deterministic ODEs. Notice also that the reactions are of order two, unlike the previous example where the reactions were at most order one. Hence the expressions for the second moments (FD equation) will only be approximate. At the steady state $\mu_x^{ss} = u$, and in order to solve the second equation in (5.24) we need to use the second moment equations. We find the diffusion $B(X)$, its expectation, $\mathrm{E}[B(X)]$, and the Jacobian:

$$E[B(X(t))] = \Gamma \cdot \mathrm{diag}\{u, E[X], \frac{u}{\varepsilon}, \frac{1}{\varepsilon}E[XY]\} \cdot \Gamma^T = \begin{bmatrix} u + \mu_x & 0 \\ 0 & \frac{u}{\varepsilon} + \frac{1}{\varepsilon}E[XY] \end{bmatrix},$$

$$J = \begin{bmatrix} -1 & 0 \\ -\frac{1}{\varepsilon}\bar{Y} & -\frac{1}{\varepsilon}\bar{X} \end{bmatrix}.$$

Then the problem simplifies to solving

$$\dot{\Sigma} = \begin{bmatrix} \dot{\Sigma}_{xx} & \dot{\Sigma}_{xy} \\ \dot{\Sigma}_{yx} & \dot{\Sigma}_{yy} \end{bmatrix} \approx \Sigma J^T + J\Sigma + B,$$

which decouples into:

$$\dot{\Sigma}_{xx} \approx -2\Sigma_{xx} + u + \mu_x\,, \quad \dot{\Sigma}_{xy} \approx -\frac{\bar{Y}}{\varepsilon}\Sigma_{xx} - \frac{\bar{X}}{\varepsilon}\Sigma_{xy} - \Sigma_{xy},$$
$$\dot{\Sigma}_{yy} \approx -\frac{2\bar{Y}}{\varepsilon}\Sigma_{xy} - \frac{2\bar{X}}{\varepsilon}\Sigma_{yy} + \frac{u}{\varepsilon} + \frac{1}{\varepsilon}E[XY] = -\frac{2\bar{Y}}{\varepsilon}\Sigma_{xy} - \frac{2\bar{X}}{\varepsilon}\Sigma_{yy} + \frac{u}{\varepsilon} + \frac{1}{\varepsilon}(\Sigma_{xy} + \mu_x\mu_y).$$

At the steady state the following expression for the means and the variances can be obtained:

$$\begin{aligned} &\mu_x^{ss} = u\,, \quad \mu_y^{ss} = 1 + \frac{\frac{\bar{y}}{\varepsilon}}{\frac{\bar{x}}{\varepsilon} + 1}\,, \\ &\Sigma_{xx}^{ss} = u\,, \quad \Sigma_{xy}^{ss} \approx \frac{\frac{-\bar{y}u}{\varepsilon}}{\frac{\bar{x}}{\varepsilon} + 1}\,, \quad \Sigma_{yy}^{ss} \approx \frac{\frac{\bar{y}^2 u}{\varepsilon}}{\frac{\bar{x}^2}{\varepsilon} + \bar{x}} + \frac{u}{\bar{x}}, \end{aligned} \tag{5.25}$$

and where $\bar{x}$ and $\bar{y}$ could be chosen to be (i) equal to the deterministic means for $x(t)$ and $y(t)$, or (ii) solved for using the stochastic means, as in equation (5.24). The two methods are demonstrated in the subsequent figures. From (5.25), it follows that for large $\bar{x}$, $\bar{x} \gg \bar{y}$, which can be obtained using large values for the inputs, $u \gg 1$, one can obtain approximate adaptation. Moreover, if additionally small values of the parameter ε, $\varepsilon \ll 1$ are picked, one can obtain approximate scale invariance as well.

Figures 5.3 and 5.4, show that the FD approximation does not approximate the true result from the SSA well, and, moreover, neither the mean nor the variance of the output adapt.

Figures 5.5, 5.7 and 5.9 illustrate the approximate adaptation of both moments for certain ranges of parameters. We also zoom into these figures to compare which method gives a better solution for $\bar{x}$, $\bar{y}$ (see Figures 5.6, 5.8, 5.10). Note also that for the parameters in Fig. 5.7 (and Fig. 5.8) we also have approximate scale invariance.

The results presented so far in this Chapter are summarized in Table 5.1.

	y_{det} adapts	μ_y adapts	Σ_{yy} adapts	FD exact
IFFL1	yes	yes	no	yes
IFFL2	yes	no	no	no

Table 5.1: Summary of adaptation results in a stochastic and a deterministic setting: y_{det} denotes the deterministic solution for y, μ_y and Σ_{yy} are its mean and variance. "FD exact" means that the differential equations for the first two moments are exact.

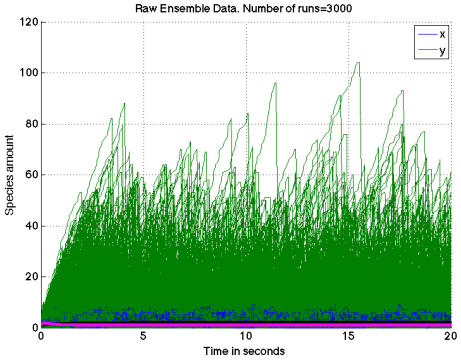

(a) SSA for the original system

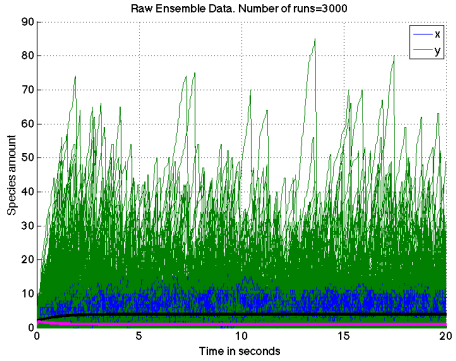

(b) SSA for the p-scaled system

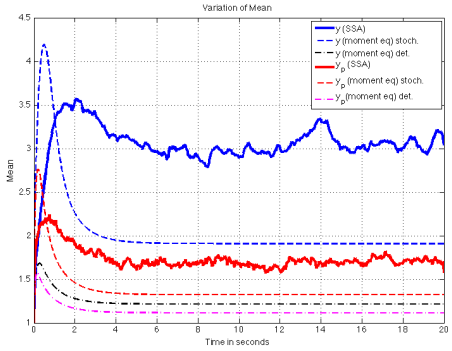

(c) Mean of y

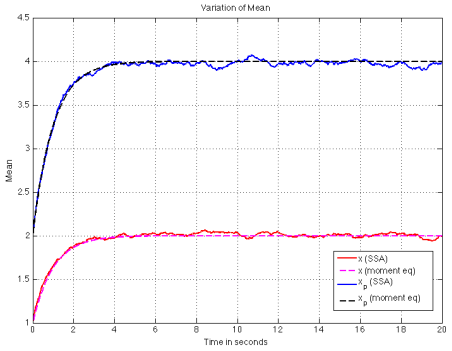

(d) Mean of x

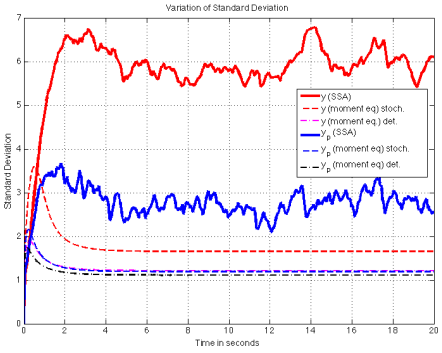

(e) Standard deviation of y

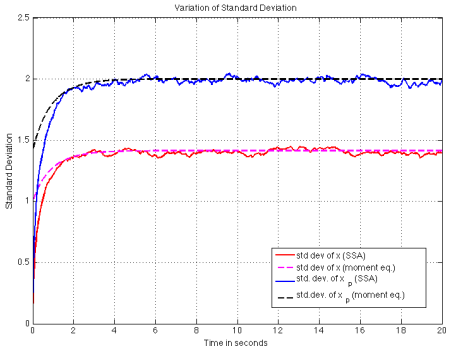

(f) Standard deviation of x

Figure 5.3: Feedforward model in which the state degrades the output. Loss of adaptation: note that neither the value of μ_y, nor the value of Σ_{yy} approach 1. Note also that the FD is not a good approximation of the SSA. Parameters used in the simulation are: $u_0 = 1$ (preadapted input), $u^* = 2$, $p = 2$, $\varepsilon = 0.1$.

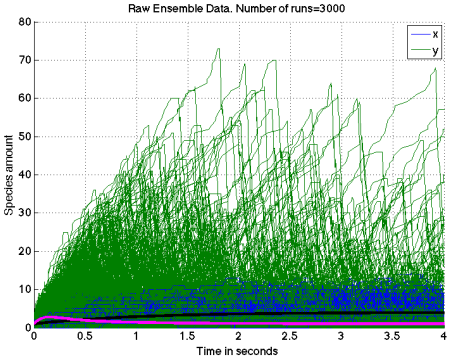

(a) SSA for the original system

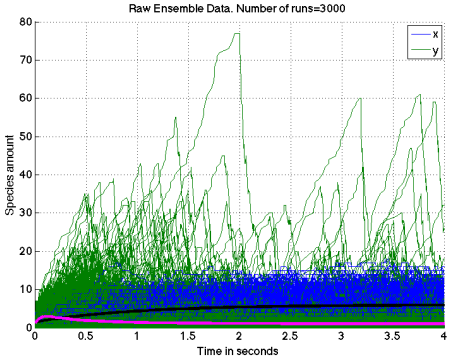

(b) SSA for the p-scaled system

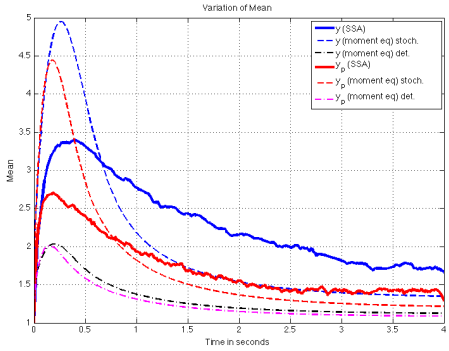

(c) Mean of y

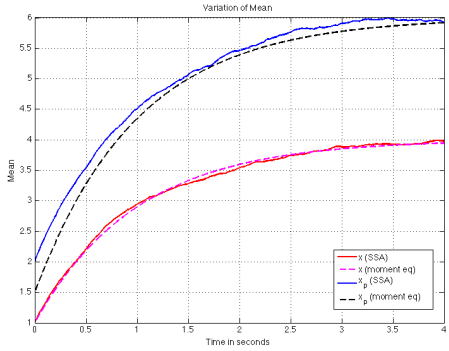

(d) Mean of x

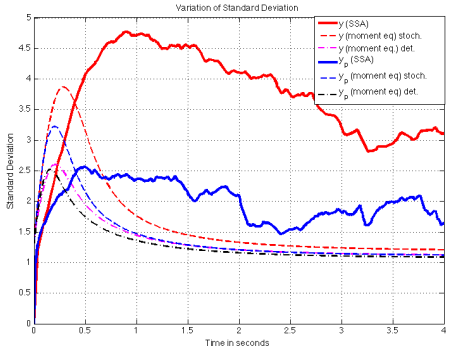

(e) Standard deviation of y

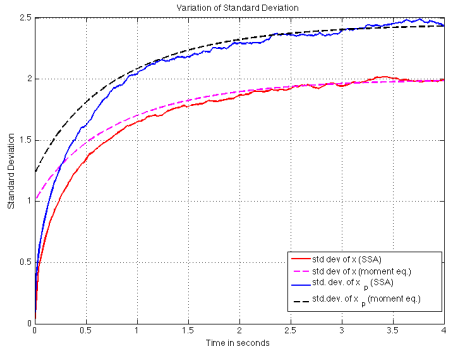

(f) Standard deviation of x

Figure 5.4: Feedforward model in which the state degrades the output. Loss of adaptation: note that neither the value of μ_y, nor the value of Σ_{yy} approach 1. Note also that the FD is not a good approximation of the SSA. Parameters used in the simulation are: $u_0 = 1$ (preadapted input), $u^* = 4$, $p = 1.5$, $\varepsilon = 0.1$

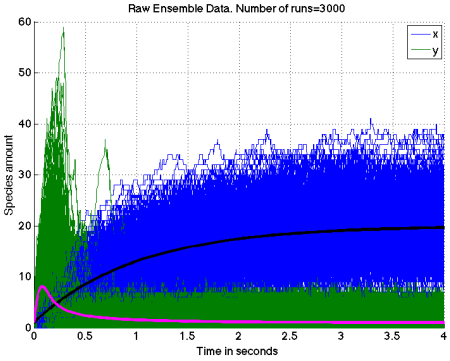

(a) SSA for the original system

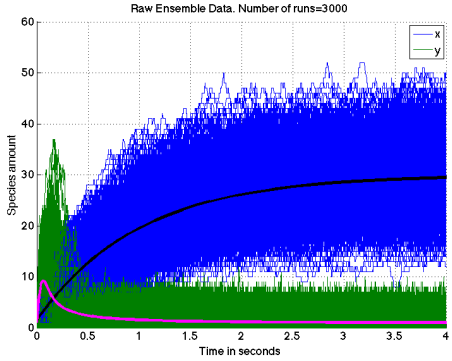

(b) SSA for the p-scaled system

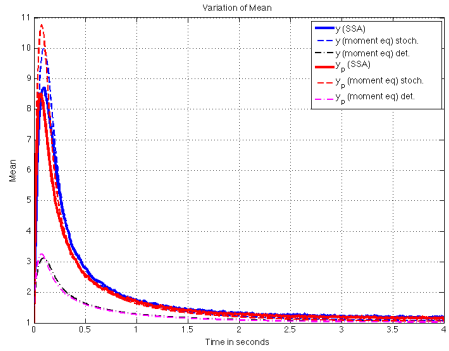

(c) Mean of y

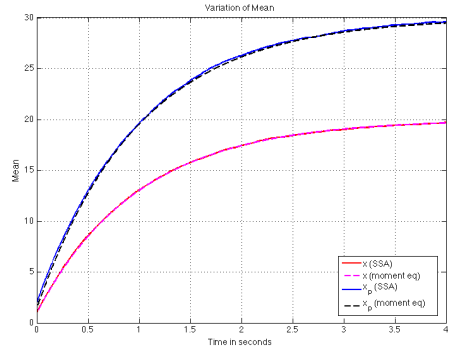

(d) Mean of x

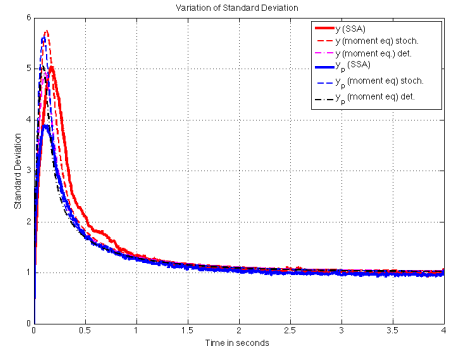

(e) Standard deviation of y

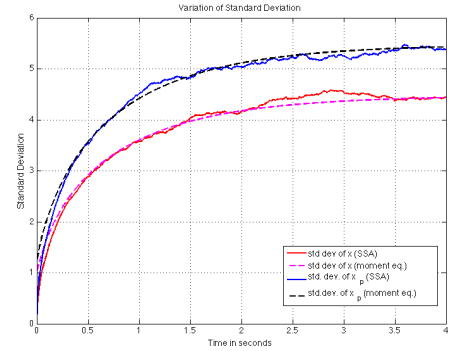

(f) Standard deviation of x

Figure 5.5: Feedforward model in which the state degrades the output. Approximate adaptation of the mean and the variance of y for certain ranges of parameters. Note also that the FD approximation of the SSA has improved. Parameters used in the simulation are: $u_0 = 1$ (preadapted input), $u^* = 20$, $p = 1.5$, $\varepsilon = 0.1$

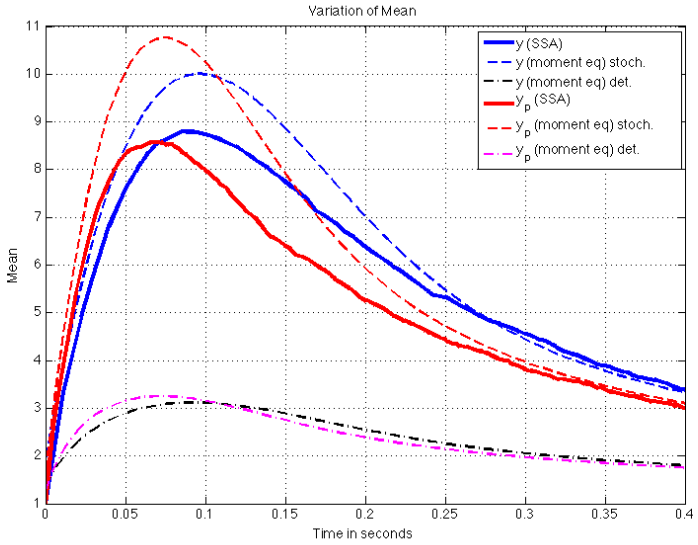

(a)

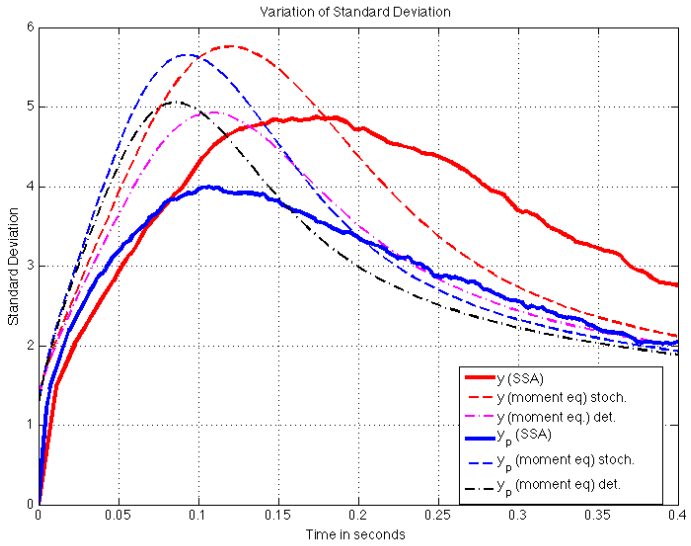

(b)

Figure 5.6: Means and standard deviation using various methods

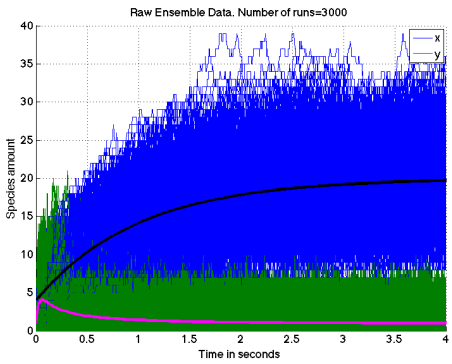

(a) SSA for the original system

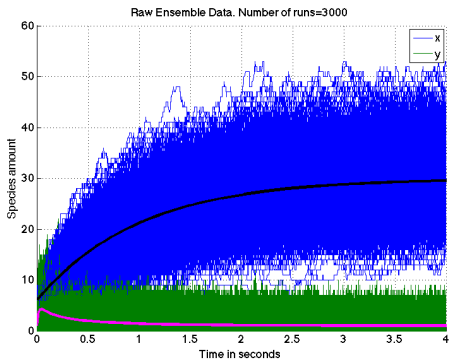

(b) SSA for the p-scaled system

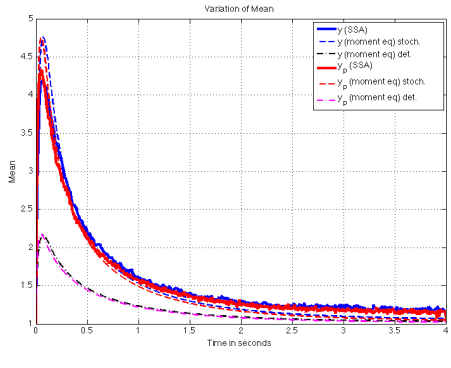

(c) Mean of y

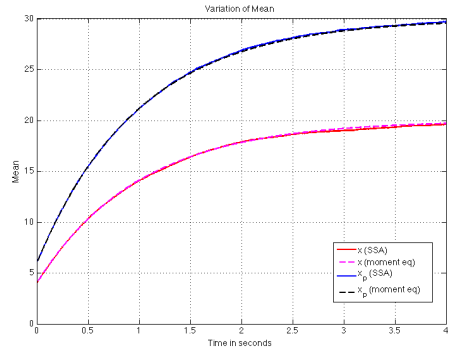

(d) Mean of x

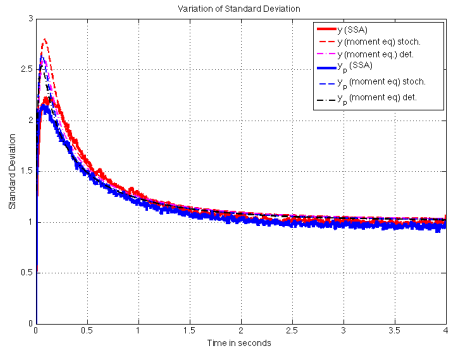

(e) Standard deviation of y

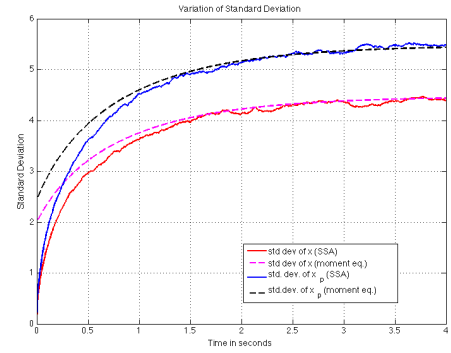

(f) Standard deviation of x

Figure 5.7: Feedforward model in which the state degrades the output. Approximate adaptation and approximate scale invariance of the mean and the variance of y for certain ranges of parameters. Note also that the FD can be used as an approximation of the SSA. Parameters used in the simulation are: $u_0 = 4$ (preadapted input), $u^* = 20$, $p = 1.5$, $\varepsilon = 0.1$

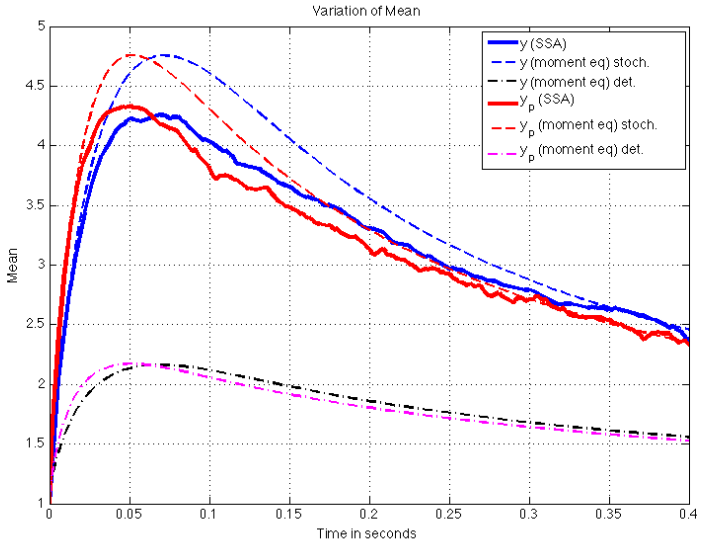

(a)

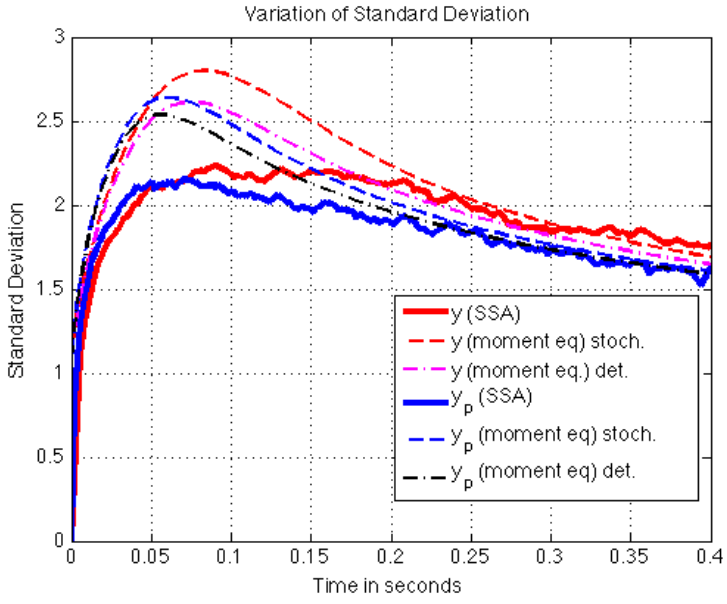

(b)

Figure 5.8: Means and standard deviation using various methods

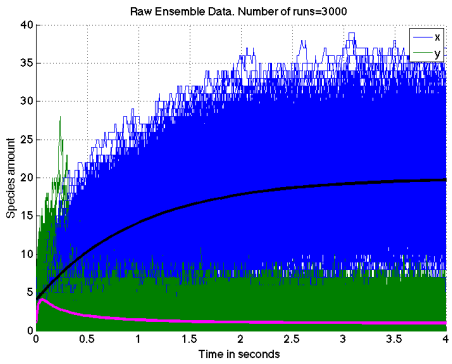

(a) SSA for the original system

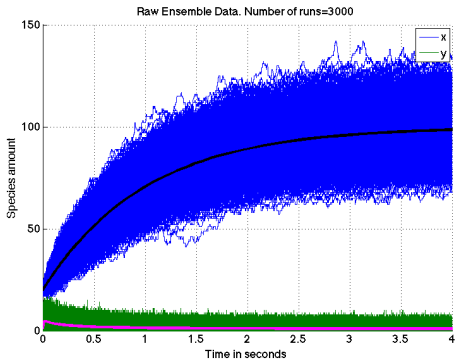

(b) SSA for the p-scaled system

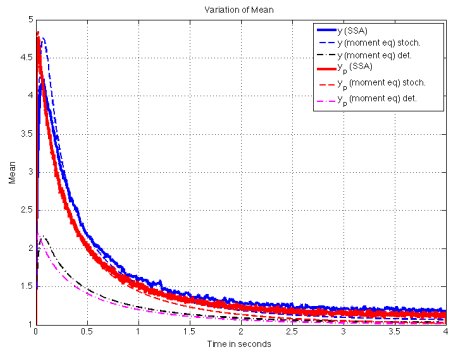

(c) Mean of y

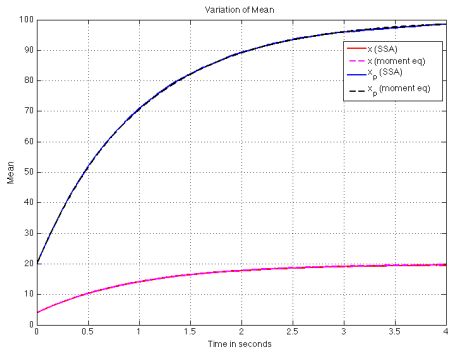

(d) Mean of x

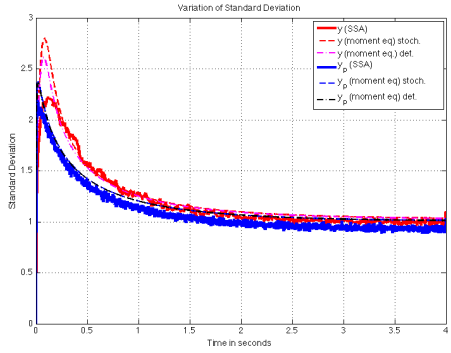

(e) Standard deviation of y

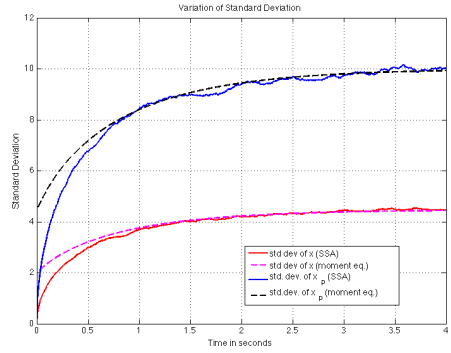

(f) Standard deviation of x

Figure 5.9: Feedforward model in which the state degrades the output. Approximate adaptation of the mean and the variance of y, for certain ranges of parameters. Note also that the FD can be used as an approximation of the SSA . Parameters used in the simulation are: $u_0 = 4$ (preadapted input), $u^* = 20$, $p = 5$, $\varepsilon = 0.1$

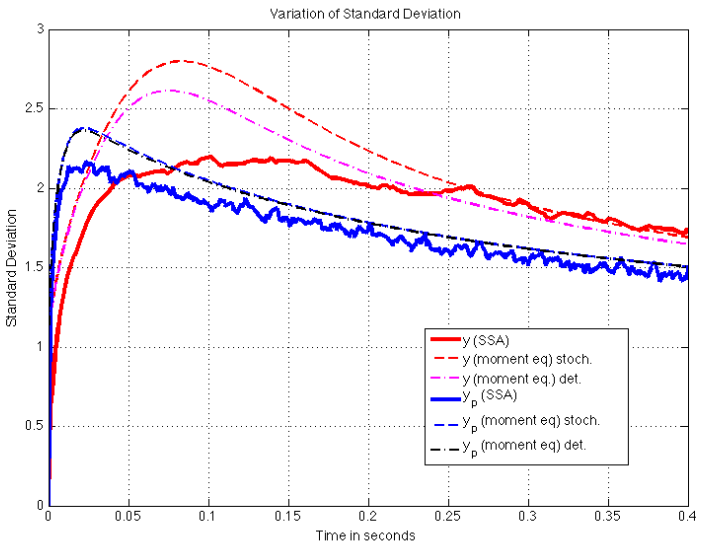

Figure 5.10: Means and standard deviation using various methods.

5.3 The two state protein model

To identify a minimal network that adapts, we modify the example discussed in [61]. We study the following reaction system:

$$\emptyset \xrightarrow{k} Y \xrightarrow{\alpha} \emptyset\,, \qquad Y \xrightarrow{u/\varepsilon} Z$$
$$Z \xrightarrow{c/\varepsilon} Y$$

The stochiometry matrix for this system is given by $\Gamma = \begin{bmatrix} 1 & -1 & -1 & 1 \\ 0 & 0 & 1 & -1 \end{bmatrix}$, with the propensities:

$$\rho_1(k) = k\,, \quad \rho_2(k) = \alpha k_1\,, \quad \rho_3(k) = \frac{u}{\varepsilon}k_1\,, \quad \rho_4(k) = \frac{c}{\varepsilon}k_2.$$

We denote

$$R(k) = \begin{bmatrix} k & \alpha Y & \frac{u}{\varepsilon}Y & \frac{c}{\varepsilon}Z \end{bmatrix}^T,$$

$$f(X,Y) = \Gamma R(k) = \begin{bmatrix} k - \alpha Y - \frac{u}{\varepsilon}Y + \frac{c}{\varepsilon}Z \\ \frac{u}{\varepsilon}Y - \frac{c}{\varepsilon}Z \end{bmatrix}.$$

Equations for the mean are given by:

$$\begin{aligned} \dot{\mu}_y(t) &= k - (\alpha + \frac{u}{\varepsilon})\mu_y + \frac{c}{\varepsilon}\mu_z, \\ \dot{\mu}_z(t) &= \frac{u}{\varepsilon}\mu_y - \frac{c}{\varepsilon}\mu_z, \end{aligned} \tag{5.26}$$

where Y is the output of interest. At the steady state $\mu_y^{ss} = \frac{k}{\alpha}$, and $\mu_z^{ss} = \frac{uk}{\alpha c}$. We next find the diffusion $B(X)$, $\mathrm{E}[B(X)]$, and the Jacobian matrix J:

$$\begin{aligned} E[B(X(t))] &= \Gamma \cdot \mathrm{diag}\{k, \alpha E[Y], \frac{u}{\varepsilon}E[Y], \frac{c}{\varepsilon}E[Z]\} \cdot \Gamma^T \\ &= \begin{bmatrix} k + \alpha\mu_y + \frac{u}{\varepsilon}\mu_y + \frac{c}{\varepsilon}\mu_z & -\frac{u}{\varepsilon}\mu_y - \frac{c}{\varepsilon}\mu_z \\ -\frac{u}{\varepsilon}\mu_y - \frac{c}{\varepsilon}\mu_z & \frac{u}{\varepsilon}\mu_y + \frac{c}{\varepsilon}\mu_z \end{bmatrix}. \end{aligned}$$

$$J = \begin{bmatrix} -\alpha - \frac{u}{\varepsilon} & \frac{c}{\varepsilon} \\ \frac{1}{\varepsilon} & -\frac{c}{\varepsilon} \end{bmatrix}.$$

Then the problem simplifies to solving

$$\dot{\Sigma} = \begin{bmatrix} \dot{\Sigma}_{yy} & \dot{\Sigma}_{yz} \\ \dot{\Sigma}_{zy} & \dot{\Sigma}_{zz} \end{bmatrix} = \Sigma J^T + J\Sigma + B,$$

which decouples into

$$\begin{aligned} \dot{\Sigma}_{yy} &= -2\Sigma_{yy}(\alpha + \frac{u}{\varepsilon}) + 2\frac{c}{\varepsilon}\Sigma_{yz} + k + \alpha\mu_y + \frac{u}{\varepsilon}\mu_y + \frac{c}{\varepsilon}\mu_z, \\ \dot{\Sigma}_{yz} &= \frac{u}{\varepsilon}\Sigma_{yy} - \Sigma_{yz}(\frac{c}{\varepsilon} + \alpha + \frac{u}{\varepsilon}) + \frac{c}{\varepsilon}\Sigma_{zz} - \frac{u}{\varepsilon}\mu_y - \frac{c}{\varepsilon}\mu_z, \\ \dot{\Sigma}_{yy} &= \frac{2u}{\varepsilon}\Sigma_{yz} - \frac{2c}{\varepsilon}\Sigma_{zz} + \frac{u}{\varepsilon}\mu_y + \frac{c}{\varepsilon}\mu_z. \end{aligned}$$

At the steady state the system simplifies to:

$$\begin{aligned} &- 2\Sigma_{yy}(\alpha + \frac{u}{\varepsilon}) + 2\frac{c}{\varepsilon}\Sigma_{yz} + k + \alpha\mu_y + \frac{u}{\varepsilon}\mu_y + \frac{c}{\varepsilon}\mu_z = 0, \\ &\frac{u}{\varepsilon}\Sigma_{yy} - \Sigma_{yz}(\frac{c}{\varepsilon} + \alpha + \frac{u}{\varepsilon}) + \frac{c}{\varepsilon}\Sigma_{zz} - \frac{u}{\varepsilon}\mu_y - \frac{c}{\varepsilon}\mu_z = 0, \\ &\frac{2u}{\varepsilon}\Sigma_{yz} - \frac{2c}{\varepsilon}\Sigma_{zz} + \frac{u}{\varepsilon}\mu_y + \frac{c}{\varepsilon}\mu_z = 0, \end{aligned}$$

and we obtain:

$$\Sigma_{yy} = \frac{c\Sigma_{yz}}{\alpha\varepsilon + u} + \frac{k}{\alpha}, \quad \Sigma_{zz} = \frac{u\Sigma_{yz}}{c} + \frac{uk}{\alpha c}, \quad \Sigma_{yz} = 0.$$

Hence,

$$\Sigma_{yy} = \frac{k}{\alpha}, \quad \Sigma_{zz} = \frac{uk}{\alpha c}, \quad \Sigma_{yz} = 0.$$

Since y was taken as the output to the system, we notice that the variance of the output also adapts. Moreover if $k = c = \alpha = 1$ then $\Sigma_{yy} = 1$, $\Sigma_{zz} = u$, $\Sigma_{yz} = 0$.

Chapter 6

Conclusions and Future Work

Motivated by questions arising in the field of molecular systems biology, with the goal to better understand and model transient behaviors of various species, this thesis' research represents a significant step towards a better understanding of two robust properties: scale invariance and adaptation, for several classes of systems found in biology. Adaptation is an essential property that many cellular systems possess, and allows them to detect changes in their environments, and readjust themselves accordingly. In addition to the asymptotic behavior that adaptation entails, we are also interested in understanding physiologically relevant transient behaviors, which we analyze through the property termed scale invariance. This property represents the invariance of the complete output trajectory with respect to rescaling of the input magnitudes, and is experimentally observed in many signaling pathways, that play roles in cell division, growth, cell death (apoptosis), etc. The misregulation of these pathways can lead to diseases, including several types of cancer.

The major contribution of this thesis lies in developing a mathematical mechanism termed "uniform linearizations with fast output", ULFO, on a study of enzyme networks. We mathematically prove that ULFO yields scale invariance, and extend the results of this study to examples relevant in systems biology. We show how on can use scale invariance and our developed mechanism for model invalidation.

Another key contribution to this topic is in the analysis of feedforward circuits, motifs commonly used in the research community as "signal processing" mechanisms that give rise to an approximate scale invariance, due to the presence of different time scales in their dynamics. We provide a fundamental limitation to this mechanism, and give a lower bound result for the scale invariance error.

Motivated by the work with our experimental collaborators who are designing novel experimental methods based on microfluidics devices that are able to generate signals of arbitrary inputs that are fed to a population of chemotactic bacteria, our contribution lies also in developing tools for the identification of time-varying parameters in nonhomogeneous Poisson processes based on observers and Kalman filters. Experimentally, discrete events such as "tumbles" or "spikes" are observed, based on images of swimming bacteria in response to the nutrient signal, and the goal is to identify a hidden continuous-time variable that drives the tumbling behavior.

The method we developed is novel in its application to biology, but it is also superior to other methods commonly used in the literature, for instance in communication networks, or neural science, where the estimation problem of a NHPP arises as well, in the sense that our method takes into account the fact that we are using information about the inputs to our estimator. We support this claim on several examples.

Topics discussed in this dissertation create several open problems that are of interest to the research community. Further analysis of scale invariance and adaptation properties in a stochastic setting is relevant to both biological and chemical problems, where it is of great interest to analyze complicated networks of simultaneously occurring chemical reactions, and understand for instance the origin of oscillations in such networks, in the light of developments in systems and synthetic biology.

Proposed method for the estimation of the rate function of a nonhomogeneous Poisson process (NHPP) can be naturally extended to finding an *optimal* estimator for an initial state of an unknown system, where the observations are k realizations of a NHPP, with the same initial state. Additionally, by feeding various inputs to the various species, and estimating the unknown underlying rate function (output of interest), one can look at the system identification problem based on the input-output data, and eventually a classification problem, where one would be able to discriminate between models of different species. Inspired by problems arising in pharmacy, and easily other experimental disciplines as well, questions regarding the number of necessary data points needed for a reliable model identification, and number of identifiable parameters are in their

own right an important research topic, and should be addressed in the further steps of this project. Even though the current focus of the estimation project are biological applications, many of the same mathematical principles apply to engineering systems.

References

[1] Adelman, T.L., Bialek, W., and Olberg, R.M. (2003). The information content of receptive fields. *Neuron*, 40(4), 823–833.

[2] Ahmed, T., Shimizu, T.S., and Stocker, R. (2010). Microfluidics for bacterial chemotaxis. *Integr. Biol.*, 2, 604–629.

[3] Al Ajarmeh, I., Yu, J., and Amezziane, M. (2010). Framework of applying a non-homogeneous Poisson process to model VoIP traffic on tandem networks. In *Proceedings of the 10th WSEAS International Conference on Applied Informatics and Communications, and 3rd WSEAS International Conference on Biomedical Electronics and Biomedical Informatics*, AIC'10/BEBI'10, 164–169. World Scientific and Engineering Academy and Society (WSEAS), Stevens Point, Wisconsin, USA.

[4] Alon, U. (2007). *An Introduction to Systems Biology: Design Principles of Biological Circuits*. Chapman & Hall/CRC Mathematical & Computational Biology, Boca Raton, FL, USA.

[5] Andrews, B., Sontag, E., and Iglesias, P. (2008). An approximate internal model principle: Applications to nonlinear models of biological systems. In *Proc. 17th IFAC World Congress, Seoul*, Paper FrB25.3, 6 pages.

[6] Angeli, D., Ferrell, J.E., and Sontag, E. (2004). Detection of multistability, bifurcations, and hysteresis in a large class of biological positive-feedback systems. *Proc Natl Acad Sci USA*, 101(7), 1822–1827.

[7] Arkin, B.L. and Leemis, L.M. (2000). Nonparametric estimation of the cumulative intensity function for a nonhomogeneous Poisson process from overlapping realizations. *Management Science*, 46(7), 989–998.

[8] Asthagiri, A. and Lauffenburger, D. (2001). A computational study of feedback effects on signal dynamics in a mitogen-activated protein kinase (MAPK) pathway model. *Biotechnol. Prog.*, 17, 227–239.

[9] Barkai, N. and Leibler, S. (1997). Robustness in simple biochemical networks. *Nature*, 387, 913–917.

[10] Bijlsma, J. and Groisman, E. (2003). Making informed decisions: regulatory interactions between two-component systems. *Trends Microbiol*, 11, 359–366.

[11] Bleris, L., Xie, Z., Glass, D., Adadey, A., Sontag, E., and Benenson, Y. (2011). Synthetic incoherent feed-forward circuits show adaptation to the amount of their genetic template. *Nature Molecular Systems Biology*, 7, 519.

[12] Block, S.M., Segall, J.E., and Berg, H.C. (1983). Adaptation kinetics in bacterial chemotaxis. *J. Bacteriol.*, 154, 312–323.

[13] Boel, R.K. and Benes, V.E. (1980). Recursive nonlinear estimation of a diffusion acting as the rate of an observed Poisson process. *IEEE Transactions on Information Theory*, 26(5), 561–575.

[14] Brockwell, A.E., Rojas, A.L., and Kass, R.E. (2004). Recursive Bayesian decoding of motor cortical signals by particle filtering. *Journal of Neurophysiology*, 91(4), 1899–1907.

[15] Bryson, Jr., A.E. and Henrikson, L.J. (1968). Estimation using sampled data containing sequentially correlated noise. *Journal of Spacecraft and Rockets*, 5, 662–665.

[16] Bryson, Jr., A.E. and Johansen, D. (1965). Linear filtering for time-varying systems using measurements containing colored noise. *IEEE Trans. Automat. Contr.*, 10, 4–10.

[17] Celani, A. and Vergassola, M. (2010). Bacterial strategies for chemotaxis response. *Proceedings of the National Academy of Sciences*, 107(4), 1391–1396.

[18] Chang, L. and Karin, M. (2001). Mammalian MAP kinase signaling cascades. *Nature*, 410, 37–40.

[19] Chen, H., Bernstein, B., and Bamburg, J. (2000). Regulating actin filament dynamics in vivo. *Trends Biochem. Sci.*, 25, 19–23.

[20] Chichilnisky, E.J. (2001). A simple white noise analysis of neuronal light responses. *Network: Computation in Neural Systems*, 12(2), 199–213.

[21] Cluzel, P., Surette, M., and Leibler, S. (2000). An ultrasensitive bacterial motor revealed by monitoring signaling proteins in single cells. *Science*, 287(5458), 1652–1655.

[22] Cohen-Saidon, C., Cohen, A.A., Sigal, A., Liron, Y., and Alon, U. (2009). Dynamics and variability of ERK2 response to EGF in individual living cells. *Molecular Cell*, 885–893.

[23] De Palo, G., Facchetti, G., Mazzolini, M., Menini, A., Torre, V., and Altafini, C. (2013). Common dynamical features of sensory adaptation in photoreceptors and olfactory sensory neurons. *Sci Rep*, 3, 1251.

[24] Donovan, S., Shannon, K., and Bollag, G. (2002). GTPase activating proteins: critical regulators of intracellular signaling. *Biochim. Biophys Acta*, 1602, 23–45.

[25] Elowitz, M., Levine, A., Siggia, E., and Swain, P. (2002). Stochastic gene expression in a single cell. *Nature*, 297(5584), 1183–1186.

[26] Erban, R., Chapman, J., and Maini, P. (2007). A practical guide to stochastic simulations of reaction-diffusion processes. *arXiv preprint arXiv:0704.1908*.

[27] Ferrell, J.E. (2009). Signaling motifs and Weber's law. *Molecular Cell*, 36(5), 724–727.

[28] Francois, P. and Siggia, E.D. (2008). A case study of evolutionary computation of biochemical adaptation. *Phys Biol*, 5, 026009.

[29] Goentoro, L. and Kirschner, M.W. (2009). Evidence that fold-change, and not absolute level, of β -catenin dictates Wnt signaling. *Molecular Cell*, 36, 872–884.

[30] Goentoro, L., Shoval, O., Kirschner, M.W., and Alon, U. (2009). The incoherent feedforward loop can provide fold-change detection in gene regulation. *Mol. Cell*, 36, 894–899.

[31] Grossman, A. (1995). Genetic networks controlling the initiation of sporulation and the development of genetic competence in Bacillus subtilis. *Annu Rev Genet.*, 29, 477–508.

[32] Hartman, P. (2002). Ordinary Differential Equations, Classics in Applied Mathematics. *Society for Industrial and Applied Mathematics (SIAM), Philadelphia, PA*, 38.

[33] Heinrich, R. and Schuster, S. (1996). *The Regulation of Cellular Systems*. Chapman & Hall New York.

[34] Henderson, S.G. (2003). Estimation for nonhomogeneous Poisson processes from aggregated data. *Oper. Res. Lett.*, 31(5), 375–382.

[35] Hoppensteadt, F.C. (1966). Singular perturbations on the infinite interval. *Transactions of the American Mathematical Society*, 123(2), 521–535.

[36] Huang, C.Y. and Ferrell, J.J. (1996). Ultrasensitivity in the mitogen-activated protein kinase cascade. *Proc. Natl. Acad. Sci. U.S.A*, 93, 10078–10083.

[37] Iglesias, P. (2003). Feedback control in intracellular signaling pathways: Regulating chemotaxis in Dictyostelium discoideum. *European J. Control.*, 9, 216–225.

[38] Iman, R.L. (2001). Appendix A : Latin Hypercube Sampling 1. *Encyclopedia of Statistical Sciences,Update*, 3(September), 408–411.

[39] Jiang, L., Ouyang, Q., and Tu, Y. (2010). Quantitative modeling of *Escherichia coli* chemotactic motion in environments varying in space and time. *PLoS Comput Biol*, 6(4), e1000735.

[40] Kaern, M., Elston, T.C., Blake, W.J., and Collins, J.J. (2005). Stochasticity in gene expression: from theories to phenotypes. *Nat. Rev. Genet.*, 6(6), 451–464.

[41] Kalinin, Y.V., Jiang, L.L., Tu, Y.H., and Wu, M. (2009). Logarithmic sensing in *Escherichia coli* bacterial chemotaxis. *Biophysical Journal*, 96, 2439–2448.

[42] Karp, G. (2002). *Cell and Molecular Biology.* Wiley.

[43] Keener, J. and Sneyd, J. (1998). *Mathematical Physiology.* Springer, New York.

[44] Keener, J. and Sneyd, J. (2009). *Mathematical Physiology 2nd ed.* Springer-Verlag, New York.

[45] Khalil, H.K. (2002). *Nonlinear Systems.* Prentice Hall, Inc., Upper Saddle River, NJ 07458.

[46] Koyama, S., Eden, U., Brown, E., and Kass, R. (2010). Bayesian decoding of neural spike trains. *Annals of the Institute of Statistical Mathematics*, 62(1), 37–59.

[47] Kremling, A., Bettenbrock, K., and Gilles, E.D. (2008). A feed-forward loop guarantees robust behavior in Escherichia coli carbohydrate uptake. *Bioinformatics*, 24, 704–710.

[48] Kuhl, M.E., Damerdji, H., and Wilson, J.R. (1998). Least squares estimation of nonhomogeneous Poisson processes. In *Proceedings of the 30th Conference on Winter Simulation*, WSC '98, 637–646. IEEE Computer Society Press, Los Alamitos, CA, USA.

[49] Kuhl, M.E. and Wilson, J.R. (1999). Least squares estimation of nonhomogeneous Poisson processes. *Journal of Statistical Computation and Simulation*, 67, 75–108.

[50] Kuhl, M.E., Wilson, J.R., and Johnson, M.A. (1997). Estimating and simulating Poisson processes having trends or multiple periodicities. *IIE Transactions*, 29, 201–211.

[51] Laming, D. (1986). *Sensory Analysis*. Academic Press, London.

[52] Lazova, M.D., Ahmed, T., Bellomo, D., Stocker, R., and Shimizu, T.S. (2011). Response-rescaling in bacterial chemotaxis. *Proc Natl Acad Sci U.S.A.*, 108, 13870–13875.

[53] Leemis, L.M. (1991). Nonparametric estimation of the cumulative intensity function for a nonhomogeneous Poisson process. *Manage. Sci.*, 37(7), 886–900.

[54] Leemis, L.M. (2004). Nonparametric estimation and variate generation for a nonhomogeneous Poisson process from event count data. *IIE Transactions*, 36, 1155–1160.

[55] Levchenko, A. and Iglesias, P. (2002). Models of eukaryotic gradient sensing: Application to chemotaxis of amoebae and neutrophils. *Biophys J.*, 82, 50–63.

[56] Lew, D. and Burke, D. (2003). The spindle assembly and spindle position checkpoints. *Annu Rev Genet.*, 37, 251–282.

[57] Ma, W., Trusina, A., El-Samad, H., Lim, W.A., and Tang, C. (2009). Defining network topologies that can achieve biochemical adaptation. *Cell*, 138(4), 760–773.

[58] Ma'ayan, A., Jenkins, S.L., Neves, S., Hasseldine, A., Grace, E., Dubin-Thaler, B., Eungdamrong, N.J., Weng, G., Ram, P.T., Rice, J.J., Kershenbaum, A., Stolovitzky, G.A., Blitzer, R.D., and Iyengar, R. (2005). Formation of regulatory patterns during signal propagation in a Mammalian cellular network. *Science*, 309, 1078–1083.

[59] Mahaut-Smith, M.P., Ennion, S.J., Rolf, M.G., and Evans, R.J. (2000). ADP is not an agonist at P2X(1) receptors: evidence for separate receptors stimulated by ATP and ADP on human platelets. *Br. J. Pharmacol.*, 131, 108–114.

[60] Mangan, S., Itzkovitz, S., Zaslaver, A., and Alon, U. (2006). The incoherent feed-forward loop accelerates the response-time of the gal system of Escherichia coli. *J. Mol. Biol.*, 356, 1073–1081.

[61] Marquez-Lago, T.T. and Leier, A. (2011). Stochastic adaptation and fold-change detection: from single-cell to population behavior. *BMC Systems Biology*, 5(22).

[62] Marsigliante, S., Elia, M.G., Di Jeso, B., Greco, S., Muscella, A., and Storelli, C. (2002). Increase of [Ca(2+)](i) via activation of ATP receptors in PC-Cl3 rat thyroid cell line. *Cell. Signal.*, 14, 61–67.

[63] Massey, W.A., Parker, G.A., and Whitt, W. (1996). Estimating the parameters of a nonhomogeneous Poisson process with linear rate. *Telecommunication Systems*, 5(2), 361–388.

[64] Masson, J.B., Voisinne, G., Wong-Ng, J., Celani, A., and Vergassola, M. (2012). Noninvasive inference of the molecular chemotactic response using bacterial trajectories. *Proceedings of the National Academy of Sciences*, 109(5), 1802–1807.

[65] Mello, B.A. and Tu, Y. (2003). Perfect and near-perfect adaptation in a model of bacterial chemotaxis. *Biophys. J.*, 84, 2943–2956.

[66] Mello, B.A. and Tu, Y. (2007). Effects of adaptation in maintaining high sensitivity over a wide range of backgrounds for Escherichia coli chemotaxis. *Biophysical Journal*, 92(7), 2329–2337.

[67] Menè, P., Pugliese, G., Pricci, F., Di Mario, U., Cinotti, G.A., and Pugliese, F. (1997). High glucose level inhibits capacitative Ca2+ influx in cultured rat mesangial cells by a protein kinase C-dependent mechanism. *Diabetologia*, 40, 521–527.

[68] Mesibov, R., Ordal, G.W., and Adler, J. (1973). The range of attractant concentrations for bacterial chemotaxis and the threshold and size of response over this range. *J. Gen. Physiol.*, 62, 203–223.

[69] Moylan, P. (1974). A note on Kalman-Bucy filters with zero measurement noise. *IEEE Trans. Automat. Contr.*, 19(3), 263–264.

[70] Nagashima, T., Shimodaira, H., Ide, K., Nakakuki, T., Tani, Y., Takahashi, K., Yumoto, N., and Hatakeyama, M. (2007). Quantitative transcriptional control of ErbB receptor signaling undergoes graded to biphasic response for cell differentiation. *J. Biol. Chem.*, 282, 4045–4056.

[71] Nesher, R. and Cerasi, E. (2002). Modeling phasic insulin release: immediate and time-dependent effects of glucose. *Diabetes*, 51 Suppl 1, S53–59.

[72] O'Malley, R.E. (1991). Singular perturbation methods for ordinary differential equations. *Applied Mathematical Sciences*, 89.

[73] Paliwal, S., Iglesias, P.A., Campbell, K., Hilioti, Z., Groisman, A., and Levchenko, A. (2007). MAPK-mediated bimodal gene expression and adaptive gradient sensing in yeast. *Nature*, 446, 46–51.

[74] Pasupathy, R. (2011). Generating nonhomogeneous Poisson processes. *JWiley Encyclopedia of Operations Research and Management Science.*

[75] Paulsson, J. (2005). Models of stochastic gene expression. *Physics of Life Reviews*, 2(2), 157–175.

[76] Prados, A., J., B.J., and B., S.R. (1997). A dynamical Monte Carlo algorithm for master equations with time-dependent transition rates. *Journal of Statistical Physics*, 89(1-3), 709–734.

[77] Rao, C.V., Wolf, D.M., and Arkin, A.P. (2002). Control, exploitation and tolerance of intracellular noise. *Nature*, 420(6912), 231–237.

[78] Ridnour, L.A., Windhausen, A.N., Isenberg, J.S., Yeung, N., Thomas, D.D., Vitek, M.P., Roberts, D.D., and Wink, D.A. (2007). Nitric oxide regulates matrix metalloproteinase-9 activity by guanylyl-cyclase-dependent and -independent pathways. *Proc. Natl. Acad. Sci. U.S.A.*, 104, 16898–16903.

[79] Roberts, M., Papachristodoulou, A., and Armitage, J.P. (2010). Adaptation and control circuits in bacterial chemotaxis. *Biochemical Society Transactions*, 38(5), 1265–9.

[80] Ross, H. and Murray, D. (1996). *E.H. Weber on the Tactile Senses*. Taylor and Francis, London.

[81] Sasagawa, S., Ozaki, Y., Fujita, K., and Kuroda, S. (2005). Prediction and validation of the distinct dynamics of transient and sustained ERK activation. *Nat. Cell Biol.*, 7, 365–373.

[82] Savageau, M.A. (1971). Concepts relating the behavior of biochemical systems to their underlying molecular properties. *Archives of Biochemistry and Biophysics*, 145(2), 612–621.

[83] Schwartz, O., Pillow, J.W., Rust, N.C., and Simoncelli, E.P. (2006). Spike-triggered neural characterization. *J Vis*, 6(4), 484–507.

[84] Shah, N.A. and Sarkar, C.A. (2011). Robust network topologies for generating switch-like cellular responses. *PLoS Comput. Biol.*, 7, e1002085.

[85] Shimazaki, H. and Shinomoto, S. (2007). A method for selecting the bin size of a time histogram. *Neural Comput.*, 19(6).

[86] Shimizu, T.S., Tu, Y., and Berg, H.C. (2010). A modular gradient-sensing network for chemotaxis in Escherichia coli revealed by responses to time-varying stimuli. *Mol. Syst. Biol.*, 6, 382.

[87] Shoval, O., Alon, U., and Sontag, E. (2011). Symmetry invariance for adapting biological systems. *SIAM Journal on Applied Dynamical Systems*, 10, 857–886.

[88] Shoval, O., Goentoro, L., Hart, Y., Mayo, A., Sontag, E., and Alon, U. (2010). Fold change detection and scalar symmetry of sensory input fields. *Proc Natl Acad Sci U.S.A.*, 107, 15995–16000.

[89] Sigal, A., Milo, R., Cohen, A., Geva-Zatorsky, N., Klein, Y., Liron, Y., Rosenfeld, N., Danon, T., Perzov, N., and Alon, U. (2006). Variability and memory of protein levels in human cells. *Nature*, 444(7119), 643–646.

[90] Skataric, M., Nikolaev, E., and Sontag, E. (2014). Fundamental limitation of the instantaneous approximation in fold-change detection models. *IET Systems Biology*.

[91] Skataric, M., Nikolaev, E., and Sontag, E. (2014). Scale-invariance in singularly perturbed systems. In *Proceedings of 53st IEEE Conference on Decision and Control (CDC 2014)*, 5511–5516.

[92] Skataric, M. and Sontag, E. (2014). Remarks on model-based estimation of non-homogeneous Poisson processes and applications to biological systems. In *Proceedings of 13th European Control Conference (ECC)*, 2052–2057.

[93] Skataric, M. and Sontag, E.D. (2012). A characterization of scale invariant responses in enzymatic networks. *PLoS Computational Biology*, 8(11), e1002748.

[94] Skataric, M. and Sontag, E.D. (2012). Exploring the scale invariance property in enzymatic networks. In *Proceedings of 51st IEEE Conference on Decision and Control (CDC 2012)*, 5511–5516.

[95] Sontag, E. (1998). *Mathematical Control Theory. Deterministic Finite-Dimensional Systems*, volume 6 of *Texts in Applied Mathematics*. Springer-Verlag, New York, second edition.

[96] Sontag, E. (2003). Adaptation and regulation with signal detection implies internal model. *Systems Control Lett.*, 50(2), 119–126.

[97] Sontag, E. (2005-2014). Lecture notes on mathematical systems biology.

[98] Sontag, E. (2010). Remarks on feedforward circuits, adaptation, and pulse memory. *IET Systems Biology*, 4, 39–51.

[99] Sourjik, V., Vaknin, A., Shimizu, T.S., and Berg, H.C. (2007). In vivo measurement by FRET of pathway activity in bacterial chemotaxis. In B.R.C. Melvin I. Simon and A. Crane (eds.), *TwoComponent Signaling Systems, Part B*, volume 423 of *Methods in Enzymology*, 363–391. Academic Press.

[100] Stryer, L. (1995). *Biochemistry*. Freeman.

[101] Sulis, M. and Parsons, R. (2003). PTEN: from pathology to biology. *Trends Cell Biol.*, 13, 478–483.

[102] Takeda, K., Shao, D., Adler, M., Charest, P., Loomis, W., Levine, H., Groisman, A., Rappel, W.J., and Firtel, R. (2012). Incoherent feedforward control governs adaptation of activated Ras in a eukaryotic chemotaxis pathway. *Sci Signal*, 5(205), ra2.

[103] Thattai, M. and van Oudenaarden, A. (2001). Intrinsic noise in gene regulatory networks. *Proc. Natl. Acad. Sci. U.S.A.*, 98, 8614–8619.

[104] Thompson, R. (1967). *Foundations of physiological psychology*. Harper and Row, New York.

[105] Tikhonov, A. (1948). On the dependence of the solutions of differential equations on a small parameter. *Matematicheskii Sbornik*, 64(2), 193–204.

[106] Tikhonov, A. (1952). Systems of differential equations containing small parameters in the derivatives. *Matematicheskii Sbornik*, 31, 575–586.

[107] Tsang, J., Zhu, J., and van Oudenaarden, A. (2007). MicroRNA-mediated feedback and feedforward loops are recurrent network motifs in mammals. *Mol. Cell*, 26, 753–767.

[108] Ullah, M., Schmidt, H., Cho, K.H., and Wolkenhauer, O. (2006). Deterministic modelling and stochastic simulation of biochemical pathways using MATLAB. *IEE Proceedings-Systems Biology*, 153(2), 53–60.

[109] Ullah, M. and Wolkenhauer, O. (2011). *Stochastic Approaches for Systems Biology.* Springer.

[110] Van Schuppen, J.H. (1977). Filtering, prediction and smoothing for counting process observations, a Martingale approach. *SIAM Journal of Applied Math.*, 32(3), 552–570.

[111] Vasileva, A.B., Butuzov, V.F., and Kalachev, L.V. (1995). *The Boundary Function Method for Singular Perturbation Problems.* SIAM.

[112] Wadhams, G.H. and Armitage, J.P. (2004). Making sense of it all: bacterial chemotaxis. *Nat Rev Mol Cell Biol*, 5(12), 1024–1037.

[113] Weber, E. (1905). *Tatsinn and Gemeingefuhl.* Verlag von Wilhelm Englemann, Leipzig.

[114] Widmann, C., Spencer, G., Jarpe, M., and Johnson, G. (1999). Mitogen-activated protein kinase: Conservation of a three-kinase module from yeast to human. *Physiol. Rev.*, 79, 143–180.

[115] Yang, L. and Iglesias, P. (2006). Positive feedback may cause the biphasic response observed in the chemoattractant-induced response of *Dictyostelium* cells. *Systems Control Lett.*, 55(4), 329–337.

[116] Yao, G., Tan, C., West, M., Nevins, J.R., and You, L. (2011). Origin of bistability underlying mammalian cell cycle entry. *Mol. Syst. Biol.*, 7, 485.

[117] Yi, T.M., Huang, Y., Simon, M.I., and Doyle, J.C. (2000). Robust perfect adaptation in bacterial chemotaxis through integral feedback control. *Proc. Natl. Acad. Sci. USA*, 97(9), 4649–4653.